

**Permeability, porosity, and depositional environment and their effect on reservoir quality in the Cretaceous Bluesky Formation Whitecourt, Alberta.**

By: Scott Doyle

Submitted in Partial Fulfillment of the Requirements  
for the Degree of Bachelor of Science, Honours  
Department of Earth Sciences  
Dalhousie University, Halifax, Nova Scotia

September 22, 2006  
Advisor: Dr. Martin Gibling

## **Acknowledgements**

I would like to thank Dr. Martin Gibling, my thesis supervisor. Your guidance and enthusiasm throughout the course of this project has been greatly appreciated. This thesis would not have been possible without your generous time and valued suggestions. Thanks to Jason Lavigne for helping me understand the petrography, and to Terry Lukie for his efforts at the core lab. I would like to thank Phil Pelletier and Art Kowal for giving me the opportunity to continue my study of the Bluesky Formation as my undergraduate thesis. Thanks to Talisman Energy for funding the study. Thanks to Hasley Vincent for his time, effort, and suggestions they were crucial to this projects completion. Thanks to Dr. Grant Wach for his suggestions, discussions, and for the use of the basin lab. Finally I would like to thank my family, girlfriend, and friends. Your love, support, and encouragement showed me there was a light at the end of the tunnel when I couldn't see it.

# **Permeability, porosity, and depositional environment and their effect on reservoir quality in the Cretaceous Bluesky Formation Whitecourt, Alberta.**

**By Scott Doyle**

## **Abstract**

Variations in porosity and permeability are common concerns when analyzing formations for reservoir quality. The Cretaceous Bluesky Formation of Whitecourt Alberta is a tight gas formation where average permeability is  $> 0.1$  mD. The Bluesky Formation in Whitecourt was deposited during a regional transgression and shows three main depositional well log signatures. "Bluesky A" is regionally extensive and interpreted as a channel mouth to shoreface deposit containing several characteristic ichnofacies and ranging in thickness from 1-4 m. "Bluesky B" is a channel deposit and or barrier bar system trending NE-SW, located primarily in the western portion of the study area near Edson, and ranging in thickness from 7 –18 m. "Bluesky C" is an estuary deposit and contains several metres of mud draped sand lenses and is moderately to heavily bioturbated.

Samples taken from 6 cored Bluesky wells have been studied to investigate why porosity and permeability vary from well to well but also within a single well. Stratigraphic columns show the Bluesky Formation fits into 3 depositional environments. Representative gamma log signatures have been identified for each of the depositional environments and are used to identify the sands in well logs. Porosity and permeability data collected using the Accumap database, and from thin sectioned samples have been studied extensively. This has allowed a comparison of the collected data for porosity and permeability with thin sections and the stratigraphic logs. By sampling and photographing sections of high and low porosity/permeability the causes for the variations became more evident. The changes in porosity and permeability are attributed to the depositional environment, sedimentary features, and the diagenetic processes the formation has undergone since it was deposited.

**Keywords:** Bluesky Formation, Whitecourt Alberta, porosity, permeability, diagenesis, stratigraphic column, thin section.

**Permeability, porosity and depositional environment and their effect on reservoir quality in the Cretaceous Bluesky Formation Whitecourt, Alberta.**

**Abstract:**

<b>1.0</b>	<b>Introduction</b> .....	1
1.1	Background.....	1
1.2	Study Area / Problem.....	1
<b>2.0</b>	<b>Regional Geology and Stratigraphy</b> .....	6
2.1	Regional Geology.....	6
2.2	Stratigraphic Context.....	7
2.3	Previous Work on Bluesky Depositional Environment.....	10
2.4	Previous Work on Bluesky Diagenesis.....	12
<b>3.0</b>	<b>Methods</b> .....	14
3.1	Background on well logs.....	14
3.2	Drill Core and Stratigraphic Columns.....	16
3.3	Porosity and Permeability Data (Accumap).....	16
3.4	Statistical manipulation of data.....	20
3.5	Thin Section Analysis.....	22
<b>4.0</b>	<b>Well Logs and Stratigraphic Sections</b> .....	25
4.1	Type Well Logs for the Bluesky Formation.....	25
4.2	Stratigraphic log descriptions.....	29
4.3	Initial interpretation of Depositional Environment.....	64
4.4	Final Interpretation of Depositional Environment.....	68
<b>5.0</b>	<b>Data analysis and manipulation</b> .....	74
5.1	Introduction to the data.....	74
5.2	Histograms of compiled data.....	74
5.3	Cross plots of compiled data.....	79
5.4	Summary of plots and histograms.....	90
<b>6.0</b>	<b>Thin sections and Diagenesis</b> .....	92
6.1	Classification .....	92
6.2	Thin Section Description.....	93
6.3	Diagenesis of the Bluesky Formation.....	104

<b>7.0</b>	<b>Discussion / Conclusions</b> .....	109
7.1	The Bluesky Formation in Whitecourt.....	109
7.2	Reservoir analysis.....	115
7.3	Future Work.....	117
<b>8.0</b>	<b>References</b> .....	119
<b>9.0</b>	<b>Appendix</b> (on enclosed CD).....	122
9.1	Sorted data set used in Chapter 5.0.	
9.2	Full size photo micrographs used in Chapter 6.0.	
9.3	Mineral abundance tables for thin sections.	
9.4	Data set used in Chapter 7.0 and sorted by log signature.	

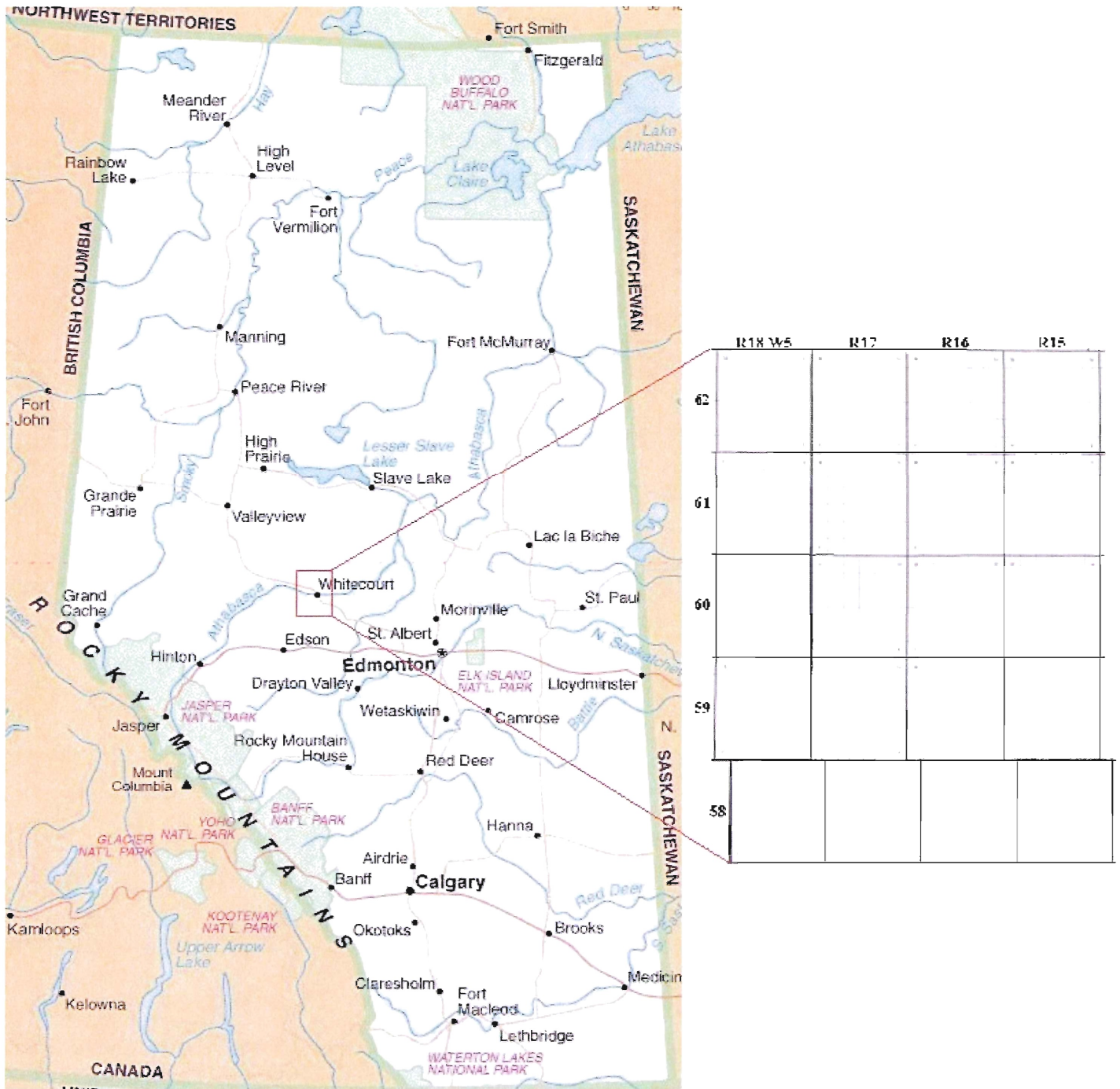
## **1.0 Introduction**

### *1.1 Background*

The Early Cretaceous (Albian ~113 My) Bluesky Formation of Western Canada lies within the Bullhead Group of the Western Canada Sedimentary Basin (WCSB). The Bluesky Formation extends from Fort St. John in eastern British Columbia to the eastern edge of the northwestern plains of Alberta. Unconventional gas reservoirs are common in the WCSB, and the Bluesky is considered unconventional because it is a tight gas reservoir. Permeability (K) is the ability of fluids to pass through a porous material (Selley, 1998). Law and Curtis (2002) defined low-permeability (tight) reservoirs as having average permeabilities less than 0.1 millidarcies. Porosity is expressed as the ratio of voids to solid rock and is commonly shown as a percentage (Selley, 1998). High porosity and high permeability are essential to the successful development of a reservoir. If either of these two properties is unsuitable, a reservoir is not likely to produce hydrocarbons. Linked to these properties is the clay content of the formation. The mineralogy and abundance of clay present can cause problems during drilling or when fracturing the formation. Problems arise due to chemical reactions and clay migration these can plug the hydrocarbon flow pathways.

### *1.2 Study Area / Problem*

The area of study is Whitecourt Alberta, located in the northwestern plains, northwest of Edmonton, in the foothills of the Rocky Mountains (Fig. 1.1).



**Figure 1.1** Study area of the Bluesky Formation near Whitecourt, Alberta. The box to the right is the actual township and range area involved in this study and shows the grid system used in western Canada. The township and range system is used so that the location of wells can be easily determined. The grid system has townships running north-south and ranges running east-west, all of which are based on the position of meridians. A Unique Well Identification number (UWI) is given to every well drilled and contains all of the data pertinent to its location within the grid system. Each Township/ Range is subdivided into 36 sections, and each section divided into 4 smaller divisions. The study area is 4 ranges by 5 townships.

The study area covers townships 62-58 and ranges 15-18, all west of the 5<sup>th</sup> meridian (Fig. 1.1) and one well outside of the area has been included to tie the study to the adjoining sections. This area is a rectangle five townships wide and four ranges high containing more than 1500 wells with penetration of the Bluesky Formation. This study incorporates data from as many of the wells in the study area as possible for the most accurate representation of the Bluesky Formation in Whitecourt.

The main question this study will attempt to answer is if, and why, the Bluesky Formation shows dramatic changes in porosity and permeability across the study area, and if so, is it depositionally or diagenetically controlled? The Bluesky Formation in this study has been separated into two main reservoir intervals and a third non-reservoir interval. These intervals have been identified using well log signatures. The first will be referred to as “Bluesky A”, a coarsening upward sequence that has been initially interpreted as a shoreface deposit. The second is Bluesky B, a thick block-shaped sequence that has been initially interpreted as a barrier-bar deposit. The third signature, Bluesky “C” is a non-reservoir interval and appears blocky but with much higher shale content than Bluesky “B”. Isopachs of the Bluesky “A” and “B” have been generated using Geographix mapping software. The isopach maps were generated from previous work done by the author during summer employment (2005) and include a map (Fig. 2.4a) for each log signature showing the gross sand present in each well. Other maps for each log signature were generated showing the net sand at a porosity cut-off of 6% for each well. A porosity cut-off is used to identify the lowest porosity that can economically produce hydrocarbons. The porosity and permeability for Bluesky B are



relatively uniform throughout the study area, but Bluesky A ranges in porosity from a high of 12% to a low of 0.

If “A” were deposited during an oscillating transgressive/regressive period in the Cretaceous and is regionally extensive, why do the porosity and permeability values vary so much? It could be predicted that “A” would appear to be homogeneous as far as permeability and porosity are concerned. This does not appear to be the case. There must have been a difference in diagenesis or depositional setting to cause the change. Bluesky “B” appears to be more homogeneous with respect to porosity and permeability, which may suggest that the changes in “A” are more depositionally related and that both log signatures have undergone the same diagenesis. It seems that the changes in “A” are a combination of both depositional setting and diagenesis.

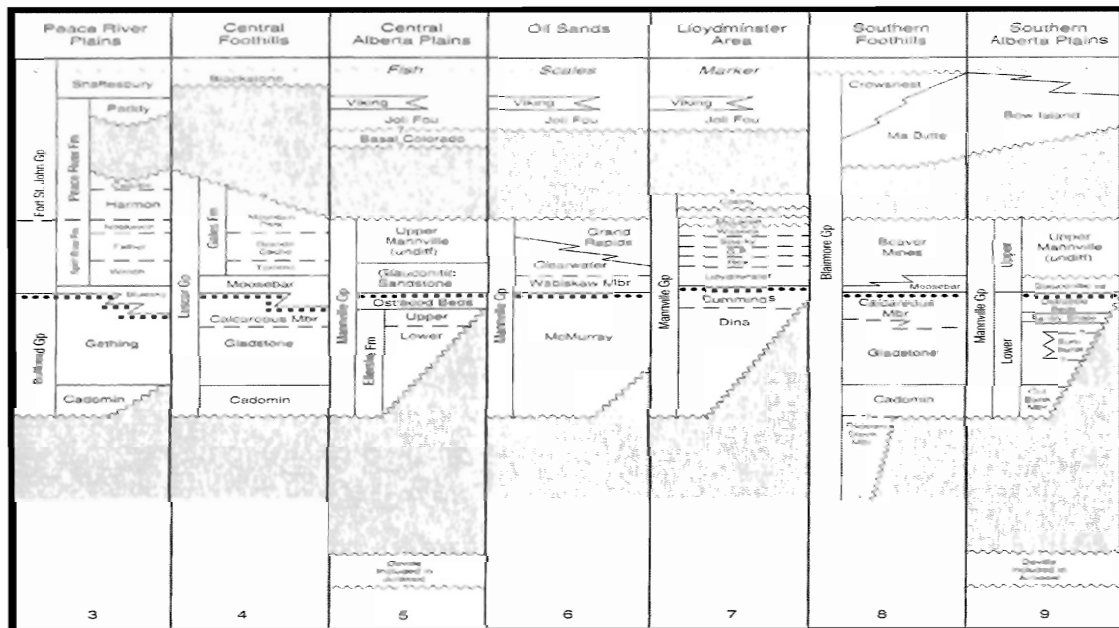
Other questions concern the location of high porosity and permeability zones with respect to potential drilling sites and what affect the presence of clays and cement in the form of kaolinite, glauconite, siderite (Fe-calcite) and ankerite (Fe-dolomite) have on the overall reservoir quality. The presence of fractures in the drill cores suggest that some parts of the Bluesky Formation will likely have much higher permeability than those areas not fractured. The author will attempt to test the relationship between the direction of the fractures and the direction of highest permeability values. Is there a relationship between high permeability and high porosity values, and can high porosity and permeability zones be mapped? Does the depositional environment have the only role in controlling the porosity and permeability values, or has burial and diagenesis played the most important role in modifying the reservoirs we see today? Has “A” been more

affected by diagenesis than “B”? Is one reservoir interval more often fractured than the other?

## 2.0 Regional Geology and Stratigraphy

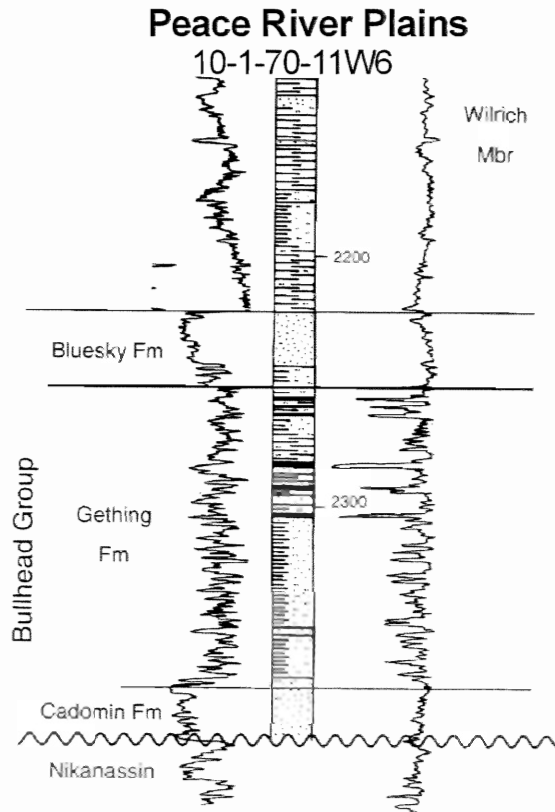
### 2.1 Regional Geology

The Mannville Group and equivalent strata comprise the oldest Cretaceous rocks over most of the WCSB and represent a major episode of subsidence and sedimentation following a long period of uplift (Hayes *et al.* 1994). They also represent the second major Cordilleran-derived clastic wedge of the foreland basin. The Bluesky Formation lies stratigraphically within the Bullhead Group representing the maximum transgression and subsequent early regressive stages of the boreal Moosebar/Clearwater Sea in the southern/central parts of the basin (Hayes *et al.* 1994). The Bluesky in Whitecourt is bounded conformably below by the Gething Formation, a terrestrial fluvial system, comprised mainly of sandstones, with local shale and coal. The Bluesky is bounded conformably above by the Wilrich Member of the Spirit River Formation, a dominantly open marine unit comprised mainly of shale.



**Figure 2.1.** Stratigraphic setting of the Bluesky Formation (column 3) and age-equivalent to the Bluesky Formation for Alberta. It also shows age equivalent units to the Bullhead group for Alberta. The Peace River Plains column best represents the stratigraphy in the study area. (Hayes *et al.* 1994).

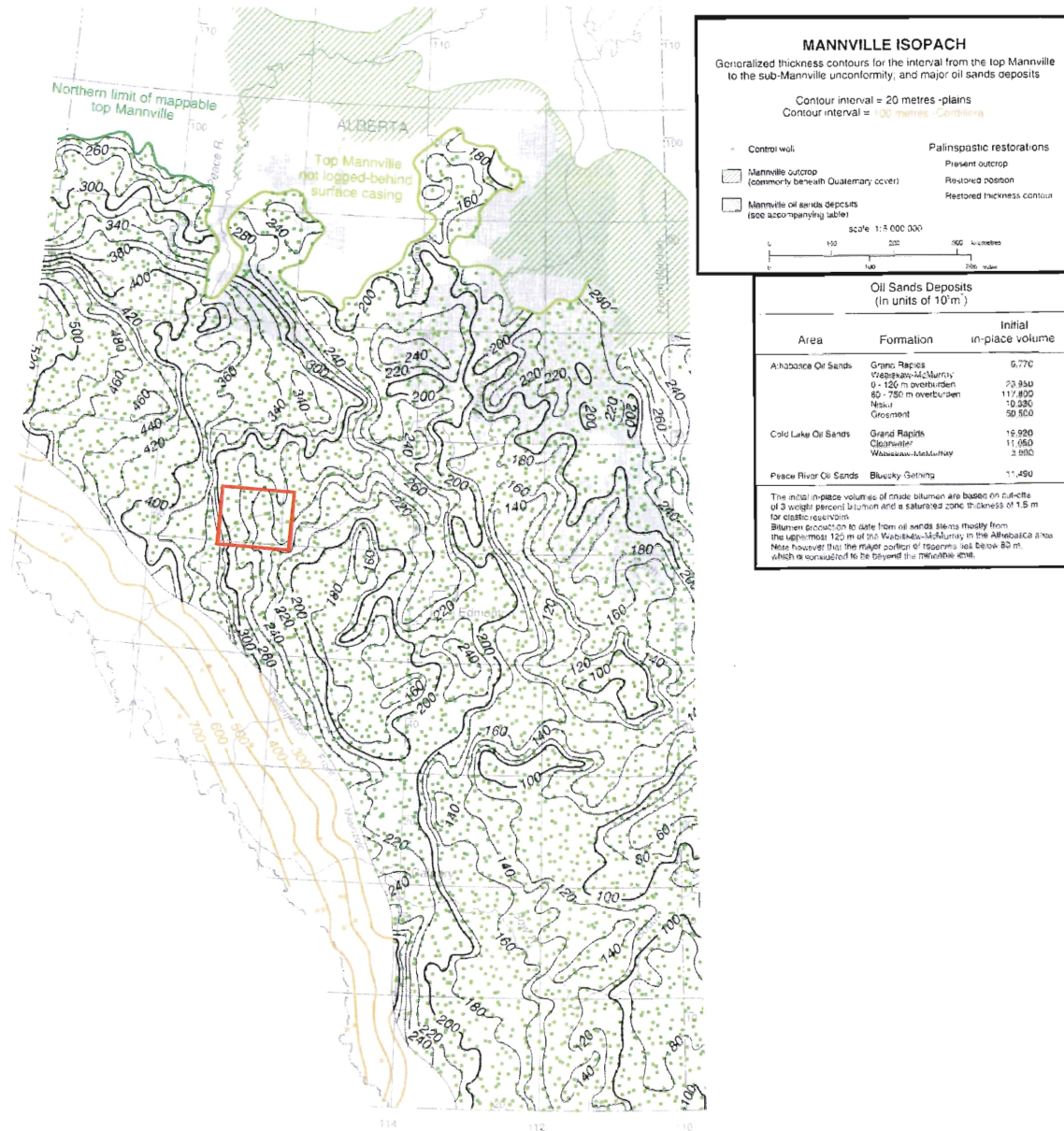
A type gamma log for the Bluesky in the Peace River Plains is very similar to the log appearance found in the Whitecourt study area. The log appearance changes in different areas of Alberta due to different conditions during deposition.



**Figure 2.2.** Gamma log on the Left and the sonic log on the right for well 10-1-70-11W6 in the Peace River Plains, to the NW of the study area. The log shape is very similar to those in the study area and shows the upper contact with the Wilrich Member and the lower contact with the Gething Formation. (Hayes *et al.* 1994).

## 2.2 Stratigraphic Context

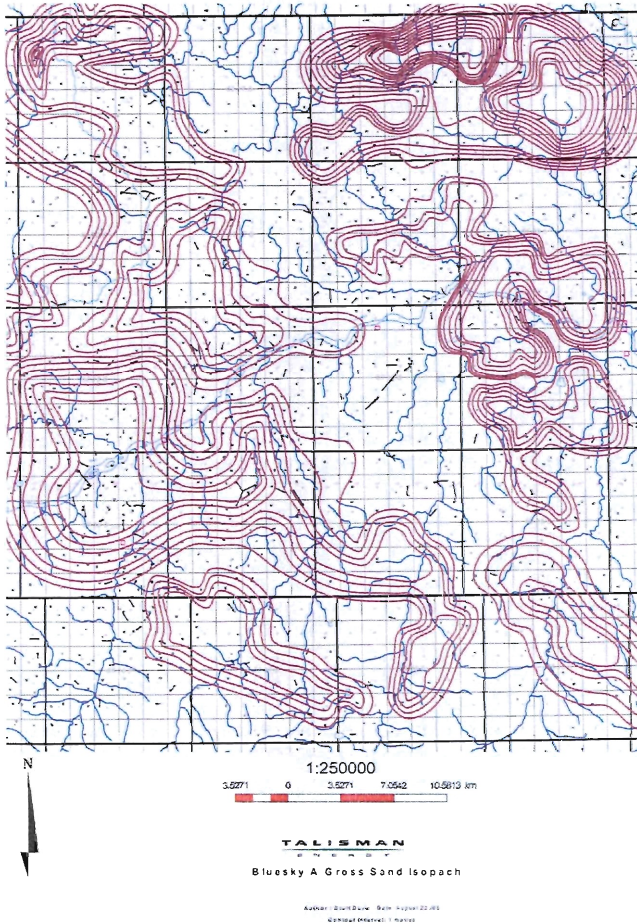
The Bluesky ranges in thickness from nearly pinching out in Eastern Alberta to 46 m in eastern British Columbia. Figure 2.3 shows an isopach map of the complete Mannville Group, which contains the Bluesky Formation. This map shows the gross thickness of the Mannville Group in Alberta. The Bluesky Formation comprises approximately 5 to 25 metres of the gross thickness of the Mannville Group in the study area.



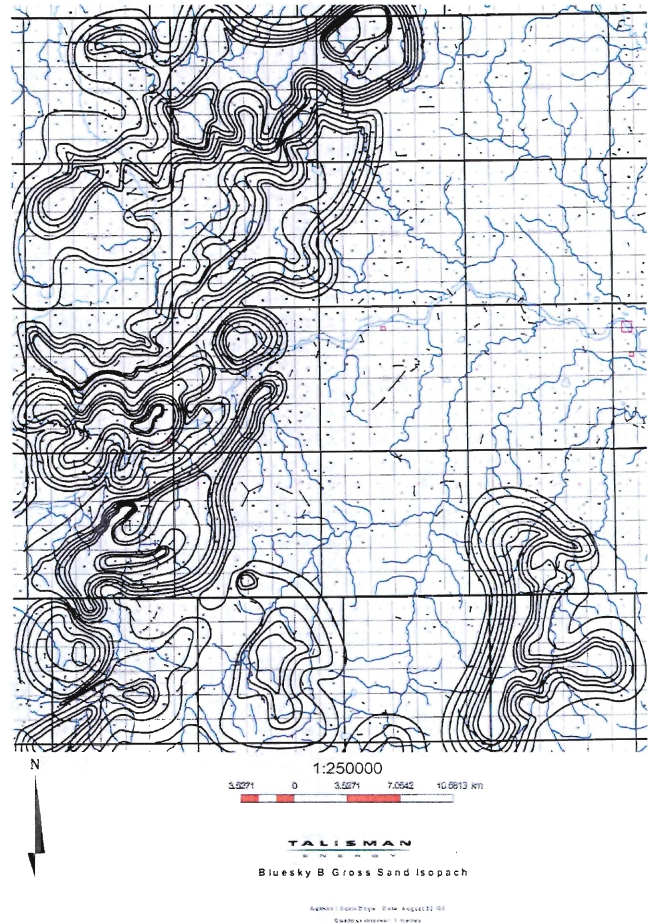
**Figure 2.3.** Isopach map for the Mannville Group, the age-equivalent to the Bullhead Group. The Bluesky Formation is stratigraphically located in the Lower Mannville Group / Bullhead Group. The study area is outlined in red. The map shows only the thickness of the Mannville for the province of Alberta and includes the study area. (Hayes *et al.* 1994).

It was not possible prior to this project to find an isopach map isolating just the Bluesky Formation possibly because it is a thin unconventional gas play. The author has mapped the Bluesky for the study area, breaking the formation into two log signatures

“A” and “B” for the isopach map, and a third, “C” for the depositional setting and the drill core analysis.



**Figure 2.4a.** This shows the gross sand thickness for the Bluesky in the Whitecourt study area for the log signature A. The contour interval is 1 m. (Doyle, 2005)



**Figure 2.4b.** This shows the gross sand thickness for the Bluesky in the Whitecourt study area for the log signature B. The contour interval is 1 m. (Doyle, 2005.)

The formation ranges from ~5 m to 25 m in the Whitecourt study area as determined by well log data. The formation is divided into two dominant lithologies for the purpose of this study: shale and sandstone. The shales are of great importance in interpreting drill core and determining a depositional environment. However, many of the cored wells do not have the basal contact with the Gething Formation, making location of the base of the formation for well log correlation difficult.

The Bluesky sandstones range from brown to brownish grey and are fine to medium grained, commonly containing glauconite. Chert granules are common and tend to give some cores a salt-and-pepper appearance. The wells examined for this study have a wide range of porosity and permeability values. Siderite is present in the sandstones and may or may not be problematic in terms of preferentially decreasing porosity and permeability locally. The sandstones show sedimentary features such as trough cross-bedding and planar parallel bedding but may also appear massive. Dewatering features such as flame structures are present but rare. Thin mud laminae are common in all the wells examined. The sandstones are home to an array of fossil traces, the types and abundances of which appear to be related to the log signature (“A”, “B”, or “C”), associated with the well.

The shales are of marine origin and contain grains of pyrite believed to have been formed in situ and these may be associated with the presence of organic debris in the form of coalified plant fragments.

### *2.3 Previous Work on Bluesky Depositional Environment*

There has been little investigation done on the Bluesky Formation in Whitecourt, Alberta to investigate the changes in porosity and permeability throughout the area. However, there have been porosity and permeability studies done on the Bluesky in other areas of Alberta and Eastern British Columbia. By piecing together several previous studies, it is possible to combine studies of permeability, porosity and depositional environments. In South Central Alberta, the Bluesky is one of the main reservoirs producing in the Hoadley gas field.

Chiang (1985) described the presence of barrier bars in the Hoadley field with thicknesses of 14-18 m and composed of medium-to fine-grained sandstone with porosity ranging from 8-16% and about 10 millidarcies permeability. These data refer to what Chiang called the “A” sand which is the uppermost sand in the Hoadley field.

Chiang did not discuss anything about the clay content other than mentioning the presence of glauconite. Also, he didn't discuss its effect on the performance of the reservoir as this is typically left to the production engineers to evaluate. From the production data given, it seems unlikely that clay is causing any problem with respect to production in the field. The discovery well drilled in 1977 flowed at 26mmcf/d after fracturing. The depositional model presented by Chiang is partially consistent with the general findings of the early stages of this study and with the formation of a barrier-bar system in or near the mouth of an estuary close to the shoreline.

Terzouli and Walker (1997) produced a study of the Bluesky in Edson, Alberta, just to the southwest of Whitecourt and described barrier-bar systems trending SW-NE. Their study used trace-fossil data to help determine a depositional model that shows a barrier bar as well as estuarine valley fill. The valley fills are channelized sand bodies and show limited trace-fossil assemblages due to the stressed environment. Their study was focused mainly on the depositional setting of the Bluesky in Edson and mentions nothing of porosity or permeability. It only briefly mentions the presence of clay in the form of slackwater mud drapes.

Lukie (2004), in an internal Talisman Energy Inc. study of the Bluesky Formation in Edson, suggested that during their study of the Bluesky, Terzouli and Walker (1997) missed some trace fossil data. Lukie (2004) suggested that their interpretation means that



the paleo-shoreline may have been trending to either the northeast or the southwest of the area.

A high concentration of glauconite is common in areas of the Bluesky Formation. Chafetz and Reid (2000) compare the strata found in the southwestern US considered to have formed under very shallow water tidal flat conditions to the numerous studies showing that glauconite generally forms only in mid-shelf to upper slope environments. The glauconite appears to be autochthonous in the high energy environment. This could have some effect with regard to the depositional environment of the Bluesky Formation, and whether the glauconite precipitated in situ or was transported there and deposited as detrital grains.

#### *2.4 Previous Work on Bluesky Diagenesis*

Lukie (2004) described good producing and poorly producing wells in Edson in a two-part study. The study relates production to diagenetic effects and the depositional environment. Porosity changes in wells in close proximity to each other show that the favoured reservoir in the Bluesky comprises a lithofacies of medium grained, trough crossbedded sandstones, having minor to no burrowing present. The unfavoured facies is the fine grained, mud laminated, and highly bioturbated sandstones.

Part 1 of the study (Lukie, 2004) suggests that changes in the size of the quartz grains in the reservoir allow for more growth of quartz crystals during diagenesis, therefore reducing porosity by increasing quartz cementation. Part 2 of the study suggests that in the good producing wells, the leaching of chert grains created intragranular porosity while the dissolution of cement created greater intergranular porosity, increasing the porosity of the reservoir. Poor producing reservoirs contain only

secondary grain moldic porosity, and are therefore defined as a poor reservoir based on petrophysical analysis.

### **3.0 Methods**

#### *3.1 Background on well logs*

This section will give a brief outline of the well logs that were used and what they indicate. The gamma ray log is mainly used to determine lithology and measures the amount of natural radiation in the form of gamma rays that the different rock layers emit. The common radioactive elements are K, U, and Th. These elements, particularly K, are common in clay minerals which comprise shale and are absent for the most part in sandstones, unless the sandstone is arkosic and high in potassium feldspar (Cant, 1992). The log generally responds by moving to the right of centre to indicate shale and to left to indicate sandstone but there are exceptions to this rule. The Bluesky follows the sand / shale pattern of sand to the left and shale to the right throughout the study area.

Three main logs are used to determine values for porosity. The density porosity log tool emits gamma radiation and measures the amount of radiation scattered back in an amount proportional to the electron density of the rock. In most cases, the electron density is related to solid material and the amount and density of the pore fluids. Density porosity is calculated by assuming a density of the solid material (i.e., sandstone 2650 kg/m<sup>3</sup>) and fluid (i.e., salt water 1146 kg/m<sup>3</sup>) (Cant, 1992).

The neutron log measures hydrogen concentrations in the rock. The tool emits neutrons of a known energy level then measures the energy of the neutrons reflected from the rock. Neutron porosities are calculated by assuming that all the pore space is filled with fluid. Since the tool is calibrated using a fluid, the presence of gas shows up as an anomalously low value (Cant, 1992).

The sonic log uses the seismic velocity of a pulse of energy, usually a sound wave, to measure the amount of open pore space in a rock. The velocity depends on lithology, permeability, and the type of pore fluid present. A drop in velocity in sandstone generally means that there is open space in the rock filled with some type of fluid or gas. It is the fluid or gas, with lower density than the rock that slows the seismic waves and gives a measure of porosity. This log is also useful in tying seismic data to well log data but was not used for that purpose in this study.

The two logs used to determine the relative permeability of the rocks in the formation were the caliper log and the SP log. The caliper log measures the diameter of the borehole using two spring-loaded arms on either side of the logging tool. It measures permeable areas as a decrease in the diameter of the hole due to the invasion of drilling fluid into the rock and a build up of mud-cake. The SP log measures the electric potential between an electrode pulled up the well and a reference electrode at the surface (Cant, 1992). Since the formation water in the uninvaded sands has a much higher concentration of salts than the water normally used to make up the drilling fluid, ions tend to flow between them to equalize the concentrations. The tool measures this difference and gives a relative permeability compared to the other rocks in the well (Mussett & Khan, 2000).

The resistivity logs (micro, shallow, and deep) are used to determine the fraction of pore space occupied by water. This can be used in the Archie's Law equation to determine the fraction of pore space occupied by hydrocarbons. Its main purpose, as identified in previous work in Whitecourt, was to help identify possible hydrocarbons based on their high resistivity (Mussett & Khan, 2000).

The best results were obtained when it was possible to use all the logs together for each well. The integration of all the log data made interpretation of the logs much easier and more accurate.

### *3.2 Drill Core and Stratigraphic Columns*

While logging drill core at the EUB core facility in Calgary, Alberta, with the aid of Terry Lukie, many detailed photographs were taken and core description sheets constructed. The cores used in conjunction with the well logs provide a more detailed analysis of what the well logs indicate. Through two visits to the core lab, the author was able to describe cores from wells that show all signatures (“A”, “B”, and “C”) and wells that show “A” with “C”, and “A” with “B”.

The rough drafts of the core sheets done during the summer work have been examined and modified so that they could be input into a program called StratDraw. This program was used to electronically draw the individual layers in the sections. The columns were exported into Corel Draw and onto a template showing grain size, location, and many other features of the core. The sections have been labeled with the appropriate stratigraphic symbols and depth indicators to show what was observed in the actual core sections. The notes taken while the cores were logged have been added to aid in the interpretation of the cored section.

### *3.3 Porosity and Permeability Data (Accumap)*

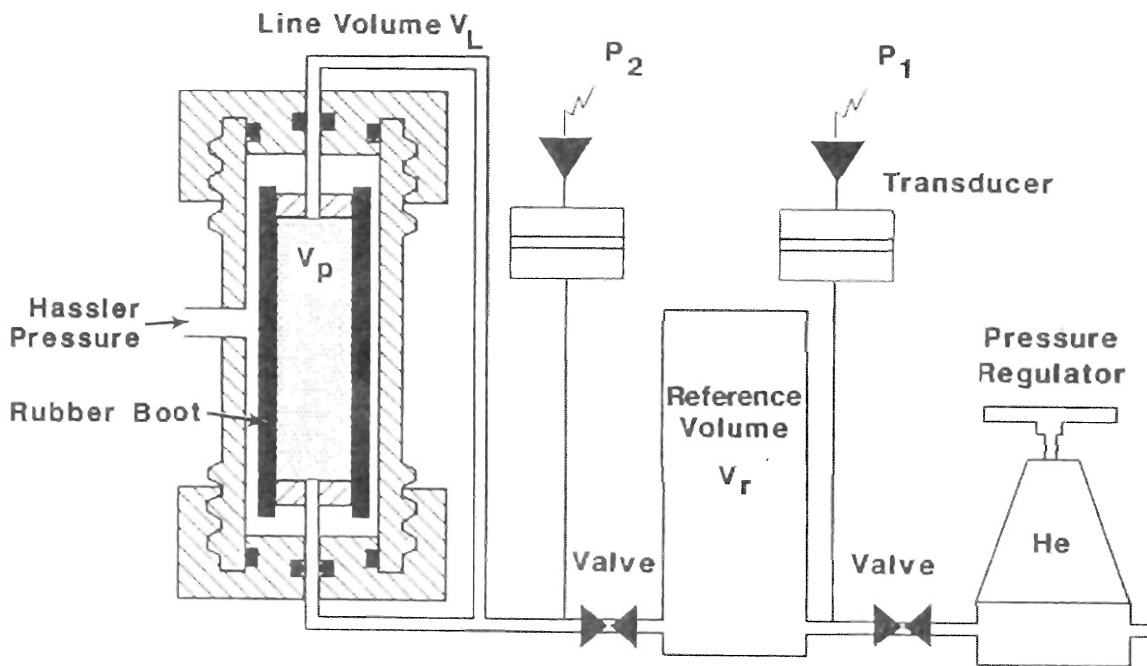
To analyze the large amount of data required to compare the porosity and permeability of different wells in the study area, an industry software program called Accumap from IHS Energy was used. Core analysis is available for the majority of the wells in the study area that have been cored through the Bluesky interval. Each suite of

analyses includes numerous porosity and permeability (K Max, K90, and K Vertical) measurements from different positions moving down the length of the core. The data have been put into an Excel spreadsheet for easier manipulation.

After a well has been cored, it is the responsibility of the laboratory running the tests to provide the EUB of Alberta with the porosity and permeability measurements taken from the core. These data become available to the general public after the well is removed from confidential status. The EUB receives all the cores drilled in the province of Alberta at the core facility in Calgary where the core is stored and can be viewed by the public for a fee. The testing that is done is determined by the company cutting the core. Generally the cores have reservoir intervals tested using the full diameter core and all other intervals tested by taking small round plugs. The full diameter core and the plugs are used to determine the porosity and permeability of the cored formation at a given depth.

To obtain the data for porosity, the samples are first cleaned and dried to remove any materials remaining from the drilling and coring process. Then Boyle's Law is used along with helium gas to determine the porosity of the sample. The formula for Boyle's Law is used in the form of:  $P_1 V_1 / T_1 = P_2 V_2 / T_2$ . Since the data collection process takes only a few minutes, the value for T does not change so the formula may be expressed in the more simple form of  $P_1 V_1 = P_2 V_2$ . A known volume of helium ( $V_1$ ) at a known pressure ( $P_1$ ) is expanded into the core sample in a matrix cup and the resulting pressure ( $P_2$ ) is read from this ( $V_2$ ) may be solved by using the simplified equation for Boyle's Law. This ( $V_2$ ) value gives the grain volume. The bulk volume is then calculated by measuring the length and diameter of the sample. The bulk volume minus the grain

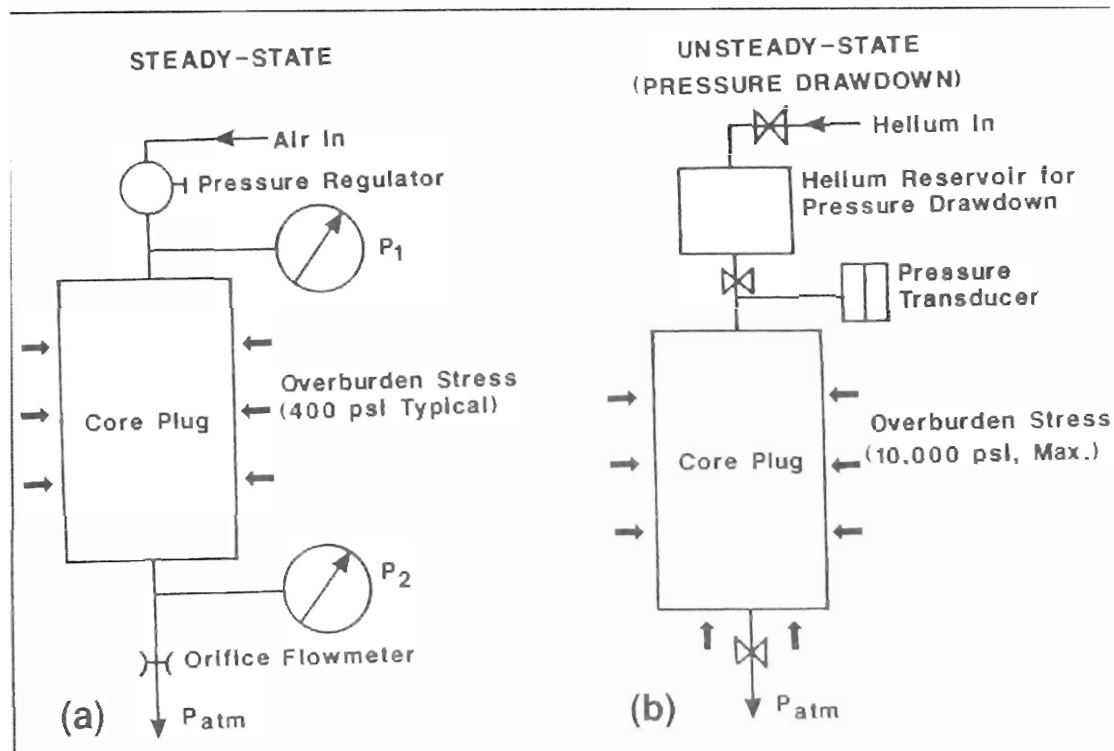
volume leaves the pore volumes. Finally the pore volume divided by the bulk volume leaves porosity of the sample. The porosities of all samples are measured under no confining stresses (D. Agar, personal communication, 2006). Figure 3.1 shows the apparatus used for calculating the porosity from a core sample.



**Figure 3.1.** The type of apparatus used to get the measurements of porosity from the cores used in this study. (Modified from Cone and Kersey, 1993)

The laboratory techniques that collect permeability data use a steady-state apparatus and the drop in pressure across the sample is kept constant so that the flow rate can be measured. The formula used to determine permeability is an integrated form of Darcy's Law:  $K_a = 2000 p_a \mu q_a L / (p_1^2 - p_2^2) A$ . The variables are the following:  $K_a$  = air permeability,  $p_a$  = atmospheric pressure (atm),  $p_1$  = upstream pressure (atm),  $p_2$  = outlet pressure (atm),  $L$  = length (cm),  $\mu$  = air viscosity (cP),  $q_a$  = gas flow rate at atmospheric pressure ( $\text{cm}^3 / \text{sec}$ ), and  $A$  = cross sectional area ( $\text{cm}^2$ ). The value for permeability is

then determined from the slope of the plot of  $V_a$  ( $V_a = q_a / A$  in cm/sec) versus  $(p_1^2 - p_2^2) / L$  which results in a straight line passing through the origin as long as the conditions for Darcy's Law are maintained (Ohen and Kersey, 1993) Figure 3.2 shows the apparatus used for calculating the permeability from a cored sample.

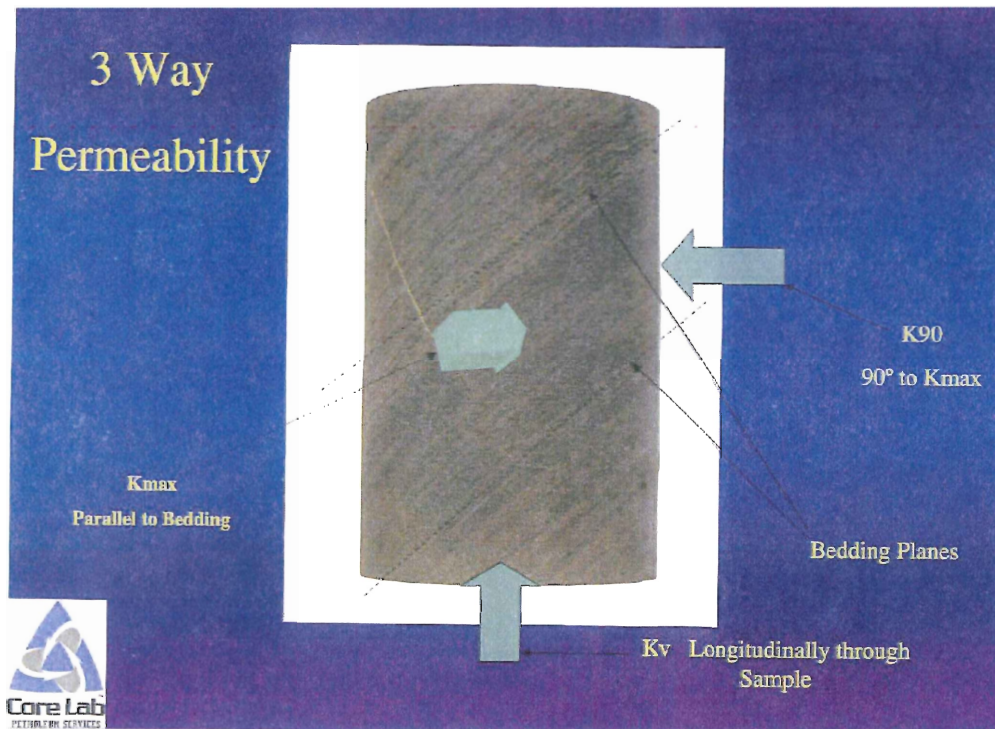


**Figure 3.2.** This figure shows a type of steady state apparatus that is used to measure the flow of a gas through the sample and from that calculate the permeability of the sample. (Modified from Ohen and Kersey, 1993).

The three types of permeability measurements taken are  $K_{max}$ ,  $K_{vertical}$ , and  $K_{90}$ .  $K_{max}$  is the permeability measurement taken along the bedding plane in both full diameter cores and in the small plug cores. The same technique for obtaining the data is used for both. The exception is that only one permeability measurement is taken for the small plug cores and it is  $K_{max}$ . The  $K_{vertical}$  measurement is taken longitudinally through the full diameter core and is not taken at all in the small plug cores. The  $K_{90}$  measurement is taken at 90 degrees to  $K_{max}$  for full diameter cores and not taken at all



for the small plug cores. Some sandblasting of the cores is necessary before horizontal permeability measurements can be taken in order to remove drilling mud from obstructing the permeability measurements. In very permeable samples, mud can invade the sample beyond the point of removal. In these samples, the horizontal permeability may show up as lower than the vertical permeability unless the core is fractured vertically (D. Agar, personal communication, 2005). Figure 3.3 shows the core and the orientation of the permeability measurements with respect to the core.



**Figure 3.3.** Orientation of the three types of permeability measurements used when acquiring the data used in this study.  $K_{max}$  is along the bedding planes oriented into the diagram,  $K_{90}$  is measured 90 degrees to  $K_{max}$ , and  $K_{vert}$  is measured longitudinally. (D. Agar, personal communication, 2006).

### 3.4 Statistical manipulation of data

The data obtained from Accumap were manipulated using several statistical methods to make the data easier to use. The first step was to eliminate any values equal to zero for porosity and permeability ( $K_{max}$ ,  $K_{90}$ , and  $K_{vert}$ ). These values represent

sections of the core that were not sampled and show up in the database as zeros. The reason for many of the Kvert and K90 values being zero is due to the sampling method used for the core as mentioned in section 3.3. The data were then entered into a spreadsheet format for ease in graphing the data and further manipulation. The next step was to calculate the basic statistics for the raw data set using a statistical program called Minitab 14. The statistics calculated were: mean, standard deviation, the minimum and maximum values, the upper (Q3) and lower (Q1) quartiles, the inner quartile range (IQR), and the location of any data values considered as outliers. Any points that are outliers on the high end are considered to represent fractured core. This method of determining fractured data has been chosen because it is more appropriate than using the often inaccurate observations of the geoscientist measuring the core in the field. Some cores appear as fractured but recorded low permeabilities, whereas some appear as unfractured but recorded extremely high permeabilities. Using the outlying method seems to eliminate most of the values that skew the fractured and unfractured data. Fractured data were considered to be anything above  $Q3 + 1.5 \times IQR$ . The low outlier cut-off values were always negative and therefore not applicable. The next step was to isolate fractured data from the unfractured data. All of the data greater than the outlier cut-off values are considered fractured and all those equal to or less than the outlier cut-off value were considered unfractured. The same statistical values mentioned above were calculated for the fractured and unfractured data sets.

From the data sets, multiple plots were generated to evaluate factors that might have contributed to fracturing, high or low permeability, and high or low porosity. Histograms were generated to see how the data are distributed for the different data sets.

For the scatter plots created in Microsoft Excel, the correlation coefficient ( $r$ ) was calculated. A table of correlation coefficients is presented in chapter 5.0. To plot the histograms, the Minitab 14 program was used. To create the histograms, the log format of the permeability data had to be used. For this, Minitab was used to take the natural log to the base of 10 of the permeability ( $K_{max}$ ,  $K_{90}$ ,  $K_{vert}$ ) values, converting them into values that could be plotted on a linear scale. The log values were then changed back to values in millidarcies for presentation purposes.

### 3.5 *Thin Section Analysis*

Using the thin section data as well as the core spreadsheet data, a comparison was made to see how cementation, grain size, and other factors affect the reservoir quality of the sand. The results from this were then used to identify high and low porosity/permeability log signatures in the study area. The thin section analyses were used not only to verify the porosity and permeability data with the core analyses but also to give grain size, degree and type of cementation, and mineralogy of both the grains and matrix. The data collected from the thin sections are crucial in integrating the various datasets and showing where the porosity and permeability is best or worst and why.

From all wells in the study area, those containing the most data for the most important categories (Table 3.1) were logged and the applicable data retrieved from the Accumap database.

Unique Well Indicator	Thin Sections	Stratigraphic Columns	Porosity / Permeability Data	Production Data
00/01-29-061-17W5/0	2	Yes	no	yes
00/03-31-060-18W5/0	1	Yes	yes	yes
00/06-25-061-18W5/0	2	Yes	yes	yes
00/07-31-058-19W5/0	3	Yes	yes	no
00/09-08-058-18W5/0	1	Yes	yes	yes
00/12-24-058-18W5/0	2	Yes	yes	yes

**Table 3.1.** Data that are available for each of the key wells as well as the work the author has prepared for this study. These wells are the best compilation possible with the existing restraints of core availability and data availability for the cored wells.

The preparation of the thin sections from samples taken at the Energy and Utilities Board of Alberta core facility was performed by Core Lab Petroleum Services. The preparation of the thin sections included the application of different types of stains to bring out the mineralogy based on reaction with the stains (Table 3.2).

Name of Stain Applied	Mineral Associated	Colour of Stained mineral
Alizarin Red S	Calcite	pink / red
Potassium Ferro-cyanide	Fe- dolomite Fe- calcite	blue / turquoise mauve / purple
Sodium cobaltnitrite	K-feldspar	yellow

**Table 3.2.** Different types of stains used on the thin sections in this study and the effect of the stain on minerals that are often difficult to identify using only petrographic methods. The Potassium Ferro-cyanide will only stain Fe-calcite mauve/purple if the section has also been treated with Alizarin Red S.

The microscope used to view the thin sections was a Leitz Labourlux 12 POL binocular petrographic microscope. The first step was to visually inspect the slides to identify the mineralogical content and percentages, followed by the textures and shape of the minerals, as well as any alteration or possible diagenetic effects such as dissolution or cementation. From the visual inspection, a rough estimate of the content of each slide and a simple look at the diagenetic history of each section was attained. These visual

inspections were used to investigate the provenance of the Bluesky as well as classify the type of sandstone present in the thin sections using the QFL classification scheme.

## **4.0 Well Logs and Stratigraphic Sections**

### *4.1 Type Well Logs for the Bluesky Formation*

The Bluesky in Whitecourt does not represent a homogeneous depositional environment and therefore contains several different characteristic well log signatures. These signatures are determined mainly by the response of the gamma ray log. The characteristic shape of the log responses have been broken into three main depositional facies or well log signatures; (petrophysical facies) “A”, “B”, and “C”. Each of the signatures was confirmed by examining drill core at the EUB core facility in Calgary, Alberta during the summer of 2005. Each signature for “A” and B” represents exclusively the deposition of sand and does not take into account the shale deposited above. Signature “C” deals with units having high sand to shale ratios. Since this study deals largely with examining the porosity and permeability of a reservoir, shale is only discussed in the depositional environment portion of the study and in the drill core descriptions.

Bluesky log signature “A” (Fig. 4.0 a.) is interpreted as regionally extensive shoreface sand that ranges in thickness from 1 – 5 m depending on the location of the well in the study area. The gamma log shape is that of a coarsening up sequence with fine materials at the base and coarser at the top and then the log fines again as the transgressive shale of the Wilrich Member begins. It is common to find moderate to heavy bioturbation in these sands with several different traces visible. This signature is generally found at the top of the Bluesky Formation and the base of the Wilrich Member. The “A” signature represents the uppermost deposited sand and may overlie “B” or “C”.

If two different sands are being deposited on top of each other, the log will not identify the change from one type of sand to another.

Bluesky log signature “B” (Fig. 4.0 b.) is preliminarily interpreted as a type of barrier or channel fill near the coastal plain. This signature is confined mainly to the western portion of the study area with some small outcrops in the S, SE, and NE. The thickness of the sand ranges from 5 – 21 m depending on the location within the study area. The well log appearance of “B” is thick and blocky, with a low percentage of clay. This depositional facies has much less bioturbation than “A” and has a very limited number of traces. This signature was originally believed to be isolated from the “A” facies but upon closer examination of the cores and well logs, the “A” signature may overlie the “B” throughout the study area but is difficult to distinguish using well logs alone. Bluesky “B” is the main target for drilling at the present time because it is the thickest reservoir.

Bluesky log signature “C” (Fig. 4.0 c.) is interpreted as an estuarine deposit through the examination of drill core. This facies was identified solely by examination of drill core because well logs do not have the vertical resolution to identify mud beds thinner than approximately 1 metre. This facies consists of thin sand lenses capped by thin mud-drapes, deposited during slackwater in a tidally influenced environment. Only one well containing this facies has been identified and because of the high percentage of mud, it may not be of reservoir quality and has only been briefly examined here for porosity and permeability. It will be mentioned again during discussion of the depositional environment.

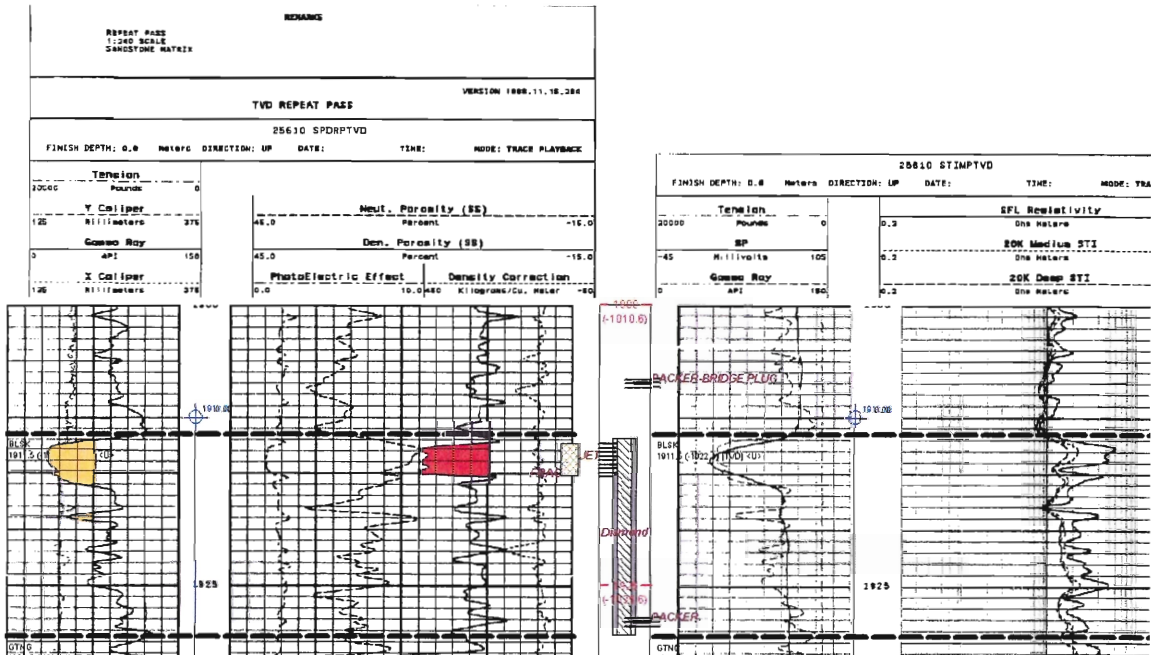


Figure 4.0 a. Type log for Bluesky log signature "A". The first track moving left to right is the gamma ray log which indicates lithology, on the same track as the gamma log is the caliper log showing hole diameter. The next track is the sonic log indicating porosity. The centre column shows what has been done to this well. The long rectangle with diagonal lines is the symbol for a cored interval. The stacked horizontal lines indicate the well casing has been perforated at the depth of the symbol. The first track to the right of the centre contains a second gamma ray log and the spontaneous potential (SP) log. The track on the far right shows the resistivity logs (micro, shallow, and deep induction). The top of each track shows the scales for each type of log. The dashed horizontal lines running left to right across the logs represent the top and bottom of the Bluesky Formation. (Logs modified from Accumap).



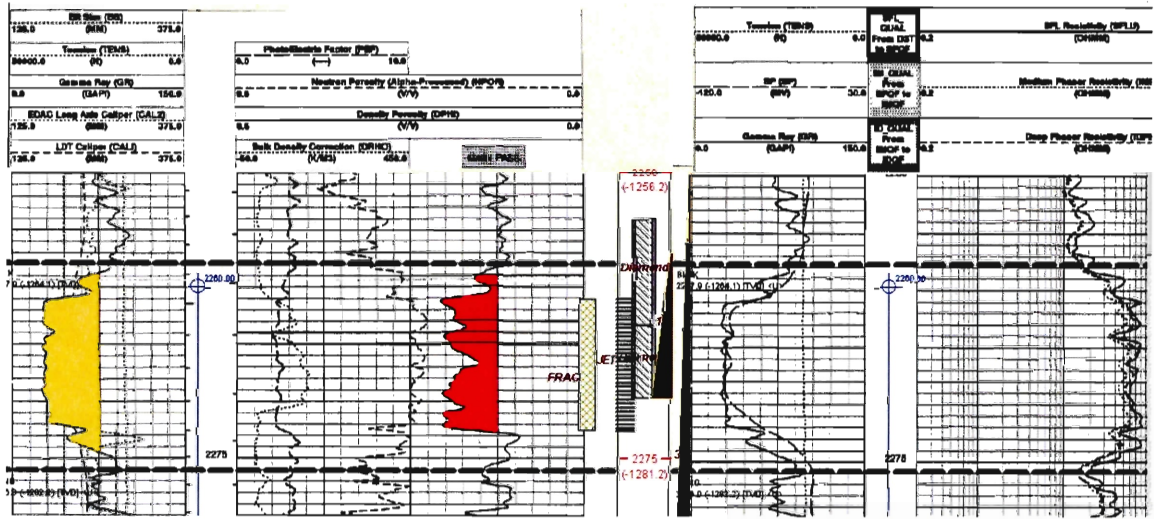


Figure 4.0 b. Type log for Bluesky log signature "B". For a description of the suite of logs refer to diagram 3.1 with the exception of the second track on the left side of the diagram. This track contains from left to right, a bulk density correction, a photo electric factor curve, a neutron porosity curve, and a density porosity curve. The inverted triangle in the centre track indicates a drill stem test (DST) has been performed on the formation. (Logs modified from Accumap).

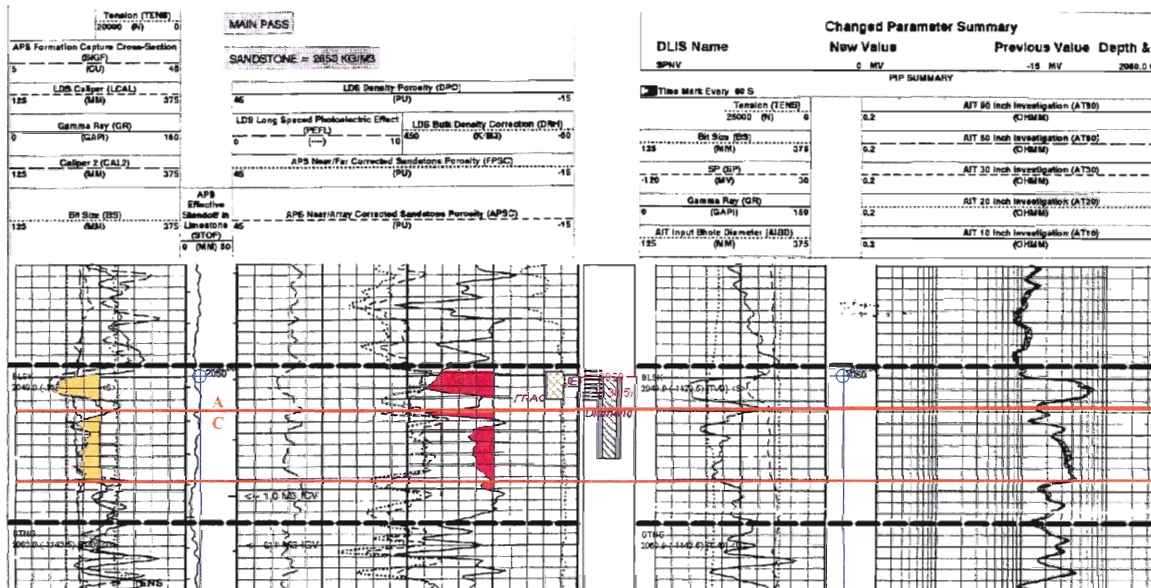


Figure 4.0 c. Type log for Bluesky log signature “C” with the top section of the core being log signature “A”. The red horizontal lines show the break between the different log signatures. For a description of the logs used refer to figure 3.1. (Logs modified from Accumap).

#### 4.2 Stratigraphic log descriptions

##### 00/06-25-061-18W5: (Fig. 4.1)

This top of the stratigraphic log shows log signature “A” covering ~ 3.25m and containing both *Macaronichus* and *Paleophycus* trace fossils indicative of a possible *Glossifungites* ichnofacies. The sedimentary structures present are rare mud laminations and planar bedding. In this upper section of the core, two thin section samples were taken and prepared for analysis. The “A” portion of the core shows cryptic bioturbation (Fig. 4.1.2).

The contact between the upper “A” signature and the lower “C” signature is marked by an abundance of carbonaceous laminae as well as some coalified wood fragments and possible siderite layers indicating waters low in sulphate and oxygen-poor conditions. The “C” signature comprises the remaining ~15.75m of the core and shows

reaction to HCl that appears to increase with depth from low to moderate. The thicker sand layers have been highly bioturbated and contain traces of *Paleophycus*, *Thalassinoides*, *Chondrites*, *Planolites*, and *Teichichnus*, indicating a *Cruziana* ichnofacies. *Teichichnus* seems to be more common throughout the middle portion of the “C” section of the core and *Planolites* appears to be decreasing with depth. There are very few identifiable sedimentary features in the “C” signature because the heavy bioturbation has destroyed the original structures. The only features discernible are dewatering features in the form of flame structures and contorted laminae.

Pyrite appears at approximately 2016 m and indicates higher concentrations of sulphate in the water which imply anoxic conditions. Mud layers beneath the pyrite contain bivalve fragments both scattered and layered, ranging in size with a maximum of 2 cm from the dorsal to ventral side. The lower portion of the core contains abundant pyrite and is heavily bioturbated by the *Cruziana* ichnofacies. The bottom of the core contains rare traces of siderite and very fissile layers of shaley material.

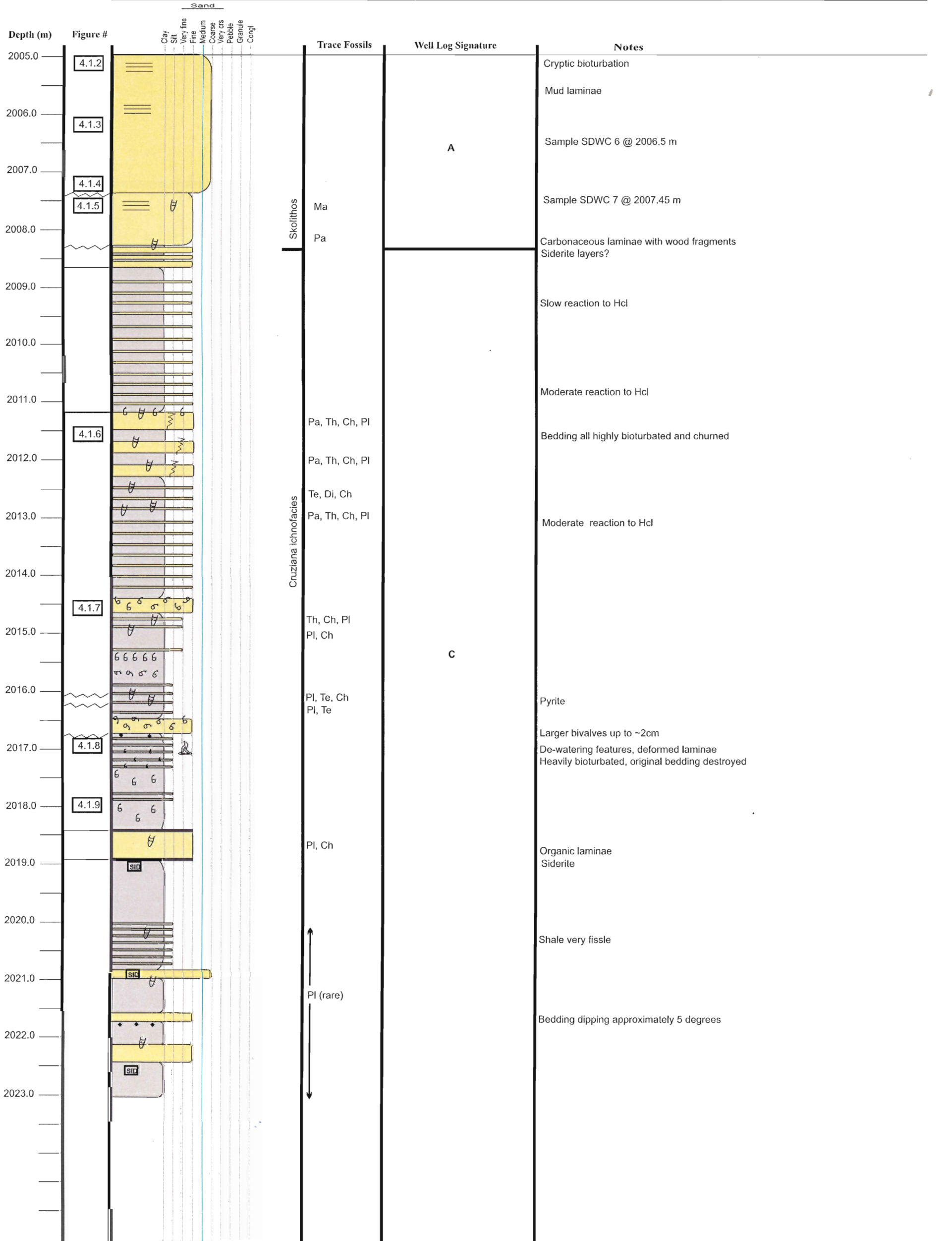








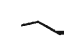

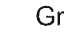


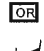




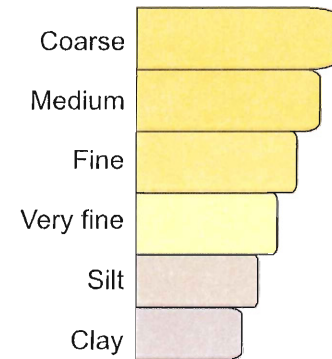
Figure 4.1 A

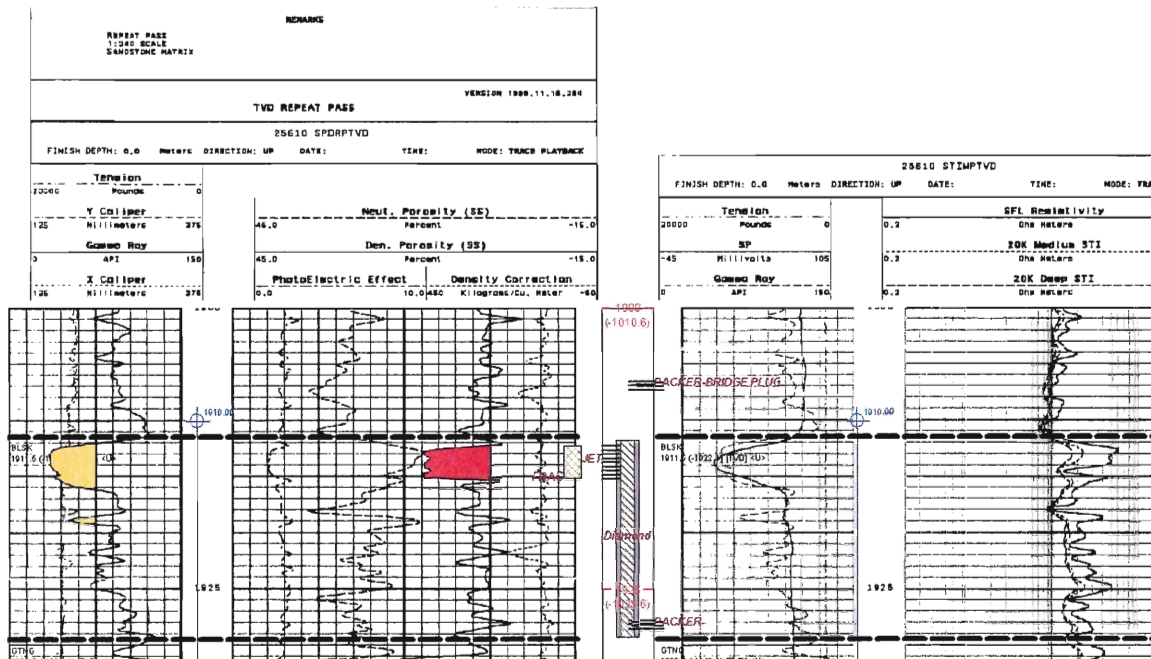
KEY TO SEDIMENTARY LOG

	Wave ripples		Flame structures
	Scour		Planar bedding
	Glaucanite		Fossil
	Trough cross bedding		Burrows
	Fining/ coarsening upward		Ripples
	Mud laminae		Planar cross beds
	Gradational		Siderite
	Churned		Organic material
	Acid Reaction		Mud clasts
			Pyrite

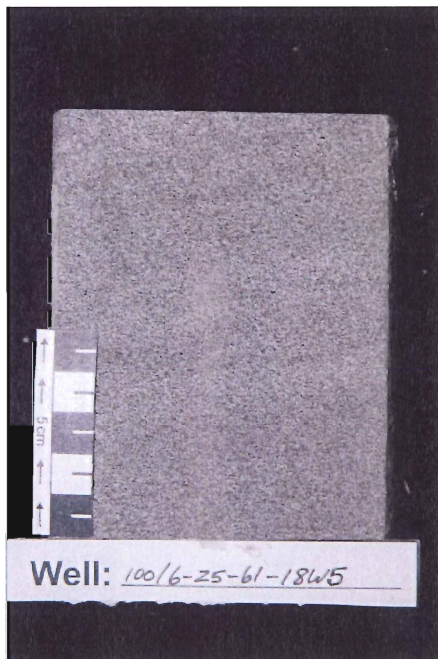
**Trace Fossils**

Ar	Arenicolites
Ch	Chondrites
Di	Diplocraterion
Ma	Macaronichnus
Op	Ophiomorpha
Pa	Palaeophycus
Pl	Planolites
Rh	Rhizocorallium
Te	Teichichnus
Th	Thalassinoides
Sc	Scoyenia





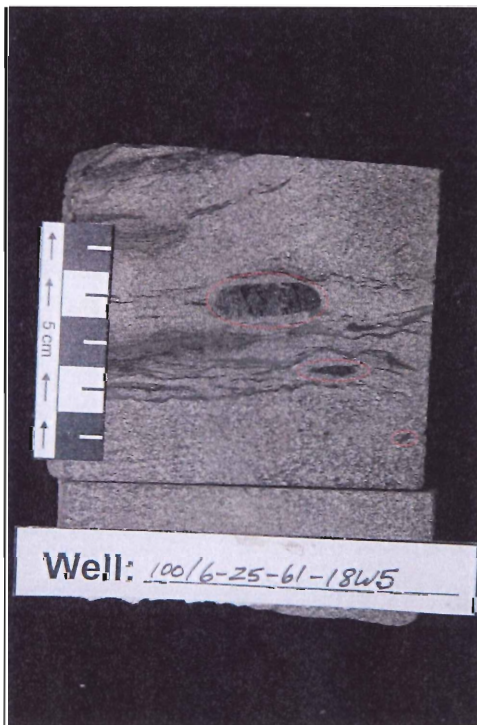
**Figure 4.1.1.** This shows the full suite of logs run in this well. This section of the Bluesky (log signature A) has a gamma ray log reading of ~40 API and appears as a coarsening up sequence. The sandstone density porosity log shows an average of 10% porosity, the SP log shows some permeability in the Bluesky interval, and the resistivity logs read above 10 ohms suggesting the presence of gas in the formation but the separation of the resistivity logs suggests the presence of water as well. The symbols between the logs represent from left to right, fracture stimulation of the reservoir, perforation of the well casing to allow gas to flow into the wellbore, a cored interval, and that they needed to put in a bridge plug because the formation was producing water. (Logs modified from Accumap).



**Figure 4.1.2.** Low angled bedding that has been altered by cryptic bioturbation. (Photo by Terrance Lukie, 2005).



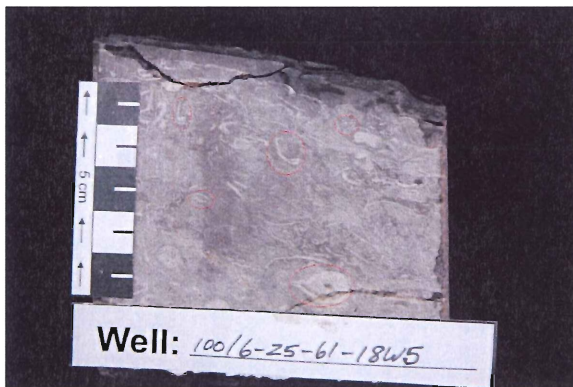
**Figure 4.1.3.** Sandstone containing low angled bedding with mud laminae and stylolites. (Photo by Terrance Lukie, 2005).



**Figure 4.1.4.** Sandstone with a slightly higher mud to sand ratio, low angled bedding, as well as carbonaceous wood fragments that are circled in red in the photo. (Photo by Terrance Lukie, 2005).

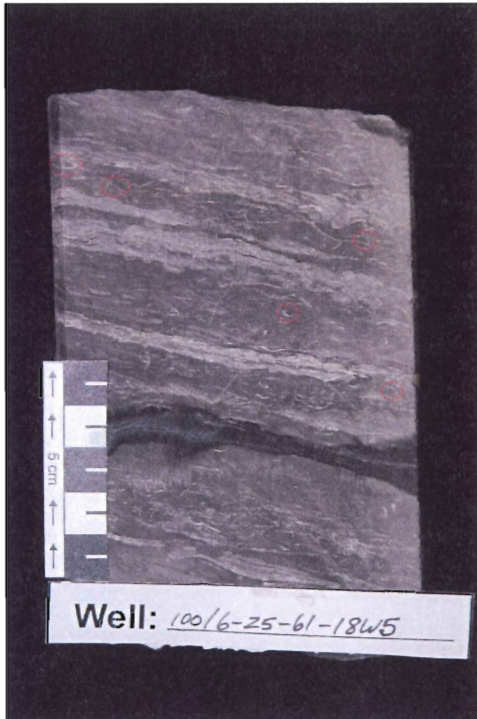


**Figure 4.1.5.** Moderately to highly bioturbated sandstone containing the trace fossils; *Paleophycus*, *Thalassinoides*, *Chondrites*, and *Planolites*. (Photo by Terrance Lukie, 2005).

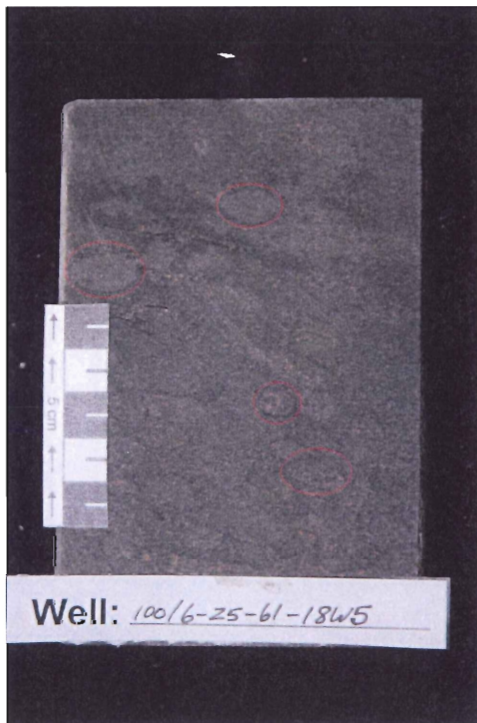


**Figure 4.1.6.** Shell lag containing both articulated and disarticulated shells. The shell in the bottom of the photo (red circle) is a good example of an articulated shell. Two disarticulated shells are present in the upper half of the photo. This has been interpreted as a storm deposit. (Photo by Terrance Lukie, 2005).

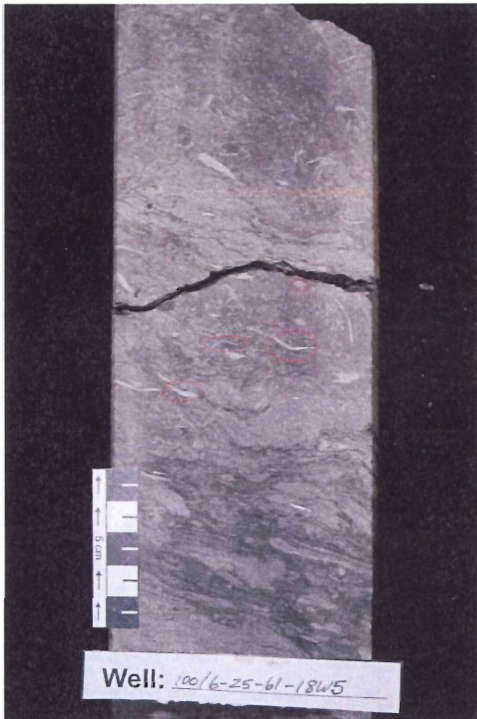




**Figure 4.1.7.** Very organic rich shale bed (dark black layer) in the surrounding shale. The lighter layers are thin sand laminae. (Photo by Terrance Lukie, 2005).



**Figure 4.1.8.** Trace fossil *Macaronichnus*. The burrows have been circled in red to emphasize them. (Photo by Terrance Lukie, 2005).

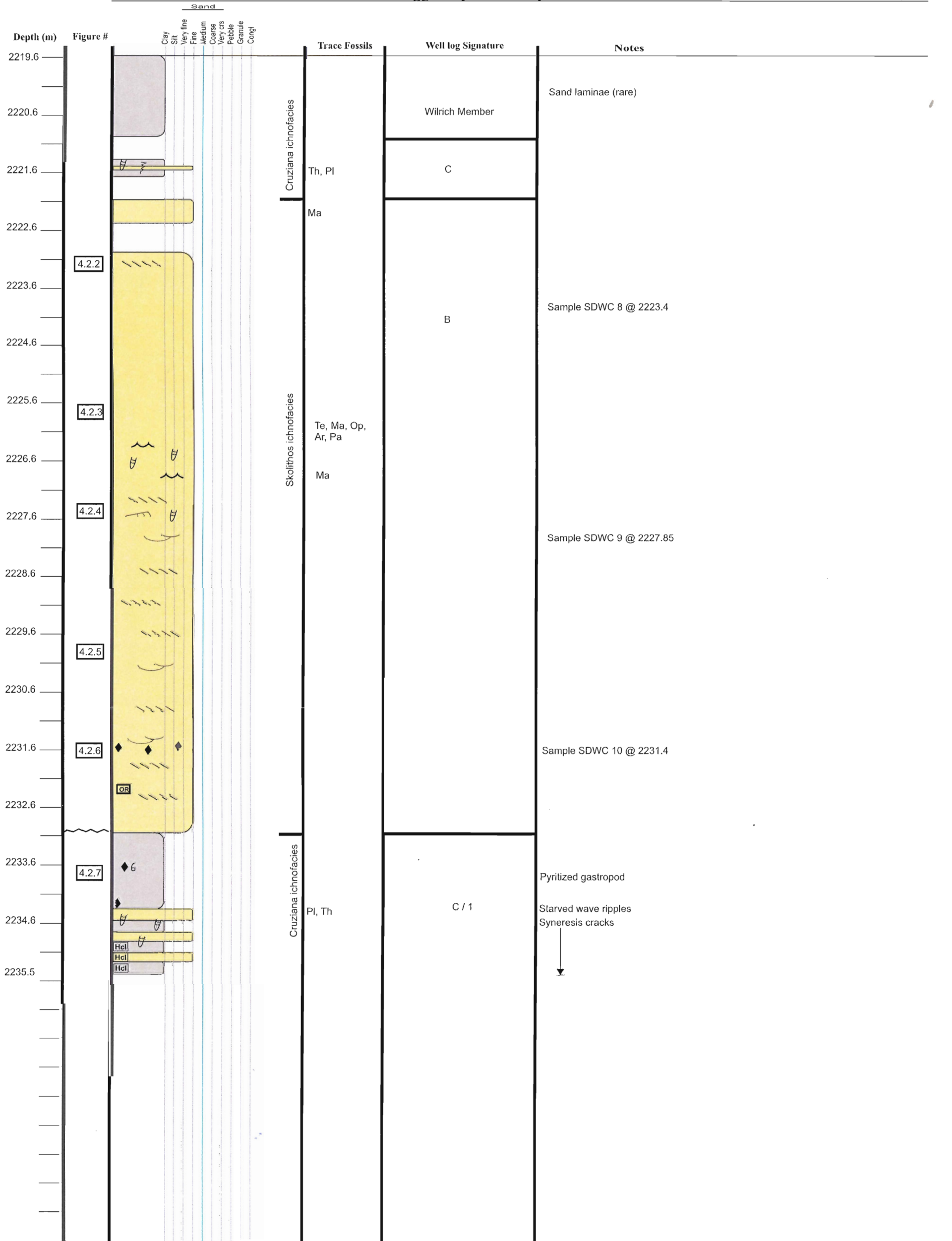


**Figure 4.1.9.** Shell lag in a muddy sandstone. The lag contains mainly brachiopod and bivalve shells, most of which are disarticulated. The largest of the shells have been circled in red for emphasis. (Photo by Terrance Lukie, 2005).

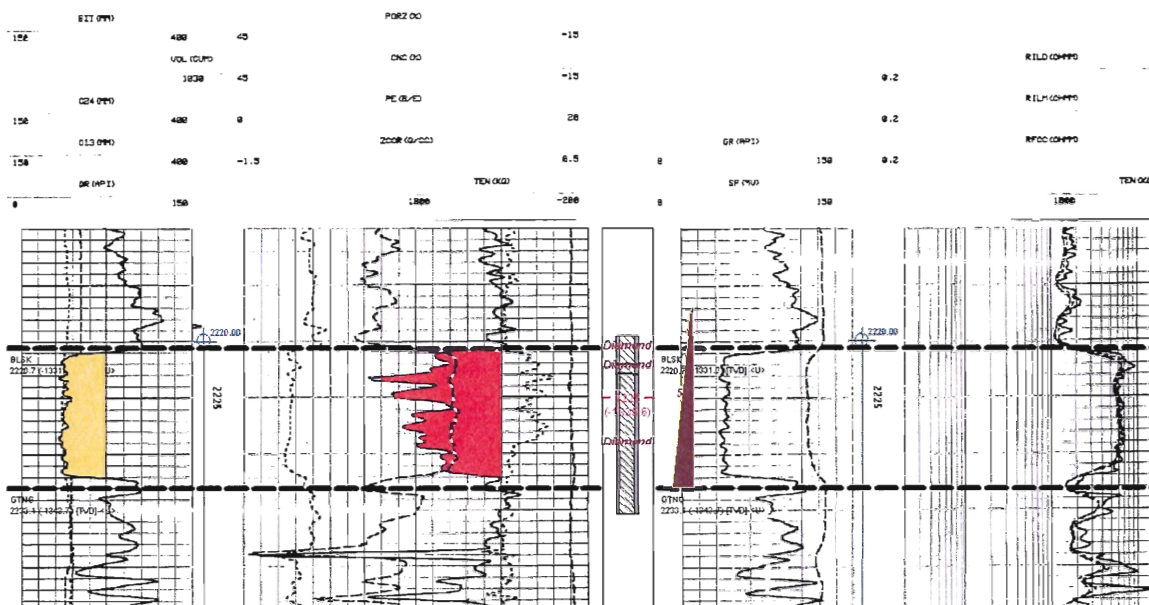
**00/07-31-058-17W5/0: (Fig. 4.2)**

The top portion of this core consists of mudstone with rare sand laminae and may be a gradational contact between the Bluesky Formation and the overlying Wilrich Member of the Bullhead Group. It may also be the “C” log signature of the Bluesky Formation. Moving down core there is a break in the log indicating missing core followed by thin sand that has been heavily bioturbated by *Thalassinoides* and *Planolites* of the *Cruziana* ichnofacies. The next section is fine sand and contains *Macaronichnus* traces. This is followed by another break in the core after which the Bluesky log signature ‘B’ is present. This ~10m thick sand body contains planar cross bedding in the upper part. A thin section sample was taken at 2223.4m. Moving down the core at ~2226 m there is bioturbation present from *Teichichnus*, *Macaronichnus*, *Ophiomorpha*,

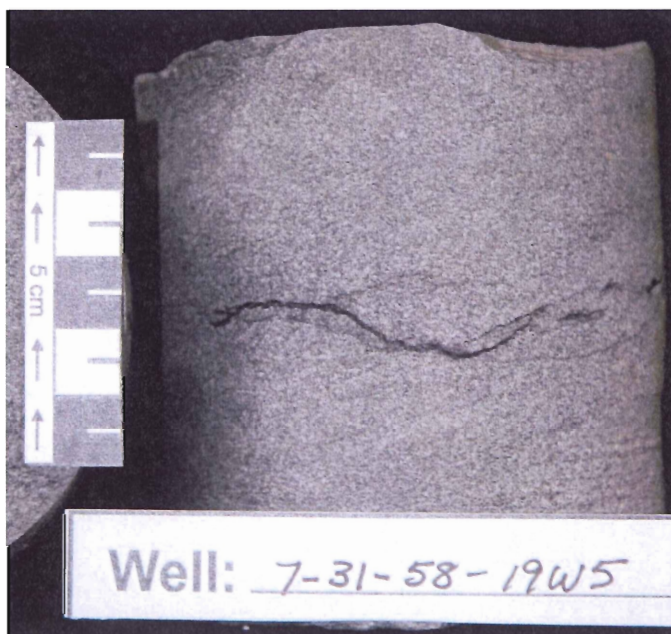
*Arenicolites*, and *Paleophycus*, all from the *Skolithos* ichnofacies. Below the bioturbated zone are wave ripples, planar cross beds, trough cross beds, and ripple cross-lamination. The next thin section sample was taken at 2227.85m. Below the base of the B log signature section, the “C” log signature appears. This section contains pyritized gastropods, starved wave ripples, and syneresis cracks. The trace fossils *Planolites* and *Thalassinoides* are present and suggest a *Cruziana* ichnofacies. The shale and sand layers in the base of this core contain calcium carbonate, probably in the form of cement that reacts moderately with dilute 10% HCl.



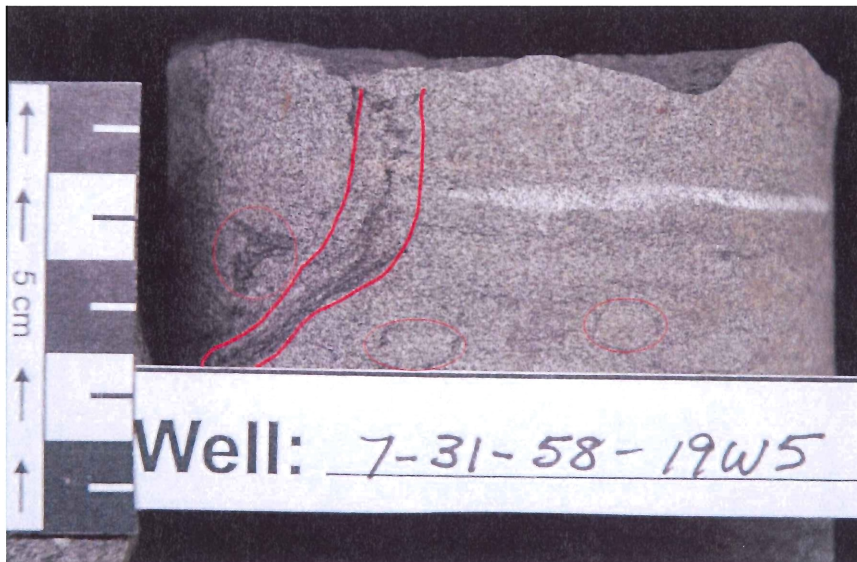
00/07-31-058-19W5



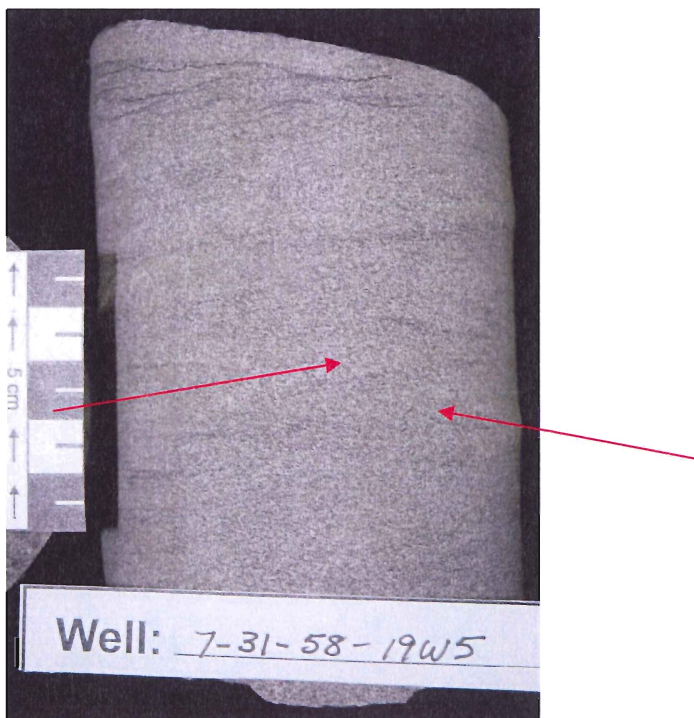
**Figure 4.2.1.** This shows the full suite of logs run in this well. This section of the Bluesky (log signature B) has a gamma ray log reading of ~37 API and appears as a thick blocky sequence. The sandstone density porosity log shows an average of ~12 %. The SP log shows some permeability in the Bluesky interval and the resistivity logs read well above 10 ohms and suggest presence of gas. The symbols between the logs represent from left to right, 2 cores taken over the shown interval, and the dark coloured triangle indicates that a drill stem test (DST) was run to determine if the formation would produce gas before casing the well. (Logs modified from Accumap).



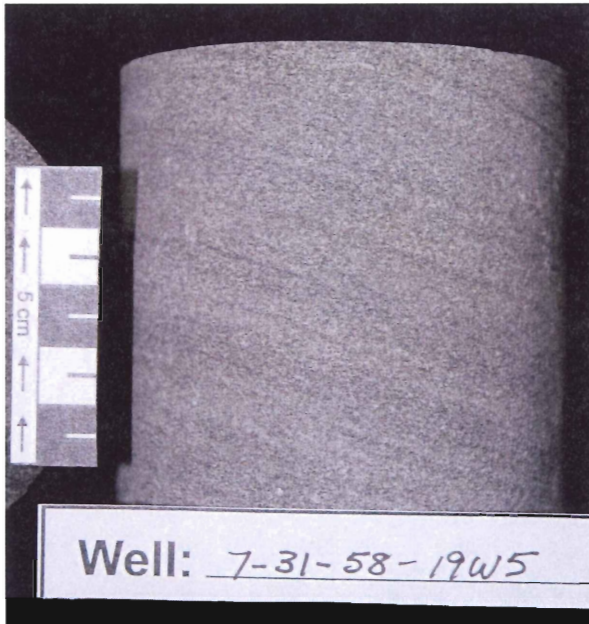
**Figure 4.2.2.** Wavy to cross bedded sandstones with mud laminations and stylolites. The somewhat diffuse nature of the bedding is the result of cryptic bioturbation. (Photo by Terrance Lukie, 2005)



**Figure 4.2.3.** Moderately bioturbated sandstone. The long vertical burrow is *Arenicolites*, the smaller round shaped burrows are *Macaronichnus*, and there may also be some *Ophiomorpha* burrows in this photo. (Photo by Terrance Lukie, 2005).



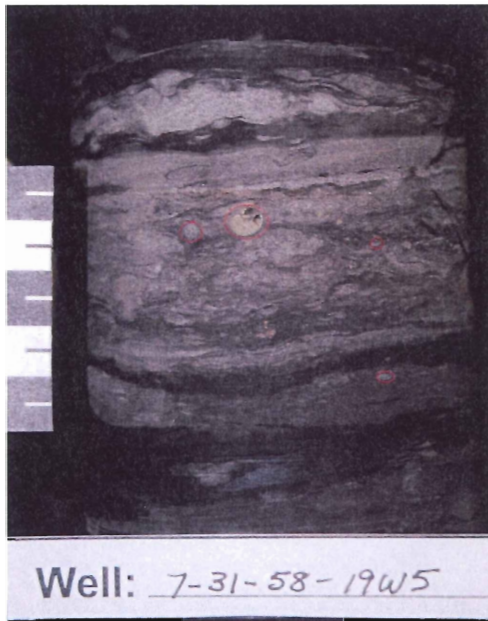
**Figure 4.2.4.** Current rippled bedding in a fine grained sandstone. The ripples are easy to see and their angle has been roughly outlined with the red lines. (Photo by Terrance Lukie, 2005)



**Figure 4.2.5.** Fine grained trough cross bedded sandstone. The bedding is sharp and easily seen in the photo. There has been little if any bioturbation in the core. (Photo by Terrance Lukie, 2005).



**Figure 4.2.6.** Planar to low angled bedding, the sands have a salt and pepper appearance caused by high chert content in the lighter colour sand. This shows little to no trace fossil content. (Photo by Terrance Lukie, 2005).



**Figure 4.2.7.** Bioturbated mudstone with high sand content. The brassy coloured fossil circled in red is a pyritized gastropod shell. The smaller red circles are planolites traces. There are also some less identifiable traces in this section of the core. (Photo by Terrance Lukie, 2005).

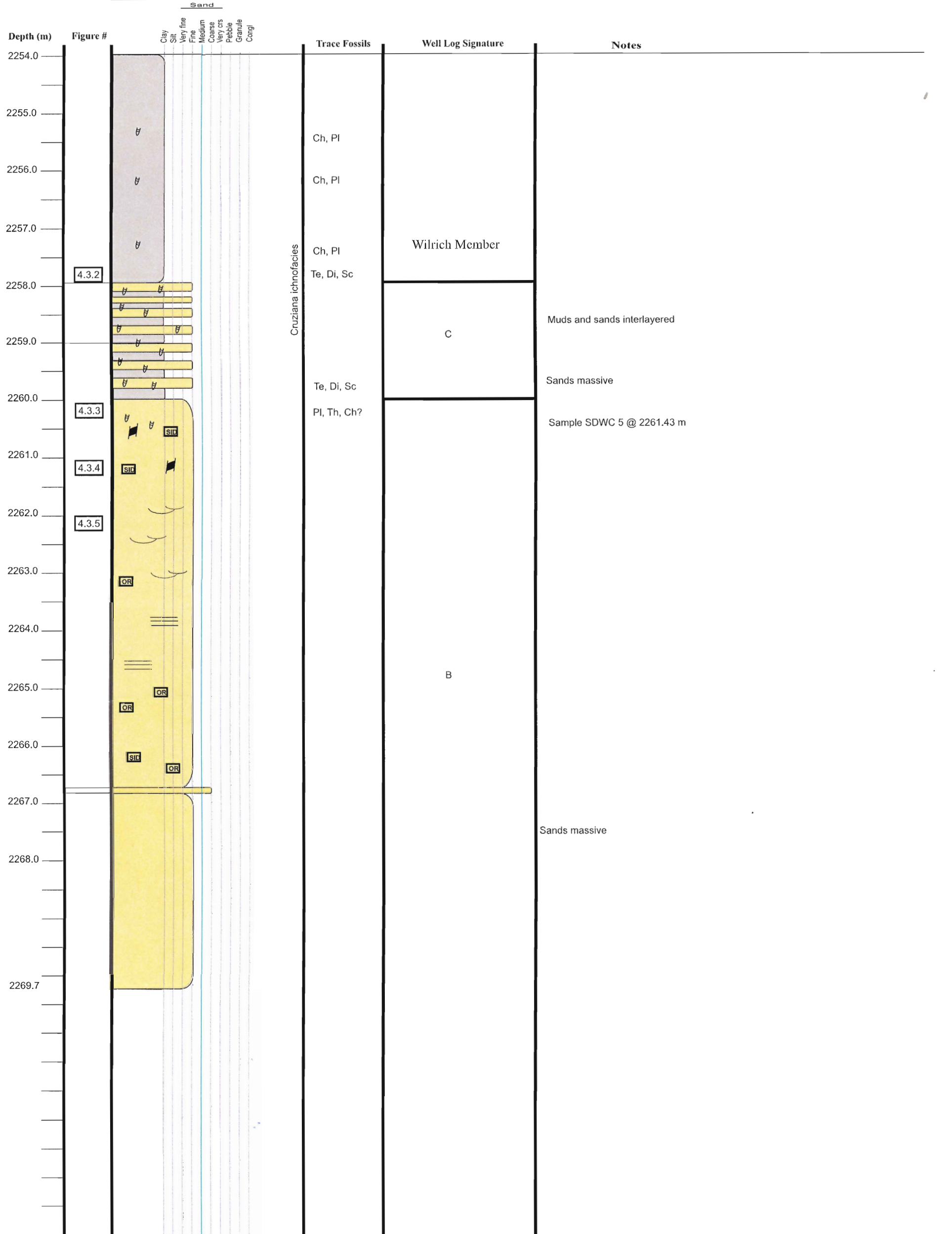
#### **00/09-08-058-18W5 (Fig. 4.3)**

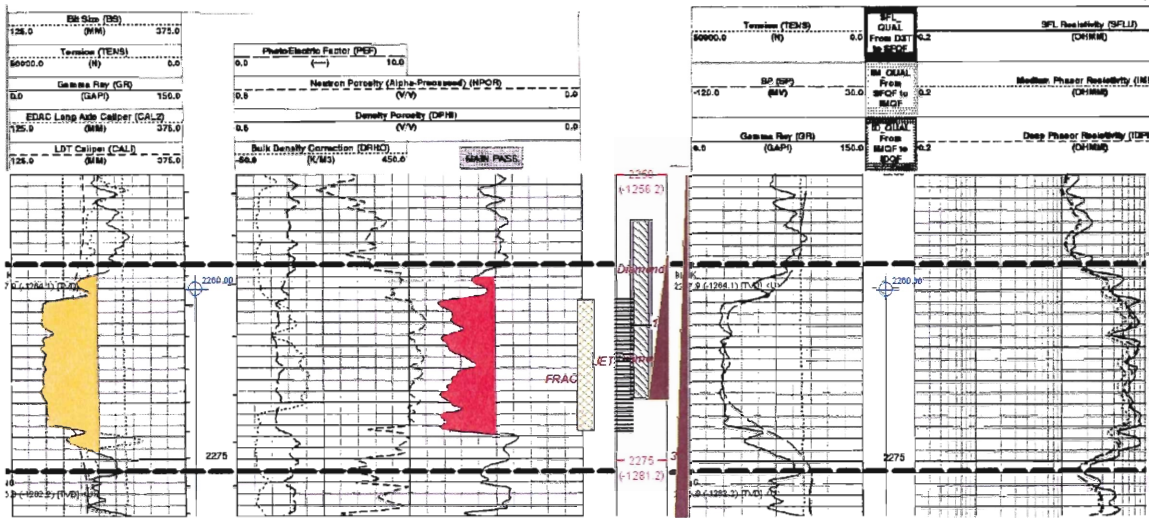
The top of this stratigraphic log begins with the Wilrich Member and moves down into the Bluesky Formation at ~ 2258 m. The Wilrich and upper section of the Bluesky contain the trace fossils *Chondrites*, *Planolites*, *Diplocraterion*, *Scoyenia*, *Thalassinoides*, and *Teichichnus*, which suggest a *Cruziana* ichnofacies. The upper Bluesky Formation in this log is a highly bioturbated sand with abundant mud laminae. The sands in this section are massive and have no visible bedding or remnant sedimentary structures. The sands with high mud content correspond to the log signature “C”.

The next portion of the core is a thick (~8 m) sand body that contains mud rip up clasts, siderite cement, and some minor bioturbation that decreases with depth. A thin section sample was taken at 2261.43m. The sands below the sample location contain trough cross bedding and some minor organic detritus. Toward the base of the core the bedding becomes planar and the siderite and organic content begins to increase. At



~2266.75m, there is a section of coarse sand below which no bedding is visible and the remaining few metres of sands are massive. This ~ 8 metre section of the core corresponds to log signature “B”.

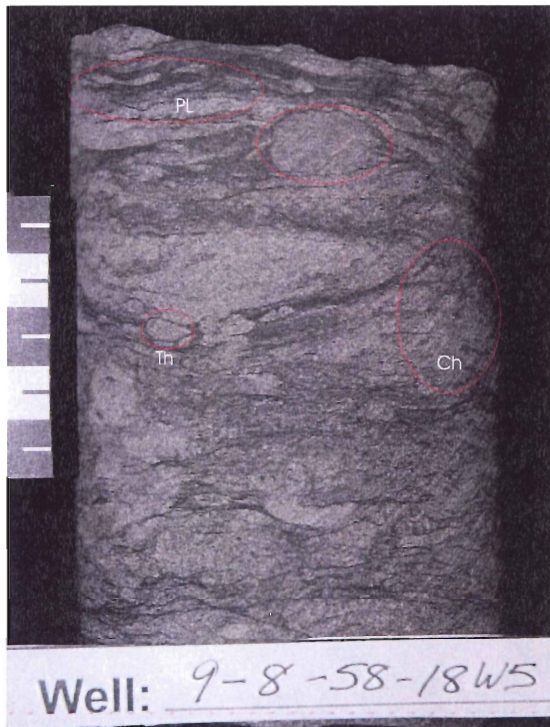




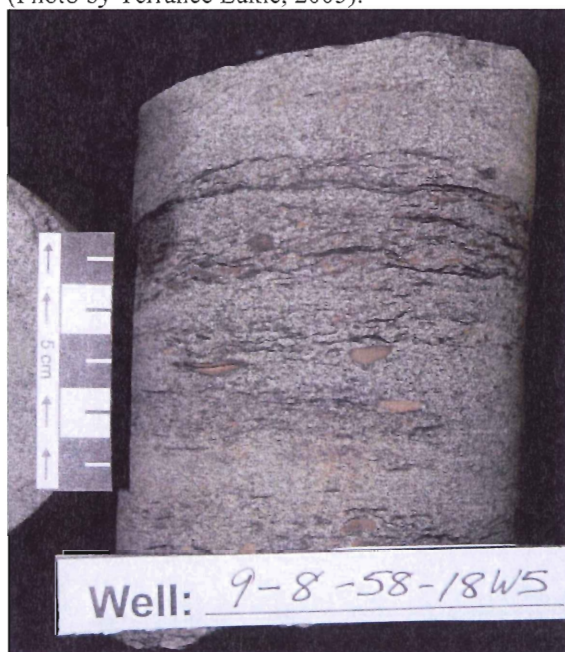
**Figure 4.3.1.** This shows the full suite of logs run in this well. This section of the Bluesky (log signature B) has a gamma ray log reading of ~33 API and appears as a thick blocky sequence. The sandstone density porosity log shows an average of ~7.5 %, the SP log shows good permeability in the Bluesky interval, and the resistivity logs read well above 10 ohms and suggest presence of gas. The symbols between the logs represent from left to right, fracture stimulation of the reservoir, perforation of the well casing to allow gas to flow into the wellbore, 2 cores taken over the shown interval, and the dark coloured triangle indicates that a drill stem test (DST) was run. (Logs modified from Accumap).



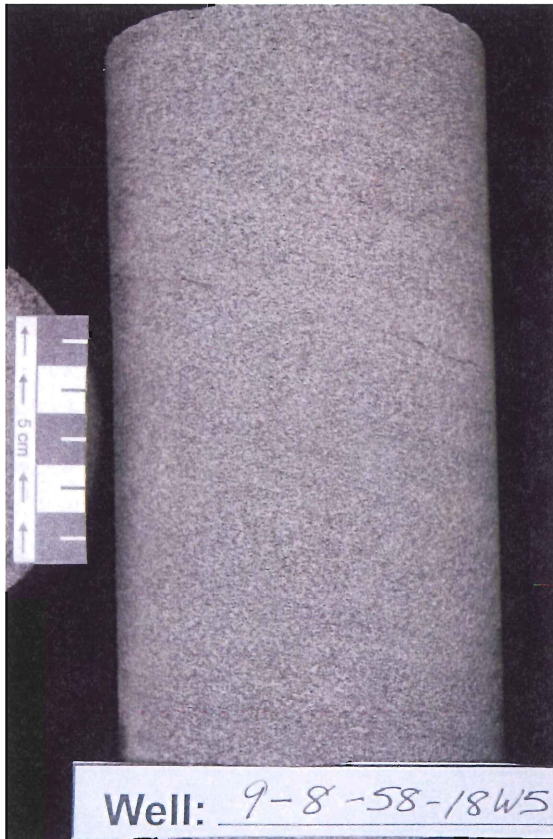
**Figure 4.3.2.** Mudstone with a high sand content. The U shaped burrow at the bottom of the core is a *Diplocraterion* trace fossil, while the long narrow burrow at the top may be *Arenicolites* or *Skolithos*. (Photo by TerranceLukie, 2005).



**Figure 4.3.3.** There is a high sand to mud ratio in this portion of the core. Examples of trace fossils are identified by red circles. The traces labeled are *Thalassinoides*, *Chondrites*, and *Planolites*. The steeply angled lines running top right to bottom left are from the coring process and are not sedimentary features. (Photo by Terrance Lukie, 2005).



**Figure 4.3.4.** Sideritized mudstone clasts in fine grained sandstone. The core also contains mud laminae but shows little if any bioturbation. (Photo by Terrance Lukie, 2005).



**Figure 4.3.5.** Trough crossbedding in fine grained sandstone with some possible cryptic bioturbation. The cryptic bioturbation is difficult to identify and the traces not identifiable. This is of little help in identifying a depositional setting. (Photo by Terrance Lukie, 2005).

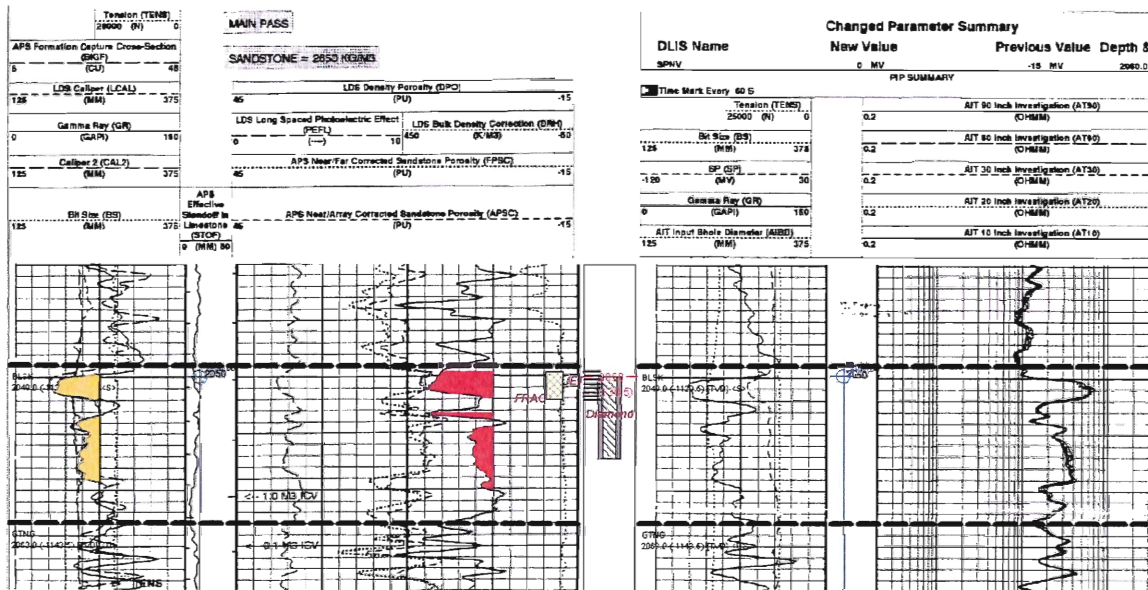
#### 00/03-31-060-18W5 (Fig. 4.4)

The top section of this stratigraphic log consists of medium grained sandstone corresponding to log signature “A”. The sand has a salt-and-pepper appearance and contains minor organic material as well as cross bedding. Approximately 0.9 m from the top of the core is a sharp contact between sand and underlying mud rich sand containing mud laminae and drapes. This section corresponds to log signature “C” and contains sand lenses with visible cross bedding. This section is highly bioturbated and contains the trace fossils *Chondrites*, and *Planolites*. The next contact at ~2052.2 m is sharp and the underlying sands are mud rich, bioturbated and contain the trace fossils *Rhizocorallium*, *Chondrites*, and *Planolites*. At ~2053 m there are distinct layers of

bivalve shells (brachiopods and gastropods), some articulated and most disarticulated.

The bottom ~ 3 m of the core contains cross bedding and flaser bedding with sand lenses containing visible cross bedding. The sands have a salt-and-pepper appearance throughout the core and contain little to no glauconite or siderite. One thin section was cut from 2053.7 m.





**Figure 4.4.1.** This shows the full suite of logs run in this well. The top section of the Bluesky is log signature A and has a gamma ray log reading of ~38 API and appears as a coarsening up sequence. The sandstone density porosity log shows an average of 9% porosity, the SP log shows some permeability in the A section, and the resistivity is well above 10 ohms and suggest the presence of gas. The lower section of the Bluesky is the C log signature. The gamma ray log reading is ~45 API and appears as somewhat blocky but with much higher API readings than any of the B signature sand bodies. The sandstone density porosity log shows an average porosity of ~3%, the SP log shows little to no permeability, and the resistivity logs read above the 10 ohm mark suggesting gas presence. The symbols between the logs represent from left to right, fracture stimulation of the reservoir, perforation of the well casing to allow gas to flow into the wellbore, and finally that the interval was cored. (Logs modified from Accumap).



**Figure 4.4.2.** The top two boxes ~ 3.00m of core from this well. The core shows both reservoir quality sands as well as high mud content sands. The core top is located in the top right corner of the photo and the bottom of this section in the bottom left of the photo. All of the tops are in the top of the photo and move in sequential order from right to left. In the core there are visible crossbedding, organic materials, and trace fossils. (Photo by Terrance Lukie, 2005).





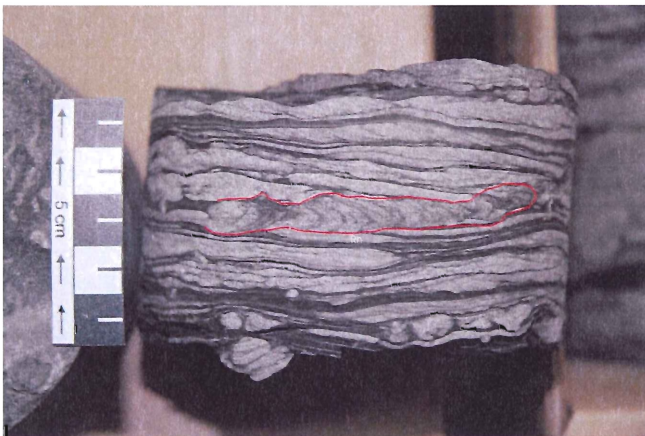
**Figure 4.4.3.** Shale/sand contact at ~2051.5 m. The contact is very sharp with a cross bedded sandstone on the right and a mudstone on the left. The shale appears somewhat more fissile at the contact. This sharp contact may indicate a regressive event. (Photo by Terrance Lukie, 2005).



**Figure 4.4.4.** The middle two boxes ~3.00 m of core from this well. The top of the core is in the top R corner of the photo and the bottom of the core in the bottom L corner. All tops are in the top of the photo and are sequential from right to left. The core has high mud content, is very highly bioturbated, and contains many mud laminae and drapes. There is a section of fissile shale more than half way down the first section of the core. The next section shows some traces and possibly some sediment loading features. (Photo by Terrance Lukie, 2005).



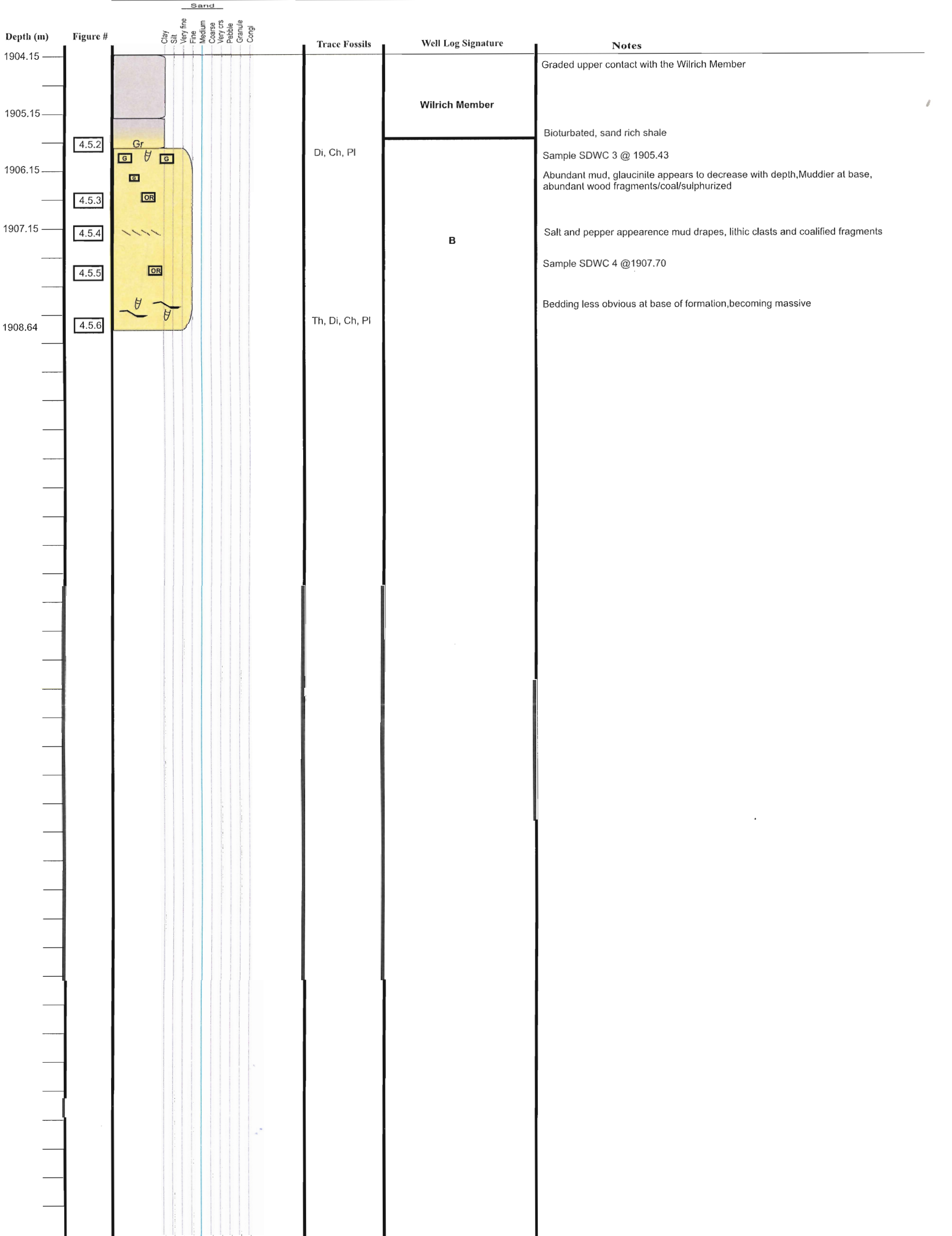
**Figure 4.4.5.** The bottom two boxes ~3.00 m of core from this well. The core shows the high mud content sands with very high bioturbation, many traces visible, and abundant many mud laminae. The core top is located in the top right corner of the photo and the bottom of this section in the bottom left of the photo. All of the tops are in the top of the photo and move in sequential order from right to left. (Photo by Terrance Lukie, 2005).

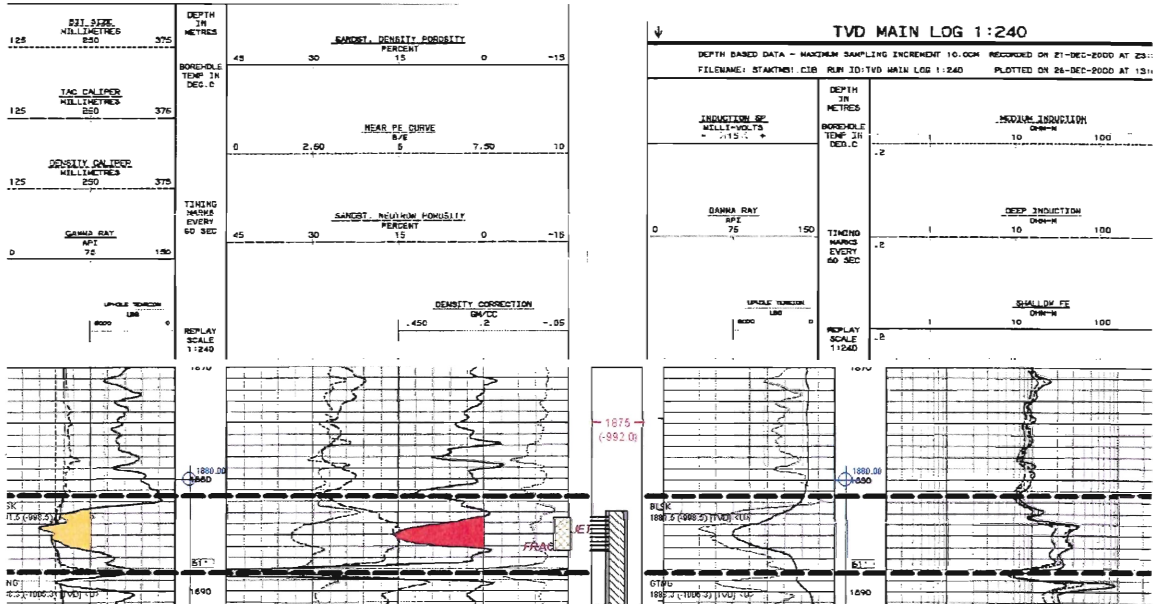


**Figure 4.4.6.** Close up of the very mud rich sandstone and several trace fossils. The long burrow running from left to right is from *Rhizocorallium*, some of the smaller round shaped burrows are likely *Planolites*, *Chondrites*, and some of the larger may be *Ophiomorpha*. (Photo by Terrance Lukie, 2005).

**00/01-29-061-17W5 (Fig. 4.5)**

The upper ~1.65 m of core in this stratigraphic log contain shale from the Wilrich Member. The contact between the Bluesky Formation and the Wilrich Member is gradational. Furthermore, the contact area is bioturbated and contains the trace fossils *Diplocraterion*, *Chondrites*, and *Planolites*. The Bluesky Formation in this core represents log signature “B”. A sample thin section was cut from 1905.43 m. The upper section of the sand contains abundant glauconite that appears to decrease with depth. The sand also contains some organic matter in the form of coalified woody material with pyrite. Moving down the core, toward the base, the glauconite disappears and is replaced by chert resulting in the common salt-and-pepper appearance and the presence of cross bedding. In addition, there are organics and mud clasts present as well as mud drapes and flaser bedding near the base. The bedding at the base of the core is much less discernible than in the upper portion of the core and appears massive.

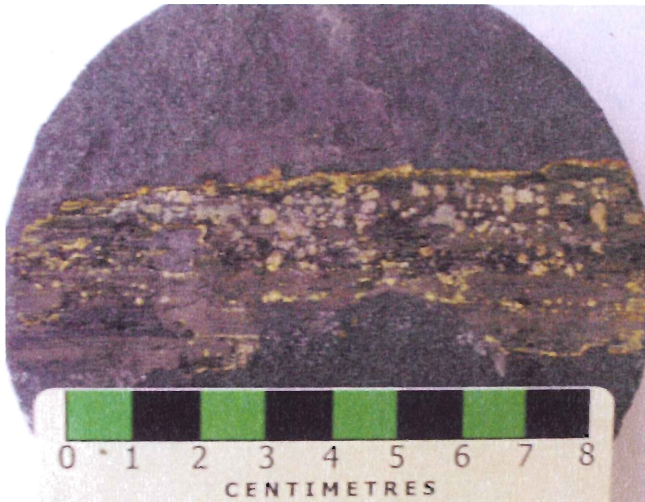




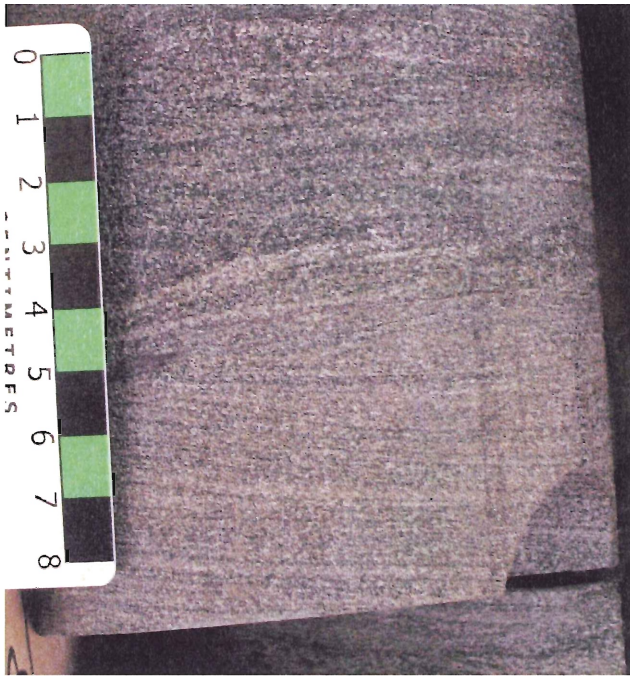
**Figure 4.5.1.** This shows the full suite of logs run in this well. This section of the Bluesky (log signature A) has a gamma ray log reading of ~45 API and appears as a coarsening up sequence. The sandstone density porosity log shows an average of 14% porosity, the SP log shows some permeability in the Bluesky interval, and the resistivity logs read above 10 ohms suggesting the presence of gas in the formation. The symbols between the logs represent from left to right, fracture stimulation of the reservoir, perforation of the well casing to allow gas to flow into the wellbore, and finally that the interval was cored. (Logs modified from Accumap).



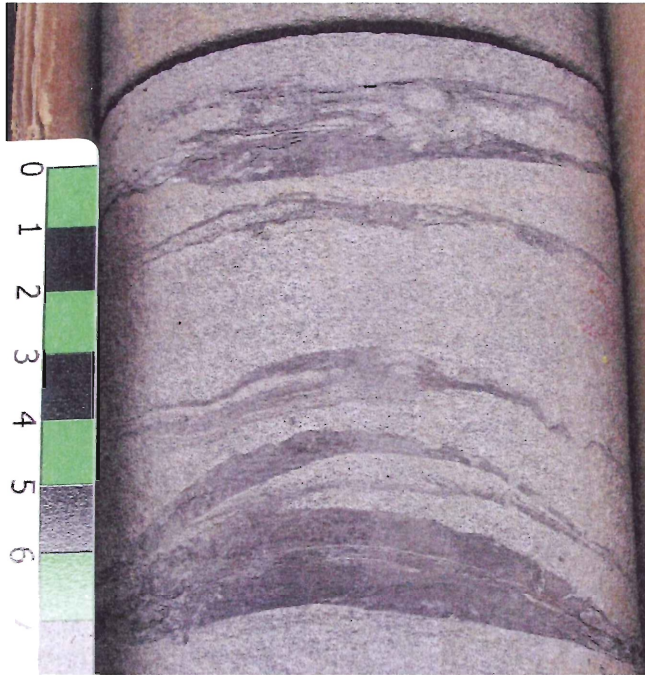
**Figure 4.5.2.** Upper contact between the Bluesky Formation and the overlying Wilrich Member. The upper shale portion has a high sand content and appears as a gradational contact. The shale contains trace fossils *Thalassinoides*, *Planolites*, and *Chondrites*. The sandstone portion of the photo has a salt and pepper appearance possibly due to a higher chert content. (Photo by Scott Doyle, 2005).



**Figure 4.5.3.** Organic material with pyrite in a section of sandstone. The sand contains some mud as well as some glauconite. The woody organic material contains what appear to be *Teredolites* (wood boring clam). (Photo by Scott Doyle, 2005).



**Figure 4.5.4.** Glauconite rich section of the core containing low to medium angled cross bedding. The bedding is easy to see due to the contrast between the light quartz rich area and the darker green glauconite areas. (Photo by Scott Doyle, 2005).



**Figure 4.5.5.** Layers of organic material within a sandstone section of the core. The layers are rare in the middle portion of the core with the organics being more common in the upper and lower ends of the core. The sand has a salt and pepper appearance and contains trace amounts of glauconite. (Photo by Scott Doyle, 2005).

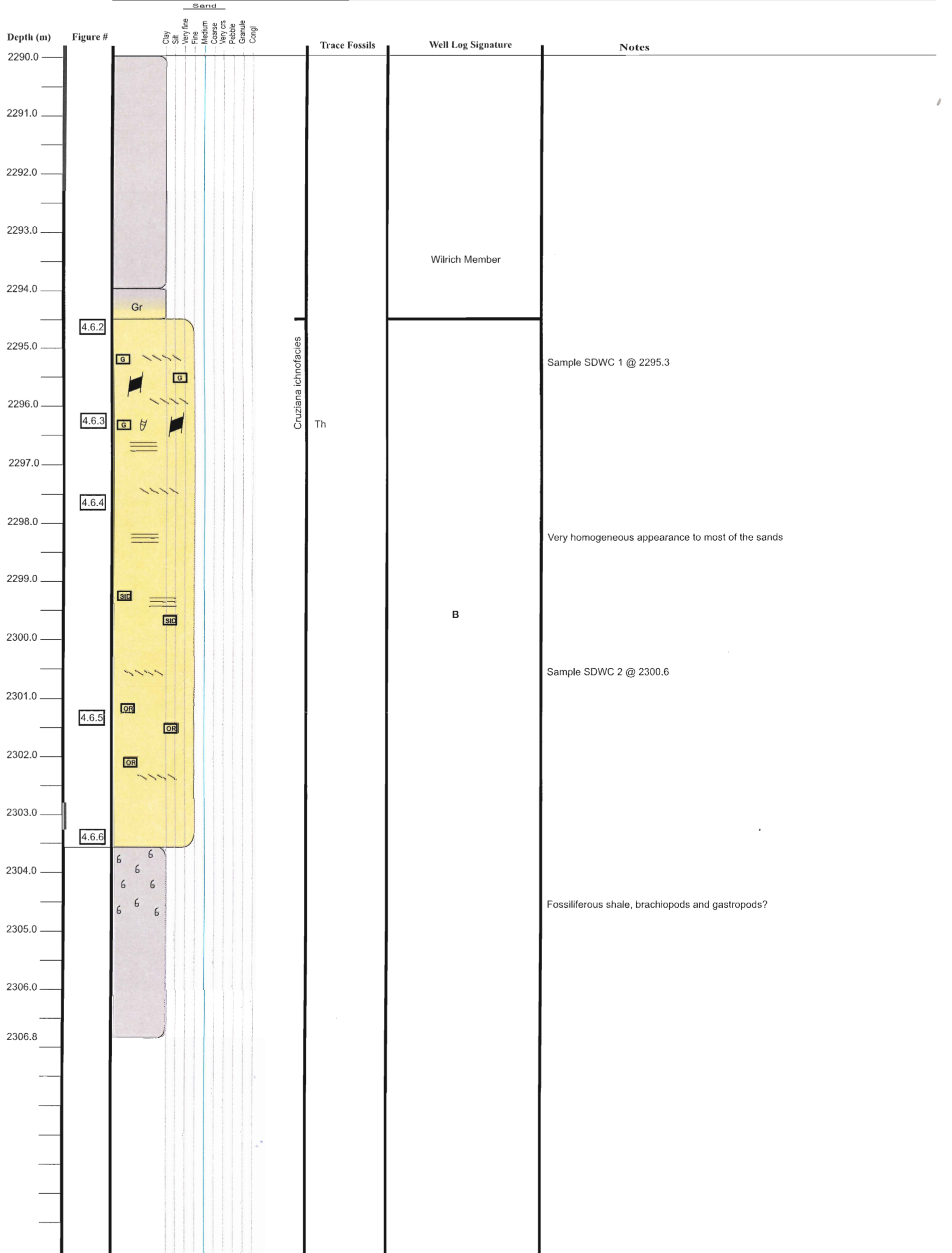


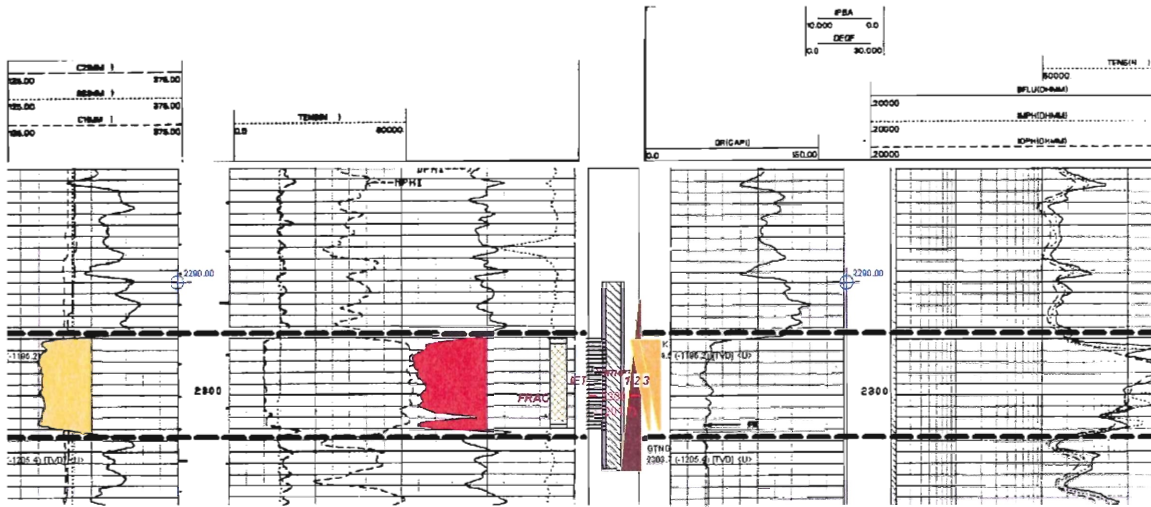
**Figure 4.5.6.** The lower sand/shale contact within the Bluesky Formation. The contact is sharp and may represent incision of the Bluesky into the underlying shale. The sands contain trace fossils *Thalassinoides* or *Diplocraterion*, *Chondrites* and *Planolites*, as well as siderite cement and abundant glauconite. (Photo by Scott Doyle, 2005).

**00/12-24-058-18W5 (Fig. 4.6)**

The top ~4 m of this core contain the shale of the Wilrich Member. Furthermore, the contact between the Bluesky formation and the Wilrich Member is gradational. The sand below the contact is thick, blocky, and has been labelled as log signature “B”. The top section of the sand contains abundant glauconite, minor mud clasts, and cross bedding. There is some minor bioturbation visible from the trace fossil *Thalassinoides* and what appears to be some cryptic bioturbation. Moving down the core, the bedding becomes planar and the sand appears homogenous with a prominent decrease in the glauconite content with depth. Toward the middle of the sand body, there are more planar beds, as well as the appearance of siderite cement. Cross bedding reappears at ~2300.50 m and some organic material appears near the base of the Bluesky sand body. The contact between the base of the sand and the underlying shale is sharp. The shale contains abundant bivalve shells (brachiopods and gastropods).



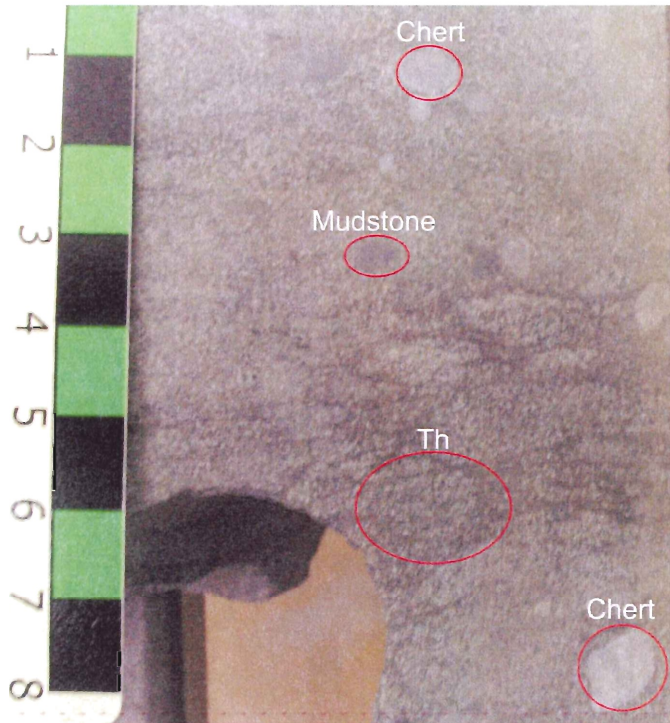




**Figure 4.6.1.** This shows the full suite of logs run in this well. This section of the Bluesky (log signature B) has a gamma ray log reading of ~32 API and appears as a thick blocky sequence. The sandstone density porosity log shows an average of ~12 %. The resistivity logs read well above 10 ohms and suggest presence of gas. The symbols between the logs represent from left to right fracture stimulation of the reservoir, perforation of the well casing to allow gas flow, 2 cores taken over the shown interval, and the coloured triangles indicate that drill stem tests (DST) were run to determine if the formation would produce before casing the well. (Logs modified from Accumap).



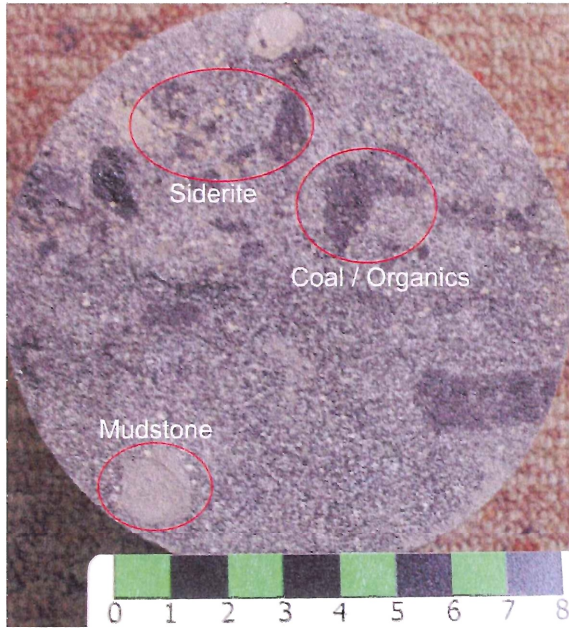
**Figure 4.6.2.** The contact between the Bluesky Formation and the Wilrich Member. The contact is gradational but roughly follows the break in the core. The lower portion of core has visible sand grains (grey specks). (Photo by Scott Doyle, 2005).



**Figure 4.6.3.** A section of the core containing bioturbation by *Thalassinoides* and containing grains of chert and mudstone. Glauconite appears as grayish green in the photo. (Photo by Scott Doyle, 2005).



**Figure 4.6.4.** Photo shows both planar and low angled bedding. Grayish green grains are glauconite. (Photo by Scott Doyle, 2005).



**Figure 4.6.5.** Photo shows siderite cement, appearing as rusty coloured grains. The core also contains mudstone clasts and abundant coaly organic material. (Photo by Scott Doyle, 2005).



**Figure 4.6.6.** The lower sand/shale contact within the Bluesky Formation. This shale separates the Bluesky Formation from the Gething Formation. The sand in this photo has much less glauconite and has a salt and pepper appearance. (Photo by Scott Doyle, 2005).

### 4.3 Initial interpretation of Depositional Environment

During this study, six cores were logged and the resulting stratigraphic logs (Figs. 4.1 to 4.6) show the sedimentary structures, fossil assemblages, grain sizes, sample depths, and any other pertinent notes regarding the cores. The cores were photographed and the photos containing important features have been included with the stratigraphic logs to help show the reasoning behind the placement of the sections into specific depositional environment categories.

The cores have been divided into 3 different log signatures based on the appearance and the content of the core. A general overview of the contents of the core and a visual representation of the division of the facies can be seen in Table 4.1.

Lithological Group	Log Signature	Grain size	Sedimentary structures	Trace Fossil Assemblage	Traces fossils	Other	Thickn ess	Interpretation
Interbedded sandstone/mudstone	<b>C</b>	very fine to medium	sands laminae, scoured contacts, de-watering features.	Cruziana, Glossifungites	Th, Pl, Pa, Te, Di, Sc, bivalve shells	siderite, pyrite, Rxn to HCl	1.0 to 15.75 m	offshore marine, sublittoral zone, firm ground?
Planar bedded medium sandstone	<b>A</b>	medium	planar bedded, scoured contacts	Skolithos	Ma, cryptic bioturbation		3.25 m	shoreface?, sandy shore?
Cross-bedded to massive sandstone	<b>B</b>	fine	planar cross-beds, wave ripples, ripple laminations, trough cross-beds, mud laminae, planar bedding, rip up clasts,	Skolithos	Te, Ma, Op, Pa, bivalve shells	siderite, pyrite, organic detritus, glauconite	4.0 to 13.5 m	channel body?, fluvial/deltaic, estuarine, tidal

Table 4.1. Shows the features present in the three different the log signatures and depositional environments present in the Bluesky Formation in the study area.

Bluesky Formation in the study area has been initially interpreted using the log signatures, gross sand isopach maps, and preliminary core observations. These have lead to an initial interpretation of a barrier bar complex (log signature B) that has been capped with a transgressive shoreface (log signature A) which has eroded the upper layers of the

barrier system leaving only some of the sedimentary structures and features that would be commonly found in a barrier complex. Estuaries are commonly associated with tidal channels and barrier mouth bars. Estuarine sediments are often a combination of clays interbedded with sands (log signature C) and are less prominent in the studied core than those of the proposed barrier complex (B) or the shoreface (A).

**Initial interpretation of “A”:**

The log signature associated with “A” has the shape of a bell curve turned on its side. Starting from the base, the curve first shows the high gamma reading (75 API) associated with high clay content and low sand content. The log reaches a minimum peak (~30 API). Here reservoir sand is present. The curve then returns to high gamma readings as it grades up into the Wilrich Shale that caps the Bluesky Formation in the study area. The “A” signature sand is thinly (6< m) distributed throughout the study area. The distribution and thickness has aided in the interpretation of a middle to upper shoreface depositional environment formed during the overall transgressive cycle that deposited the Bluesky. The gross sand isopach map (Fig. 2.4a) of the Bluesky signature “A” sand shows that the sand bodies are present throughout most of the study area. Much of the original interpretation of the “A” signature sand has been taken from the gross sand isopach map.

**Initial interpretation of “B”:**

The log signature associated with “B” is a blocky shaped curve with abrupt changes in the gamma ray log from a high API response in the underlying shale to a low response (~30 API) throughout the reservoir portion. It is increasing to ~75 API as the

curve moves into the overlying shale of the Wilrich. The gamma reading is fairly consistent with respect to the clay/sand ratio throughout the reservoir varying only slightly. The gamma log indicates the sand body is one unit consisting of one log signature. However, when compared to drill core, the small oscillations in the upper portion of the gamma log may actually correspond to what has been proposed as “A” signature sand lying on top of the “B” signature sand. Using the thickness of the sand (> 6 m) from gross sand isopach maps and the orientation of the “B” signature sands, the author has made a preliminary interpretation of a barrier complex composed of several migrating barriers along a coastal plain. These migrating barriers have been topped by a transgressive middle to upper shoreface (signature “A”).

#### **Initial interpretation of C:**

The log signature “C” started originally as a way to describe any large volume of sandy material that didn’t fit into either the “A or B” category. After looking at cores and then re-examining the gamma logs, it became evident what appeared to be the “B” signature sand with a higher clay/sand ratio was not a “B” signature but a different signature completely. Signature “C” can usually be found underlying the “A or B” sands or in a few cases overlying them. Identifying this signature solely based on logs is challenging and is most easily done with the use of drill core data as well. The drill core contains lenticular to flaser bedding and suggests frequent slackwater conditions in a lagoonal depositional setting. When considering the depositional setting with respect to the other facies present in the cores, it appeared that the “C” sand was deposited in a lagoonal or estuarine setting. The initial interpretation of the depositional setting is summarized in Figure 4.7.

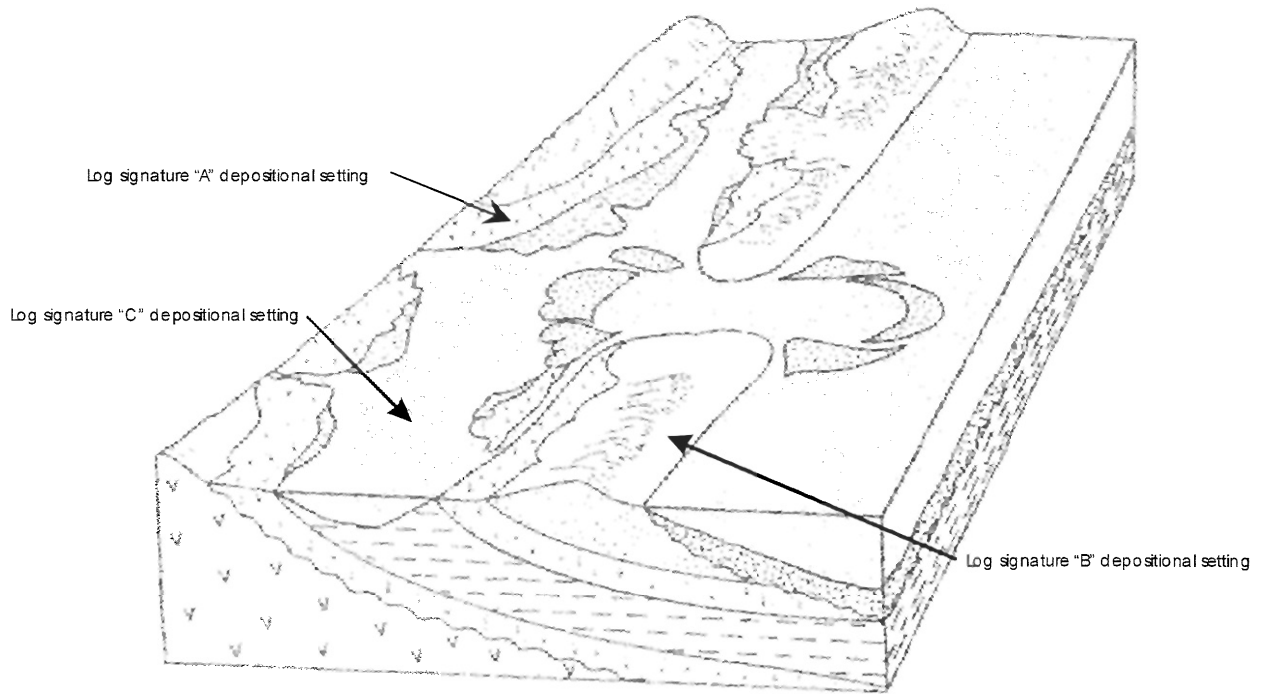


Figure 4.7. The initial model used to describe the depositional setting of the Bluesky Formation in the Whitecourt study area. The different log signatures are shown with the associated setting they were thought to have been deposited in. (Modified from Facies Models, Reinson, 1992).

The overall setting of the Bluesky Formation in Alberta is marine and transgressive. The formation contains several large barriers that fit with the author's interpretation.

However, given the size of the study area, it is possible that several different small scale depositional settings could be present even though the overall depositional model is that of a barrier complex. Because of this, further investigation was necessary including processing of core data and comparison of the data to known depositional settings. The purpose of the initial interpretation was to show the thought process behind labelling the well log signatures and proposed depositional model. The high mud content in this facies indicates at the least a periodically low energy environment.



#### 4.4 *Final Interpretation of Depositional Environment*

The final interpretation of the depositional environment is based on the log signatures presented thus far, the gross sand isopach maps, the core analysis, stratigraphic logs, and thin section analysis and descriptions. Using these additional methods to determine the depositional environment, the final interpretation has changed slightly from the initial interpretation. The log signatures remain “A”, “B”, and “C” however their placement within the overall Bluesky Formation depositional setting has changed slightly to accommodate the new information acquired during this study.

##### **Final Interpretation of “A:**

The coarsening up shape of the “A” log signature may indicate several possible environments purely from the well log analysis aspect. After looking at the drill core, the trace fossil assemblage became especially useful. The trace fossils present in the “A” sand are most commonly *Macaronichnus* and *Paleophycus* and belong to the *Skolithos* and *Glossifungites* ichnofacies. The living environments for these ichnofacies range from fluvial/deltaic to sublittoral to shoreface as seen in Figure 4.8.

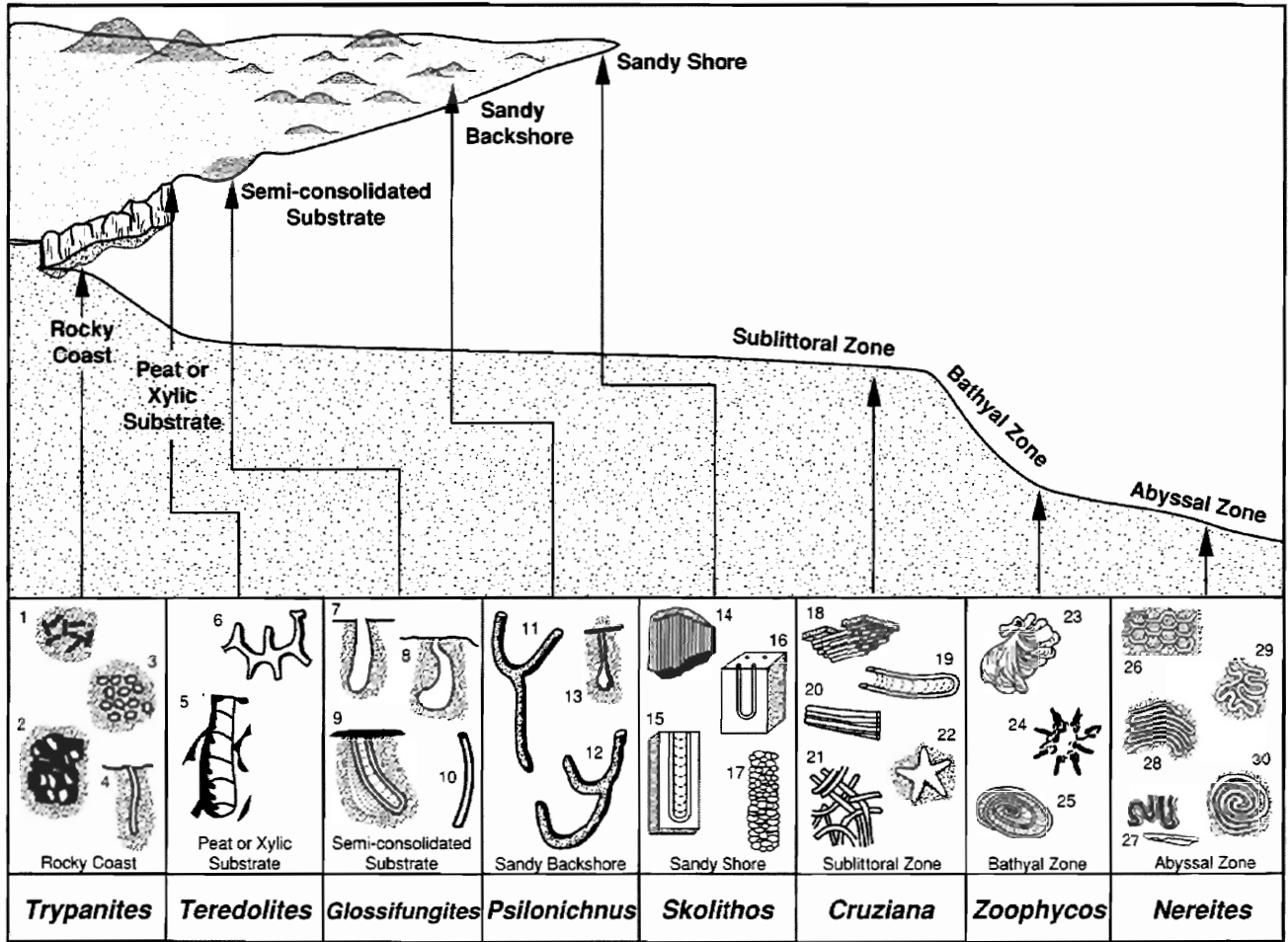


Figure 4.8. This figure shows the environments for the various types of trace fossils and classifies them by burrow type and location. (Pemberton and MacEachern, 1995).

The range of these fossils helps to narrow down the depositional environment and eliminate some of the possible candidates. The low trace fossil diversity and the limited number of burrows in the core may indicate a high energy environment.

The migration of two dimensional dunes has resulted in planar cross bedding and suggests unidirectional flow (Prothero and Schwab, 1996). The lack of any other sedimentary features also lends support to the idea that flow may have been of a higher velocity. The flow was not fast enough to create anti-dunes or planed off ripples but was

fast enough to create planar cross bedding. The sediment load in the water would have been a limiting factor for the trace fossil diversity.

From the core analysis, gamma log appearance, and the trace fossil content, the depositional environment for the “A” log signature is something proximal to the coastal plain and part of a tidally influenced system.

### **Final Interpretation of “B”**

The blocky shape of the “B” log signature may indicate several possible environments purely from the well log analysis aspect. The trace fossils present in the “B” sand are most commonly *Teichichnus*, *Macaronichnus*, *Ophiomorpha*, *Arenicolites*, and *Paleophycus*. *Thalassinoides*, *Chondrites* and *Planolites* are present in the top of one core but the dominant ichnofacies is *Skolithos*. The living environment for these ichnofacies is sandy shore type settings (Fig. 4.8).

The core contains trough and planar cross beds indicating unidirectional flow conditions and the migration of both two and three dimensional dunes. The core also contains mud clasts and organic material, suggesting proximity to a terrestrial source. The type log for the “B” signature appears to have the “C” signature deposited above it. This could be explained with “B” as a barrier and “C” being a regressive pulse that moves basinward to cover the barrier. Another plausible explanation is that “B” is part of a channel system and “C” was deposited as a transgressive pulse on top of the channels as the coastal plain back steps. The trace fossils along with the sedimentary features suggest that the “B” signature sand is part of a channel system or maybe part of a partially eroded barrier bar. The typical sequences found in a transgressive barrier model namely flood tide delta, marsh, and backshore dune deposits do not appear in the cores. Although these

sequences are not identified in the cores, many of their features are present. Due to the limited number of cores available, a transgressive barrier cannot be ruled out (Reinson, 1992).

### **Final Interpretation of “C”**

The erratic shape of the “C” log signature and the high gamma ray response may indicate several possible environments purely from the well log analysis aspect. The trace fossils present in the “C” sand are *Planolites*, *Chondrites*, and *Rhizocorallium*, belonging to the *Cruziana* ichnofacies. The living environment for these ichnofacies is the sublittoral zone or lower shoreface to marine settings (Fig. 4.8). The trace fossil assemblage does not correlate well with the sedimentary features found.

The core contains flaser bedding, mud drapes and mud laminae, indicating possible slack water conditions. The core also contains some planar cross bedding in sand lenses, indicating unidirectional flow, dewatering features, siderite, organic laminae, and shell layers, suggesting proximity to the coastal plain. The presence of syneresis cracks suggests an environment with changing salinities. The type log for the “C” signature appears to have the “A” or part of a “B” signature deposited above it with a shale layer separating them. This could be explained with “C” as an estuary and “A” being a transgressive shoreface or tidal channel that moved landward to cover the estuary. Relying primarily on trace fossils does not give a clear picture of the depositional environment. The sedimentary features suggest that the “C” signature is part of an estuary although the trace fossils suggest it is sublittoral. The typical features found in an estuary appear in the core but due to the limited number of cores, it cannot be regarded as

the only depositional environment possible. Other possible environments include a back-barrier lagoon (Reinson, 1992).

Figure 4.9 shows the range of environments for some of the trace fossils found in this study.

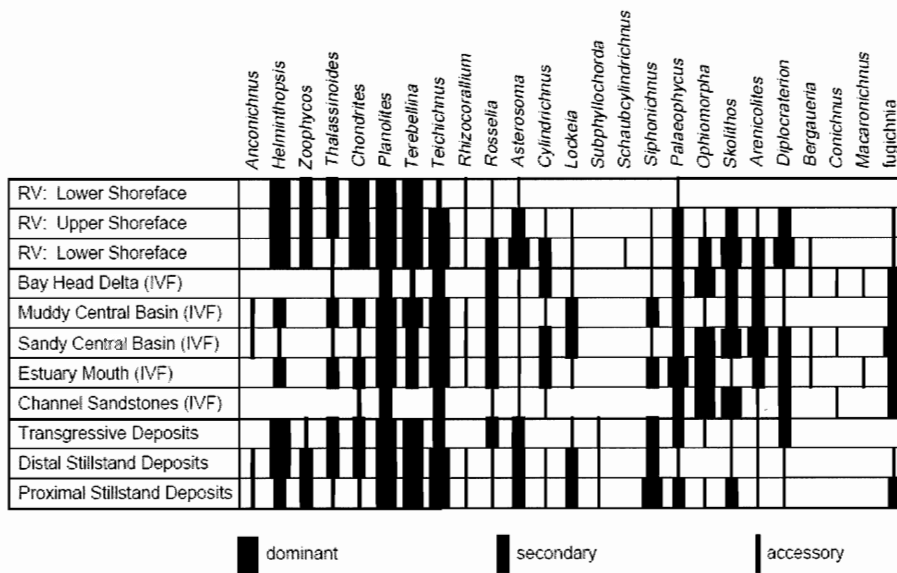
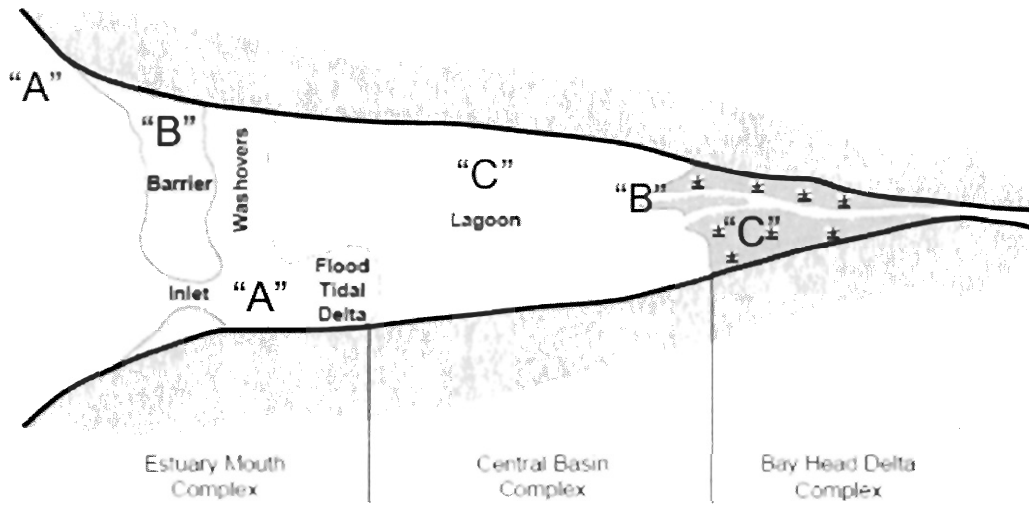


Figure 4.9. Different trace fossils and the range of environments they can survive in. (Pemberton and MacEachern, 1995).

The overall depositional setting is proximal to the coastal plain and contains channel systems, an estuary system, possible barrier complexes, shorefaces, and a lagoonal system. Figure 4.10 shows the depositional environment from a plan view with the possibilities for each log signature labelled.



**Figure 4.10.** This figure shows the plan view of the depositional environment described above for the Bluesky Fomation in Whitecourt Alberta. The log signatures and their location in the depositional environment are labelled A, B, and C. (Pemberton and MacEachern, 1995).

## 5.0 Data analysis

### 5.1 Introduction to the data

Table 5.1 shows a brief summary of the data that will be presented in chapters 5.2 and 5.3, as well as some statistical data from the plotted data sets.

Figure #	Name of plot	Plot Type	Data set used	Correlation coefficient	Trend
5.1	K max	Histogram	all data values	N/A	N/A
5.2	Porosity	Histogram	all data values	N/A	N/A
5.3	K 90	Histogram	all data values	N/A	N/A
5.4	K vert	Histogram	all data values	N/A	N/A
5.5	K max vs Porosity	Log-linear, scatter plot	all data values	0.141	somewhat linear
5.6	K max vs K 90	Log-log, scatter plot	all data values	0.826	linear
5.7	K max vs K vert	Log-log, scatter plot	all data values	0.242	somewhat linear
5.8	Depth vs Kmax	Linear-log, scatter plot	all data values	0.009	non-linear
5.9	Depth vs Porosity	Linear-log, scatter plot	all data values	0.072	non-linear
5.10	K max vs Porosity	Log-linear, scatter plot	fractured	0.114	non-linear
5.11	K max vs K 90	Log-log, scatter plot	fractured	0.999	linear
5.12	K max vs K vert	Log-log, scatter plot	fractured	0.183	non-linear
5.13	K max vs Porosity	Log-linear, scatter plot	unfractured	0.441	somewhat linear
5.14	K max vs K 90	Log-log, scatter plot	unfractured	0.996	linear
5.15	K max vs K vert	Log-log, scatter plot	unfractured	0.663	somewhat linear
5.16	K max vs Porosity	Log-linear, scatter plot	sampled wells	0.436	somewhat linear

**Table 5.1.** Plots used in chapters 5.2 and 5.3 as well as statistical data for each plot. This table encompasses the measurements taken from 883 data points in 36 cores.

The purpose of these cross plots and histograms is to make apparent any factors that may contribute to increases and decreases in permeability and porosity in the Bluesky Formation study area.

### 5.2 Histograms of compiled data

The data in the following histograms have been modified so they could be plotted in the Minitab program. The log to base 10 was calculated for all the permeability values and the corresponding permeability values have been presented in the histograms. A

histogram splits data into bins based on the frequency with which values occur in a data set.

Figure 5.1 is a histogram of K max for all of the data collected. The shape of the histogram is multi-modal and non-symmetric. The centre of the data set is approximately at 1.0 mD. There appears to be both high and low outliers. The values to the high and low end of the plot may be associated with fracturing in the formation. The figure shows that the majority of the data fall between 0.1 and 10 millidarcies. The data beyond these points are interesting because they represent the most and least favorable conditions from a reservoir standpoint. The thin section analysis to follow (Chapter 6.0) sheds some light on the reason for the high and low tails of the histogram.

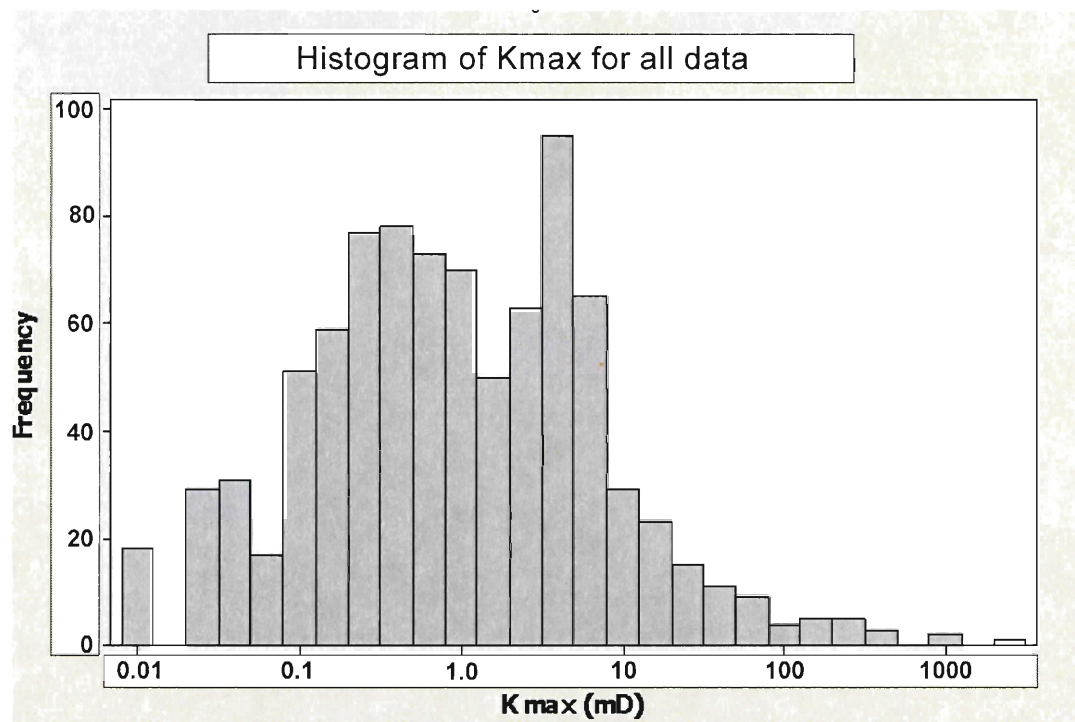


Figure 5.1. Histogram of all the maximum permeability values from the data set.



Figure 5.2 shows a histogram of porosity for all data collected. The shape of the data set is bi to multi-modal and non-symmetric. The centre is approximately 0.095, the majority of the data fall between 5 and 12 % porosity. There appears to be some high outliers that may be associated with coarser grain sizes and less cemented parts of the formation or possibly with fractures. The low end values may be associated with finer grain sizes or more cemented areas.

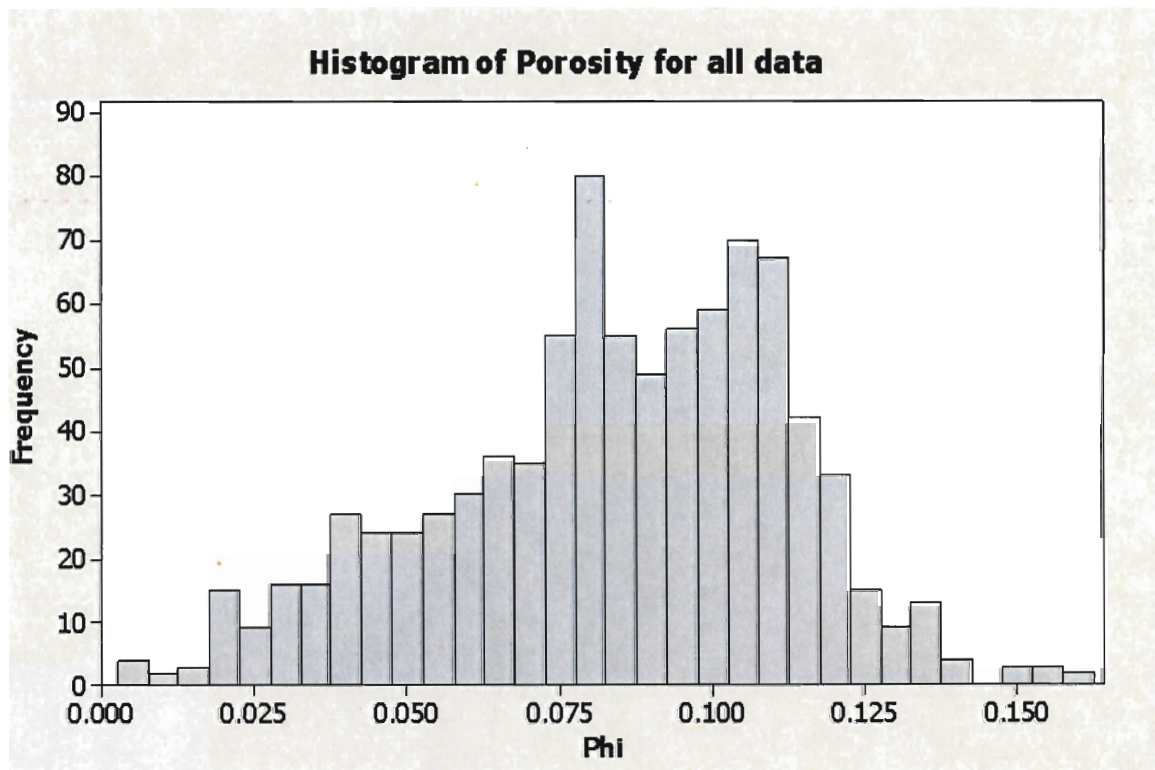


Figure 5.2. Histogram of all the maximum porosity values from the data set.

Figure 5.3 is a histogram of K 90 for all data with a non-zero value for K 90 and K vert. The shape of the data set is bi-modal and shows some symmetry, although skewed to the high end of the scale. The centre is approximately 1.0 mD and there are high and low end outliers. The high end outliers may be associated with fractures or bedding features in the horizontal direction or coarse grain sizes. The abrupt drop in frequency at the higher permeability end of the histogram indicates permeability does not reach above 10 mD in the K90 horizontal direction.

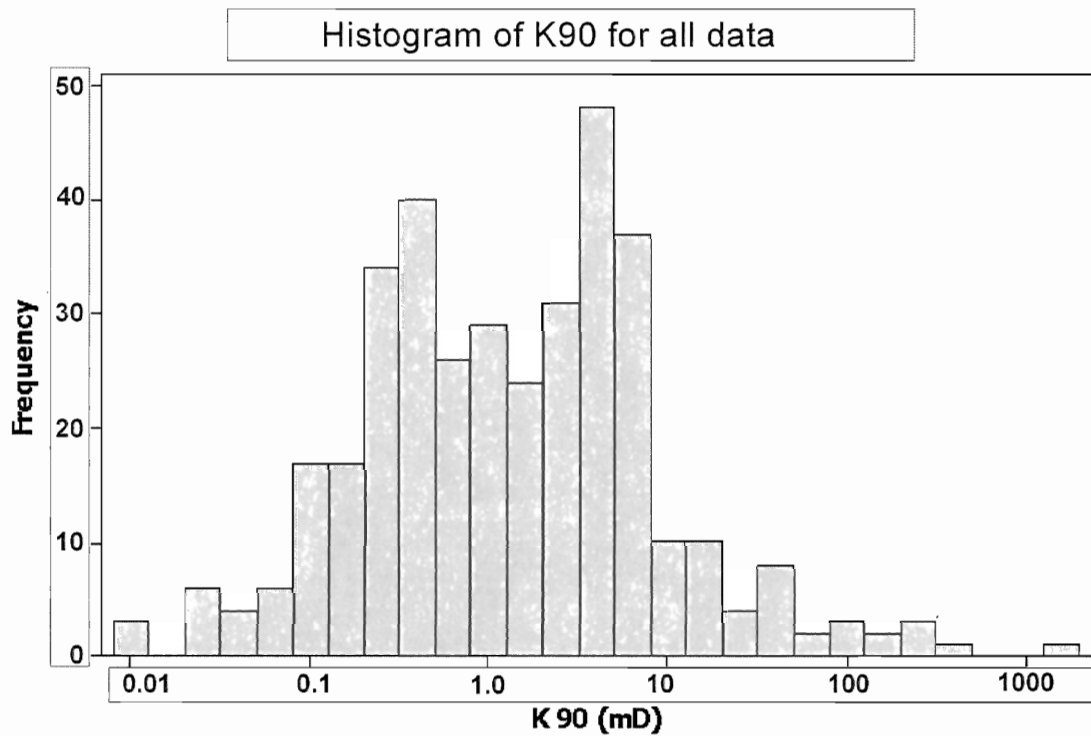
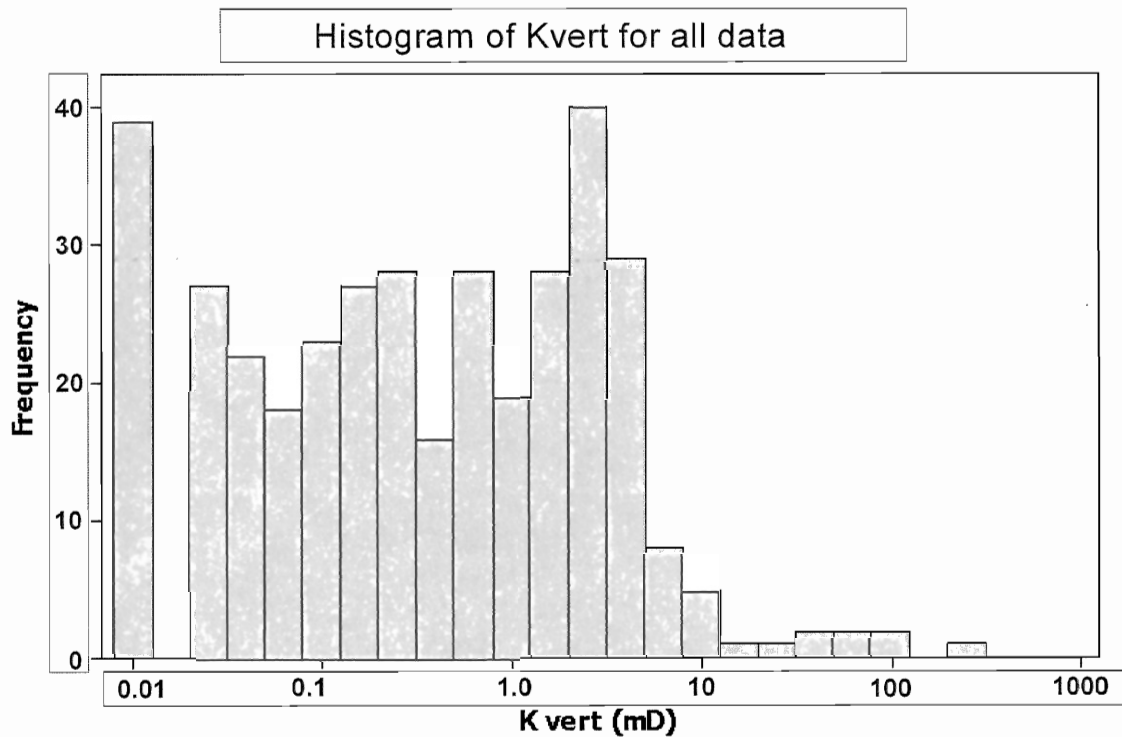


Figure 5.3. Histogram of all the permeability measurements taken 90 degrees from the maximum permeability direction.

Figure 5.4 shows a histogram of  $K_{vert}$  for the data with a non-zero value for  $K_{90}$  and  $K_{vert}$ . The shape of the data set is nearly uniform and has a centre at 0.32 mD. The data at the high end of the scale may be associated with fractures in the vertical direction or may represent a homogeneous coarse grained sand with no vertical barriers to flow.



**Figure 5.4.** Histogram of all the permeability measurements taken vertically through the core (refer to figure 3.3).

### 5.3 Cross plots of compiled data

The plot of Kmax vs Phi (Fig. 5.5) is the maximum permeability measurement taken along bedding plotted against porosity. This plot contains all measurements of maximum permeability and porosity from all 37 of the wells used in this study, both fractured and unfractured data. This plot shows a somewhat linear trend with a broad scatter of points and a correlation coefficient of 0.141. The main body of the plot shows an increase in porosity with an increase in permeability. The majority of the data points fall within the area  $\Phi > 0.06, < 0.12, K_{max} > 0.1, < 10.0$ . Some data points have unusually low Kmax values for a given porosity level. A possible explanation for this might be cementation of the reservoir or closed pore throats from quartz or clay.

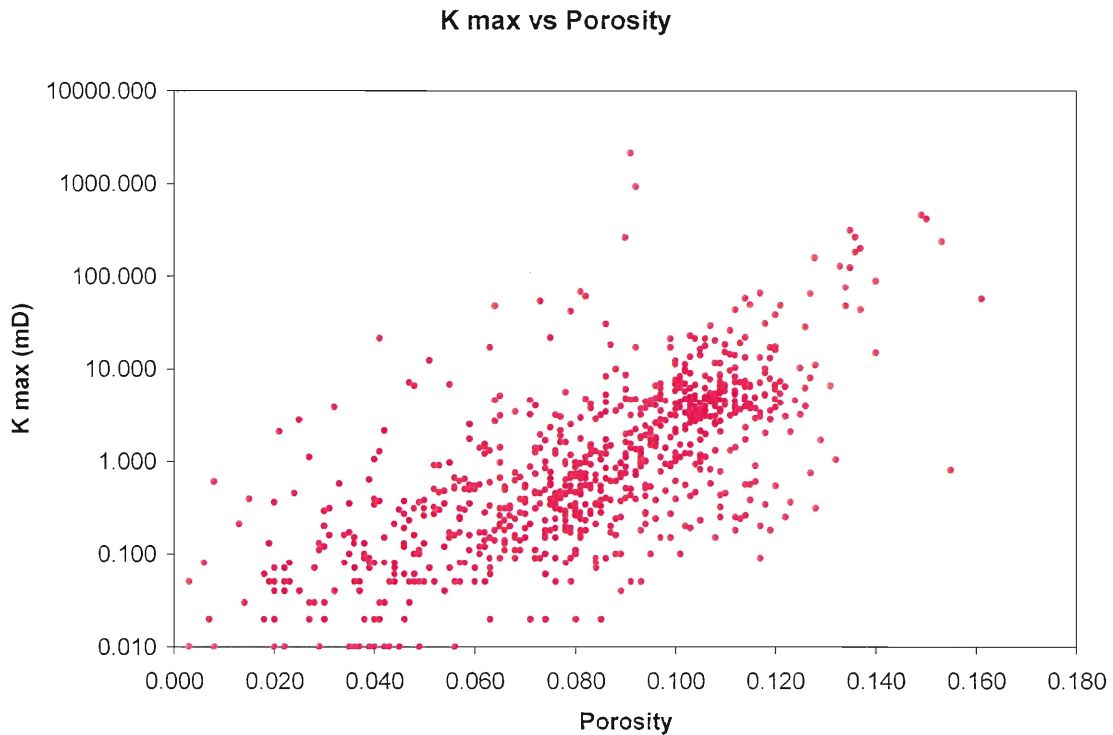
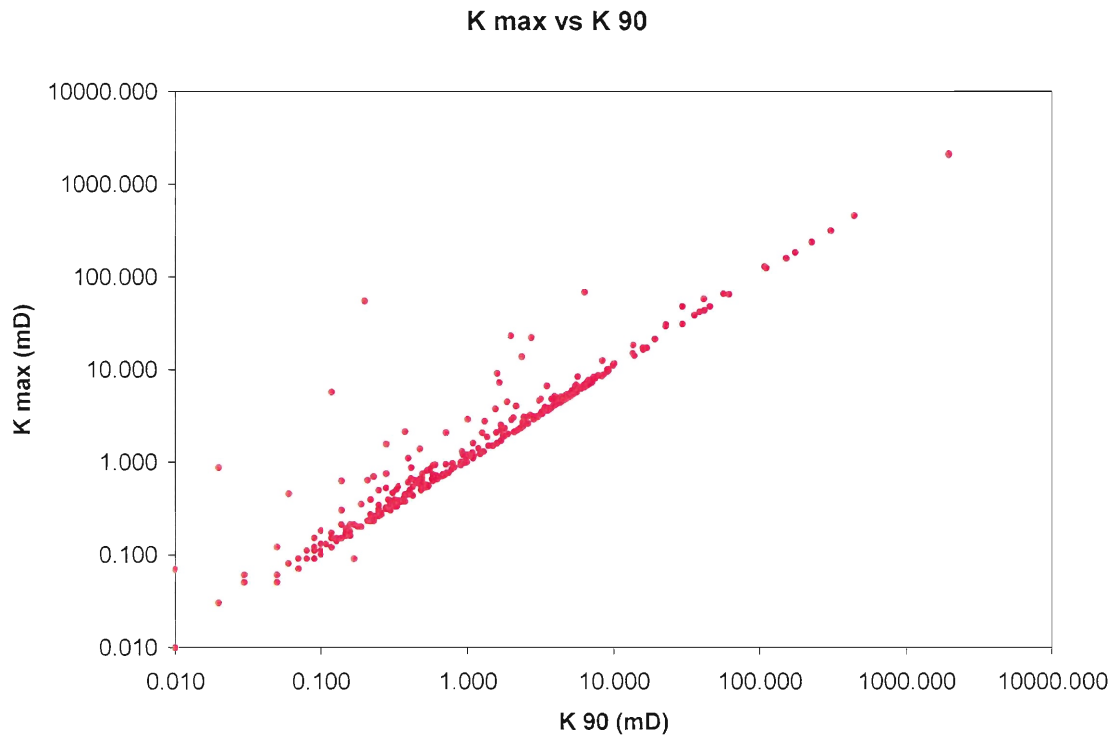


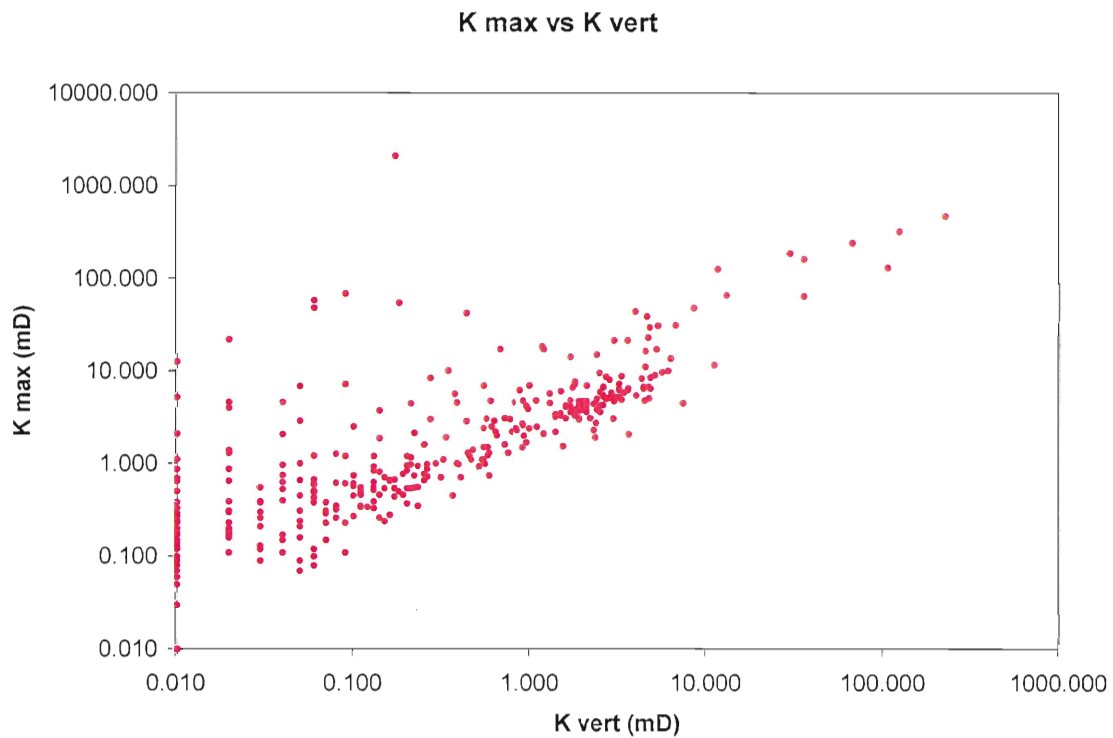
Figure 5.5. Cross-plot of porosity against maximum permeability for all of the data points in the data set.

Figure 5.6 shows a plot of Kmax vs K90. K90 is the permeability measurement taken 90 degrees from the K max measurements. The plot shows a linear relationship between the two permeability measurements with a correlation coefficient of 0.826. There are a few obvious outlying data values with low porosity and high permeability which may be related to fractures in the core. In this plot, there is very little difference between K max and K 90. This is seen in the correlation coefficient being very near 1.



**Figure 5.6.** Cross-plot of maximum permeability against permeability taken 90 degrees from the maximum direction.

Figure 5.7 shows a plot of K max vs K vert. K vertical (K vert) is the measurement of permeability taken vertically on the cylindrical core sample (Fig. 3.3). The plot shows a somewhat linear trend with correlation coefficient 0.242, indicating that the majority of the data points for K max are considerably greater than K vert, which is to be expected. The area where K vertical and K max are both high may represent areas with coarse grain sizes and no cementation, or possibly vertical fracturing. Another possibility is homogeneous sand with few vertical barriers to flow. The points that have both high K max and K vert values are valuable for hydrocarbon recovery because of easier migration of the fluid or gas.



**Figure 5.7.** Cross-plot of maximum permeability against permeability taken vertically through the core (refer to figure 3.3).

Figure 5.8 shows a plot of depth (sub-surface) vs K max to determine if present-day depth has any effect on permeability values. The plot shows a non-linear trend with a correlation coefficient of 0.009. The data falls into groups based on the availability of data at certain depths and shows a slight trend of increased permeability with depth. This could potentially be explained by the formation fining upward. At any given depth, permeability has a very wide range. This indicates no correlation of permeability with depth.

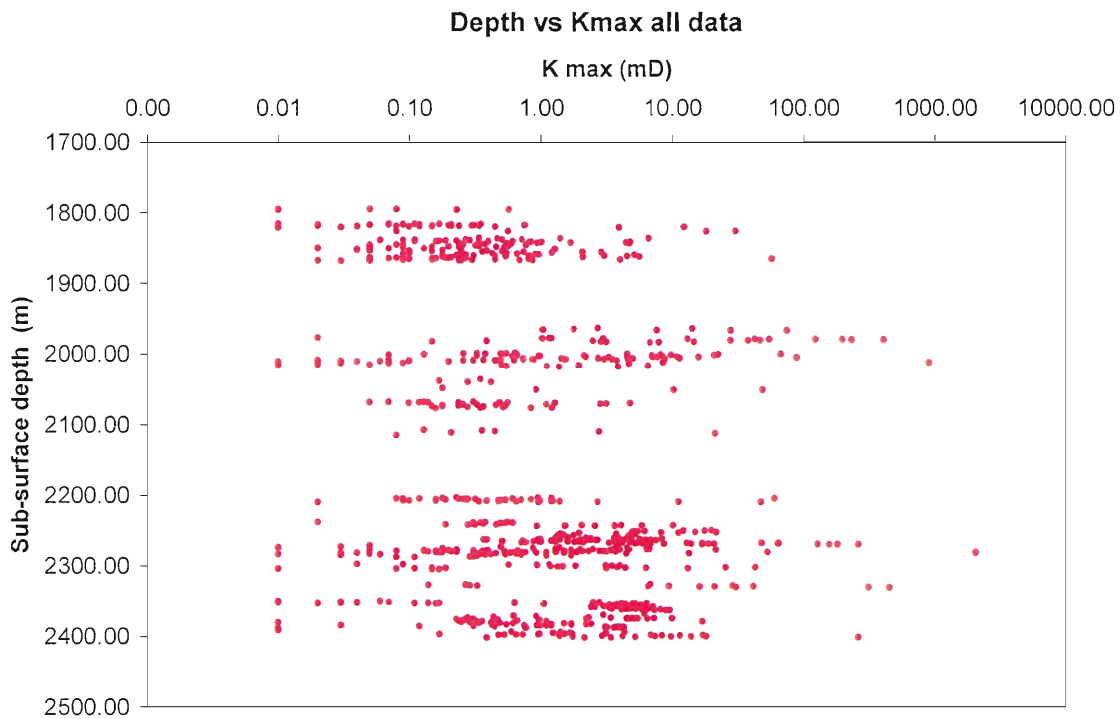


Figure 5.8. Cross-plot of maximum permeability against sub-surface depth for all the data points in the data set.

Figure 5.9 shows a plot of depth vs porosity to determine if present-day depth plays any role in porosity values. The plot has a non-linear trend and a correlation coefficient of 0.072. The data appear in groups which is an artifact of the availability of data at a given depth. From this plot, it is apparent that porosity greater than 0.12 is unlikely at any depth. This is likely a function of grain size and cementation. The porosity shows no decrease with depth, the opposite of what might be expected. This may suggest that burial depth and compaction have had little effect in decreasing porosity. The multi-stage burial and uplift process must be taken into account when looking at the relationship of depth with porosity and permeability and the Bluesky Formation also dips to the SW. Thus, the present-day depth may bear little relationship to the original geological depth of burial.

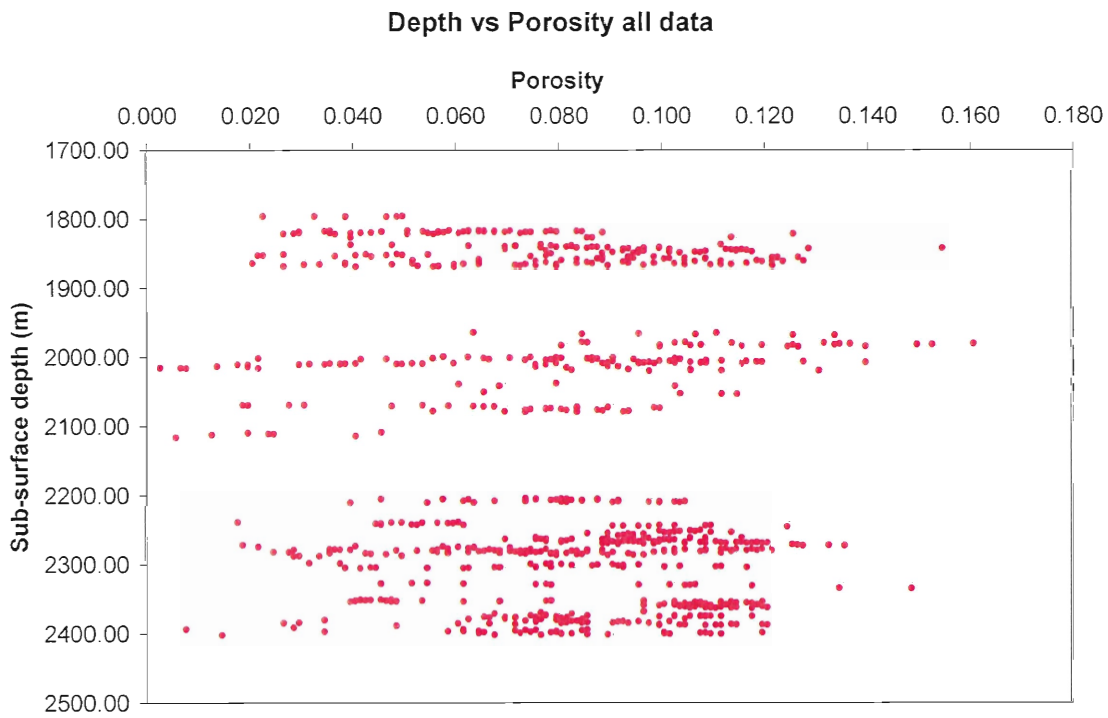
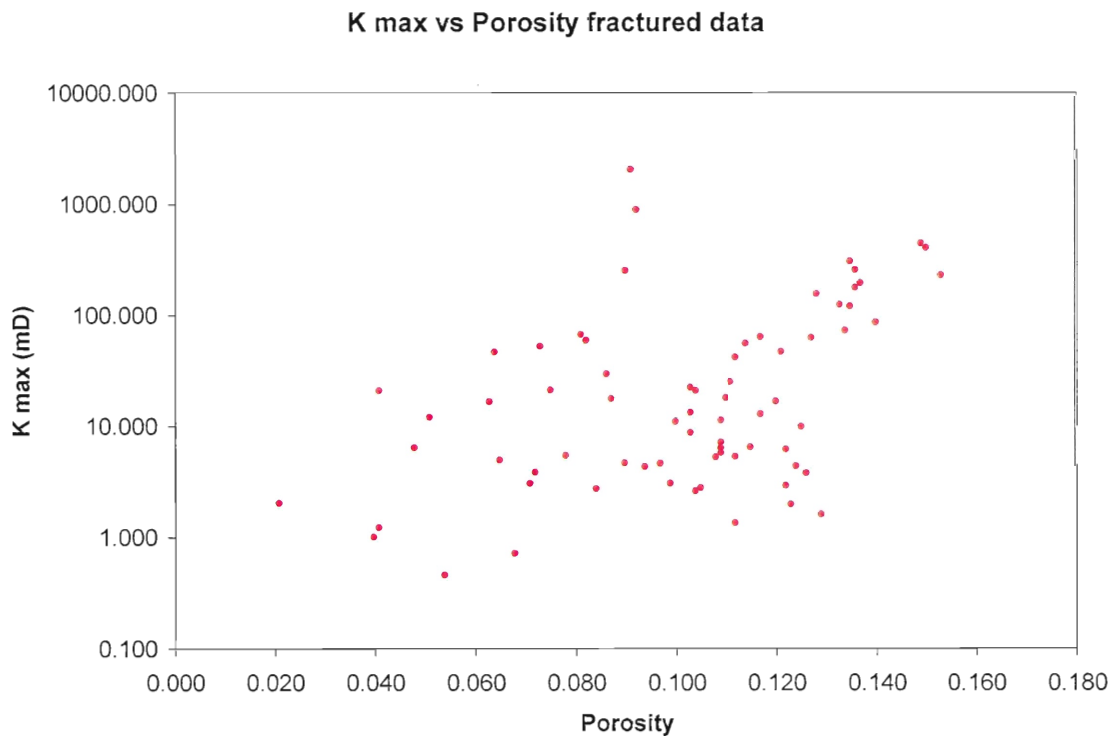


Figure 5.9. Cross-plot of porosity against sub-surface depth for all data points in the data set.

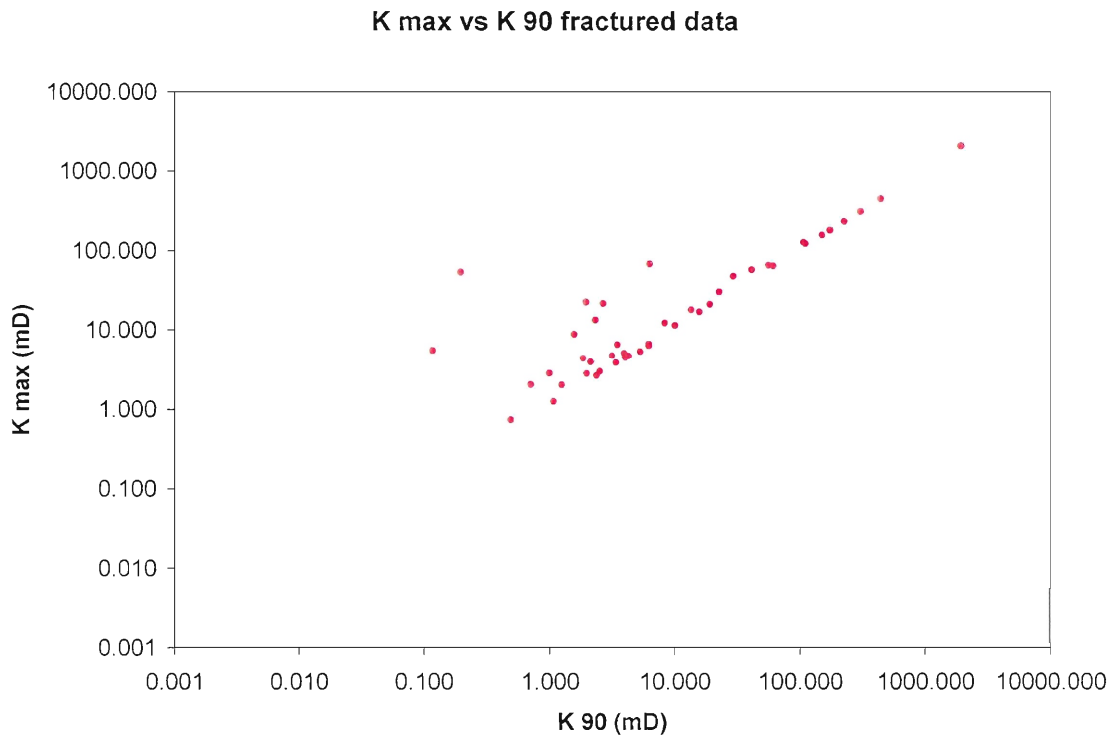


Figure 5.10 shows a plot of the fractured data values of K max vs porosity. These data show a weak trend with a correlation coefficient of 0.114. These values have been determined as anomalous from statistical methods outlined in chapter 3. This plot shows that there is no consistent correlation between high permeability and high porosity values in the fractured data set. For any given value of permeability, there is a wide range of porosity values. However, there does appear to be some clustering of data points with porosities between 0.09 and 0.14 and Kmax between 1.0 and 100. When compared to Figure 5.1, it appears that fracturing may affect both permeability and porosity with higher recorded values for both.



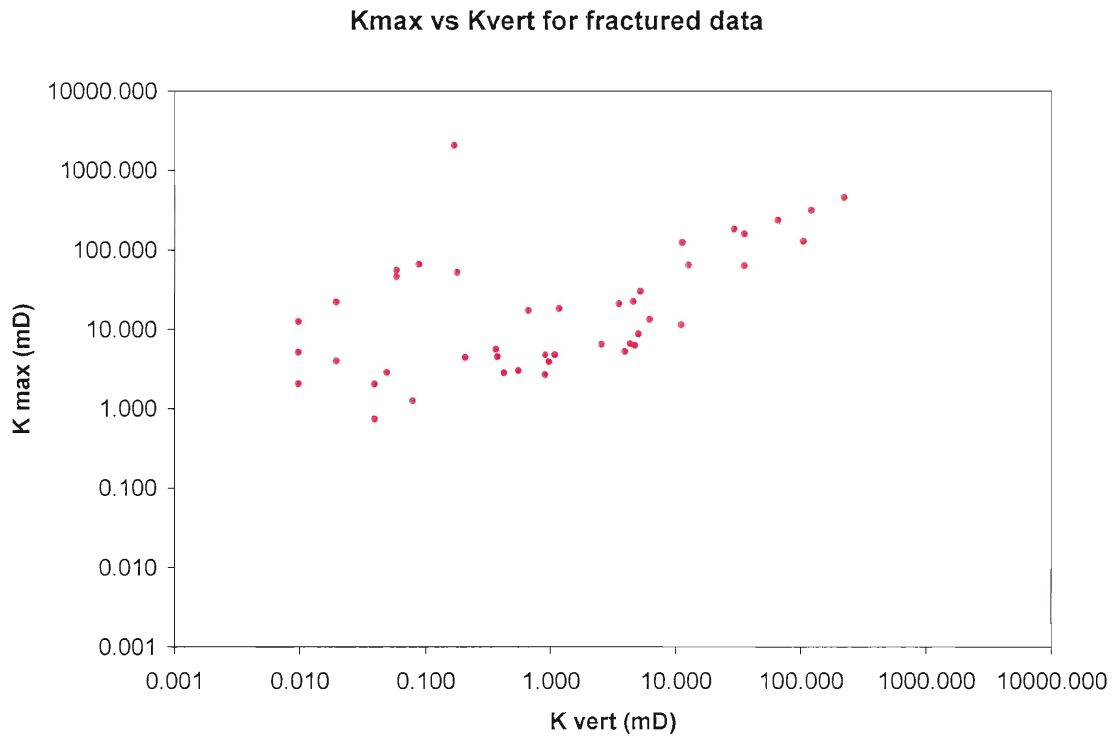
**Figure 5.10.** Cross-plot of porosity against maximum permeability for all fractured data points in the data set.

Figure 5.11 shows a strong linear relationship between K90 and Kmax for the data considered to be fractured, having a correlation coefficient of 0.999. This is important and may suggest that higher permeability values have more relation to bedding and sedimentary features and less relation to possible fractures. Comparing figure 5.7 to figure 5.2, it is evident that the data considered to be fractured may actually have sedimentary or diagenetic features along bedding that causes the increase in permeability.



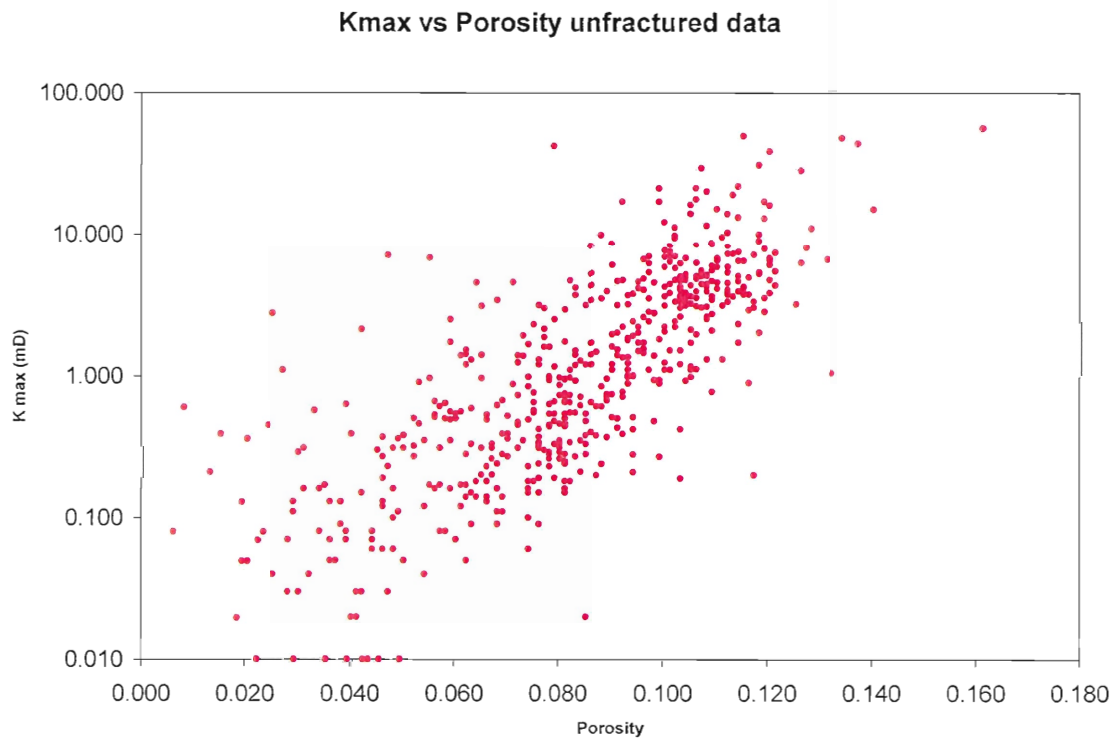
**Figure 5.11.** Cross-plot of maximum permeability against permeability taken 90 degrees from the maximum direction for all fractured data points.

Figure 5.12 shows a plot of  $K_{max}$  vs  $K_{vert}$  for all of the data considered to be fractured. This plot is similar to figure 5.7 and shows that wells having high permeability along bedding also may have high permeability vertically. The trend of the plot is weakly linear, having a correlation coefficient of 0.183. This plot indicates that the data considered to be fractured may indeed be fractured or there may be bedding or sedimentary features creating high permeability in both the horizontal and vertical direction, e.g.: sand having a low percentage of mud or clay. At the low end,  $K_{max}$  is equal to 100 times  $K_{vert}$  and at the high end,  $K_{max}$  is equal to  $K_{vert}$ .



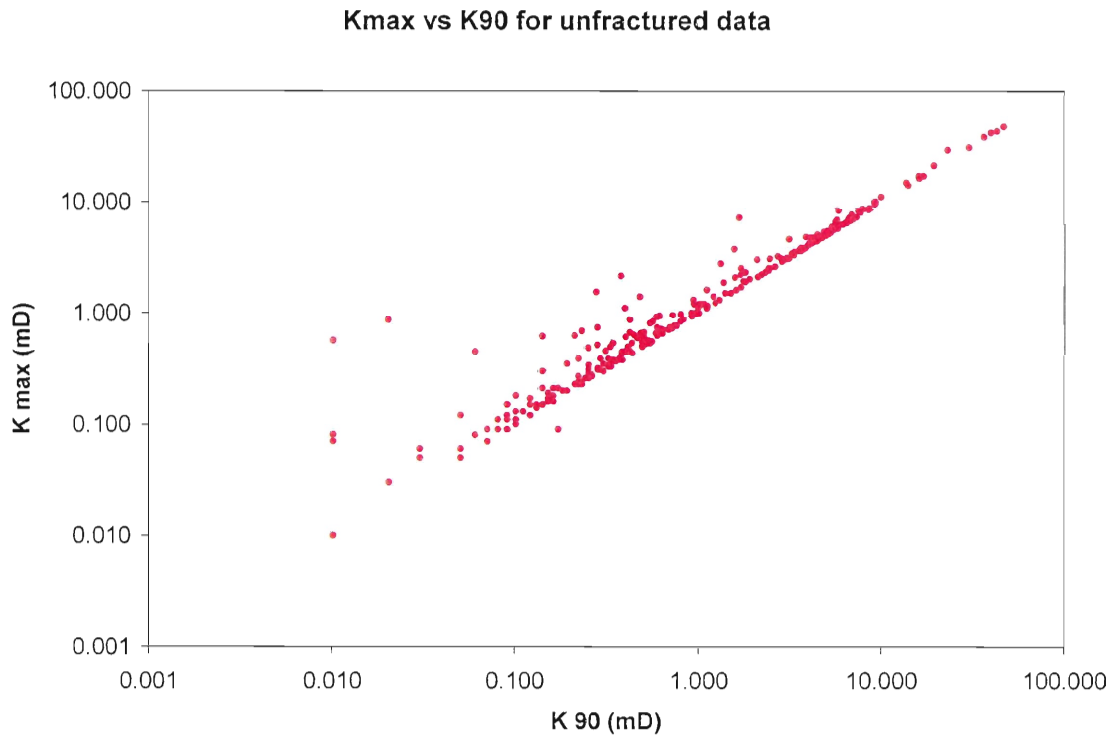
**Figure 5.12.** Cross-plot of maximum permeability against permeability taken vertically through the core (refer to figure 3.3).

Figure 5.13 shows a plot of K max vs porosity for all the data points considered to be unfractured using the statistical method outlined in chapter 3. The plot shows a linear trend between K max and porosity for all the unfractured data points, having a correlation coefficient of 0.441. This coefficient is much higher than the coefficient in Figure 5.7. There appears to be a modest trend of low porosity values associated with low permeability values. For these data, there is evidence of high porosity and corresponding high permeability. The main body of the data is outlined by  $K_{max} > 0.100$  and  $< 100$  and  $\Phi > 0.06$  and  $< 0.120$ . There may be some relationship between high and low porosity permeability values and the diagenetic and sedimentary features found in the rock.



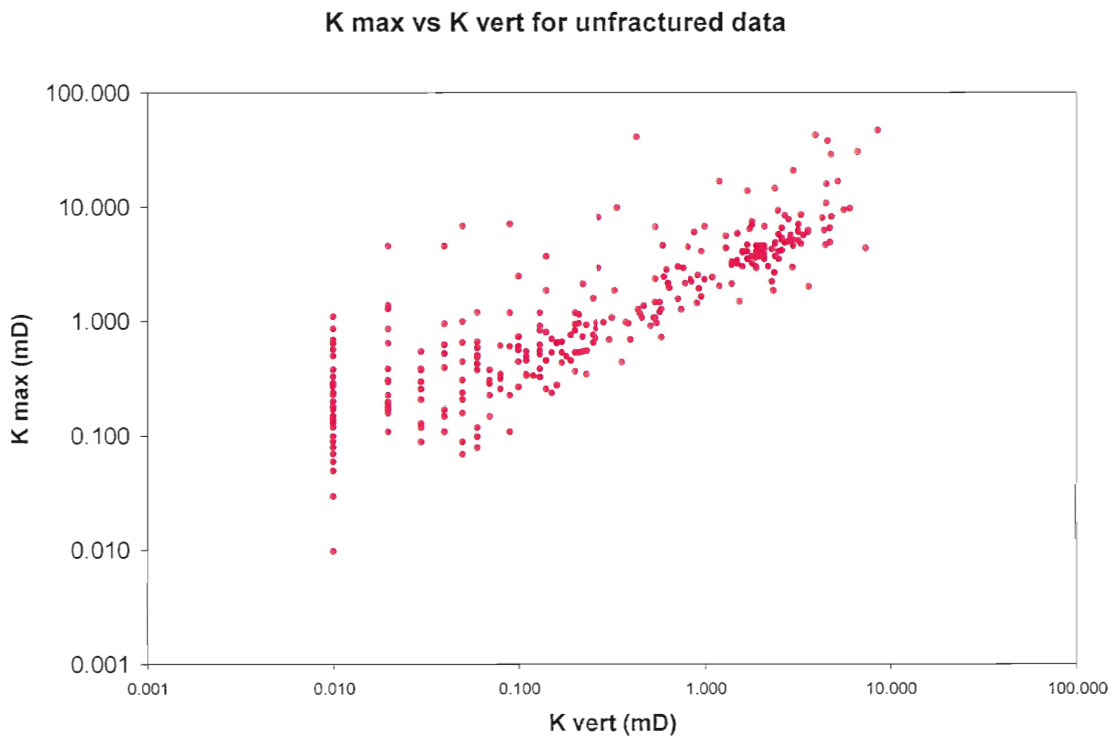
**Figure 5.13.** Cross-plot of porosity against maximum permeability for all unfractured data points in the data set.

Figure 5.14 shows a plot of  $K_{max}$  vs  $K_{90}$  for the data considered to be unfractured. This plot shows a strong linear trend with a correlation coefficient of 0.996. By eliminating any data that may be fractured, this plot shows that an increase in  $K_{max}$  generally leads to an increase in  $K_{90}$ . This indicates that for this data set it is probable the factors controlling higher permeability are related to bedding or sedimentary features in the horizontal direction. However, there are some outlying data points that do not conform to the  $y=x$  line.



**Figure 5.14.** Cross-plot of maximum permeability against permeability taken 90 degrees from the maximum direction for all unfractured data points.

Figure 5.15 shows a plot of K max vs K vert for all of the data points considered to be unfractured. This plot shows a linear trend having a correlation coefficient of 0.663. The moderate correlation coefficient may indicate homogeneous sands with no barriers in the vertical direction. Another explanation is partially cemented fractures in the core that does not yield anomalously high permeability values that would be excluded from this data set. This would represent a limitation of using a statistical method for determining extreme data values and identifying them as fractured or unfractured.



**Figure 5.15.** Cross-plot of maximum permeability against permeability taken vertically through the core for all the unfractured data (refer to figure 3.3).

#### 5.4 *Summary of plots and histograms*

The histograms in this chapter give a good overall view of the frequency of high and low porosity and permeability values contained in the data set. The high permeability values found in the data set may be explained in several ways and the porosity appears to be broadly linked to permeability. It seems possible that the controlling factor for high permeability, at least in part, controls high porosity. It is expected that horizontal (K max) values should be the highest of the permeability measurements. In cases where this is not true, it may be related to fracturing in the formation in either the horizontal or vertical direction. For situations where K 90 is higher than K max, the fractures would be in the horizontal direction. For situations where K vert is higher than K max, the fractures would be in the vertical direction. For examples where K 90 is equally as high as K max, the sands in the formation may be homogeneous and have no specific directional barriers to horizontal flow.

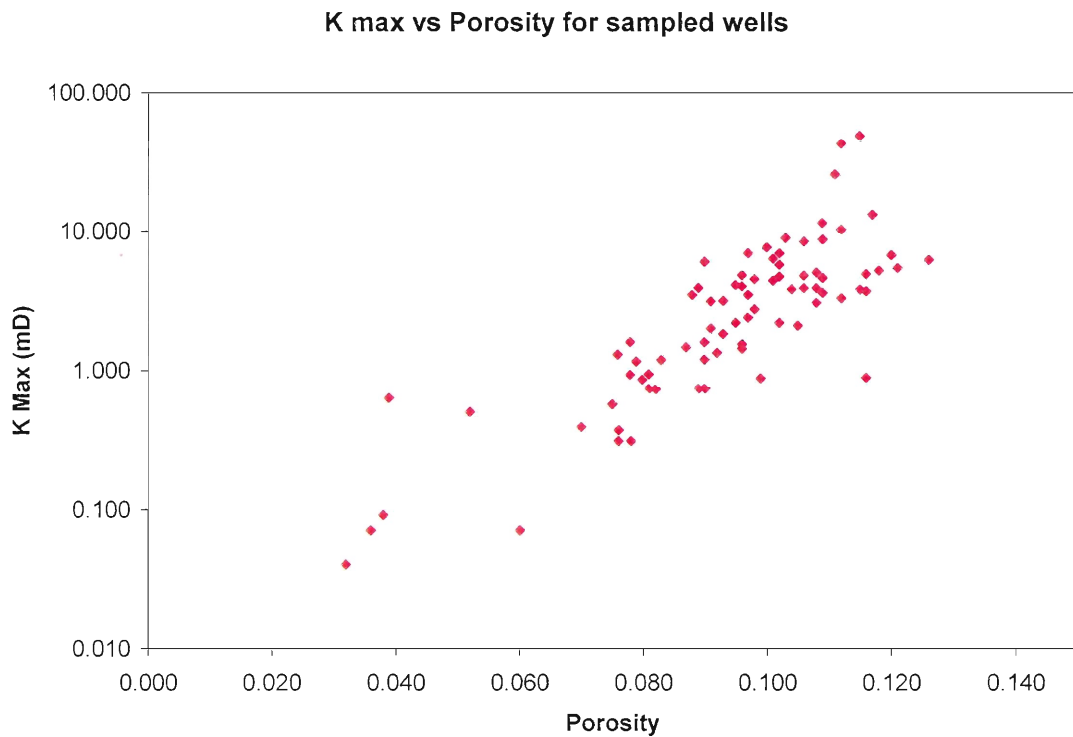
High permeability in the horizontal direction may be created by diagenetic processes taking place after deposition and burial of the sediments. Finer grain sizes and diagenesis could also reduce permeability and porosity with the formation of cement, overgrowths, and stylolites related to compaction of the sediments. Although fracturing and diagenesis may be responsible for the variations in permeability in the data set, the nature of the depositional environment may be the first step in a complex series of steps that determine permeability and porosity for the Bluesky Formation.

This study includes thin section and core analysis from six wells. From those six wells, four have actual porosity and permeability data that have been incorporated into the plots and histograms previously shown. Table 5.3 shows the wells with available data

and the values for minimum, maximum, and mean K max and porosity. Figure 5.16 shows a plot of the mean values of K max against porosity for these four wells.

UWI	K max			Porosity		
	Min	Max	Mean	Min	Max	Mean
00/03-31-060-18W5/0	10.3000	48.8000	20.007	0.1120	0.1150	0.1135
00/12-24-058-18W5/0	0.0400	42.9000	5.9800	0.0320	0.1170	0.0876
00/09-08-058-18W5/0	0.3700	8.7000	3.9980	0.0700	0.1260	0.0997
00/06-25-061-18W5/0	0.0700	11.5000	2.5440	0.0360	0.1160	0.0883

**Table 5.3.** Porosity and permeability statistical data for the wells sampled and logged for this study.



**Figure 5.16.** Cross plot of K max vs porosity for four of the wells used in the thin section and core analysis portion of this study.

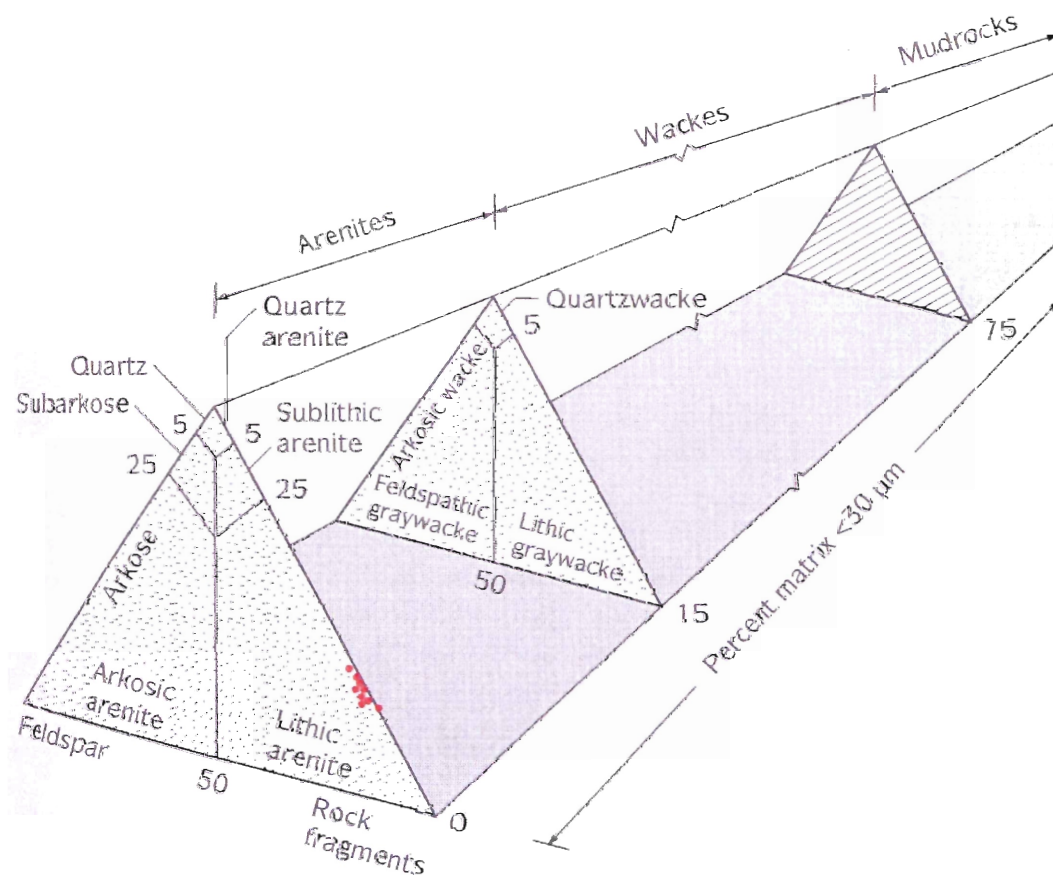
With thin sections, core data, and photos, it may be possible to determine, at least in part, what factors control the permeability and porosity of the Bluesky Formation in the study area.



## 6.0 Thin sections and Diagenesis

### 6.1 Classification

The thin section study of the Bluesky Formation involved using a petrographic microscope to identify the mineral content, mineral percentages, and grain shape and diagenesis. The data collected from the study is presented (Tables 6.1 to 6.11) in the Appendix. The mineralogical framework remained relatively constant over the study area. The mineral percentages did not remain the same and the largest changes occurred in the minerals associated with cementation of the rock. The sections have been analyzed and their percentages have been plotted on a QFL ternary diagram. Figure 6.0 shows the location of the Bluesky thin sections on the QFL diagram.



**Figure 6.0.** Standard QFL diagram used for classifying sandstone based on their composition. The Bluesky samples are shown with the cluster of nine overlying red dots and represent a lithic arenite. The samples taken from the shale intervals were not included on the diagram. (Modified from Dott, 1964).

The figure classifies the Bluesky Formation as a lithic arenite and is based on the nine sandstone thin section samples used in this study. It does not include any of the sampled shale intervals. The Bluesky lithic sandstones contain a very high percentage of lithic grains, a moderate to low percentage of quartz, and virtually no feldspar. An arenite is a texturally clean or matrix poor sandstone (Prothero and Schwab, 1996). Lithic arenites contain quartz (30-80%) and rock fragments (5-50%). The mix of light coloured quartz and dark coloured lithics give the sandstone a salt and pepper appearance (Prothero and Schwab, 1996). This classification agrees with most orogenic clastic wedges consisting of lithic arenites. This is not surprising because of the physical disintegration of mountainous supracrustal rocks associated with collisional orogenies (Prothero and Schwab, 1996).

## 6.2 Thin Section Description

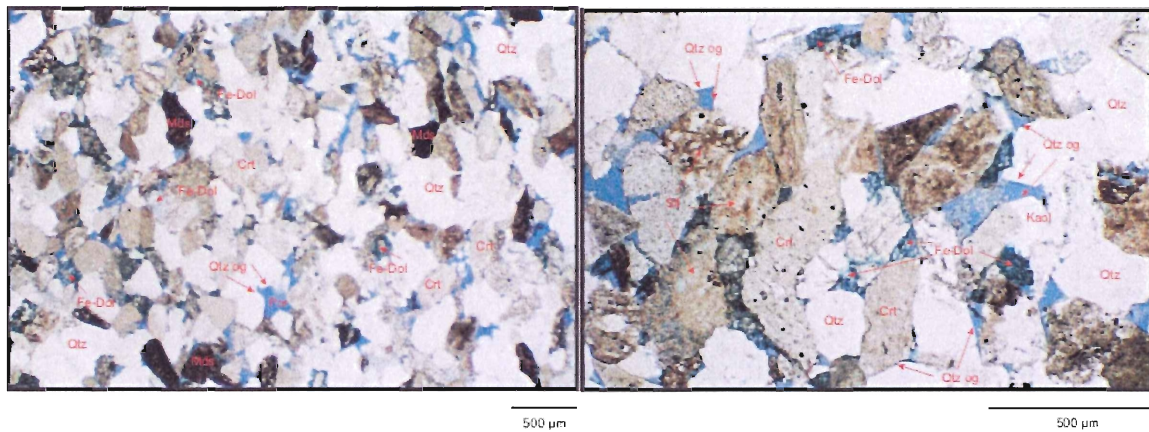
All of the thin sections were photographed (Figs. 6.1 to 6.11) and show some of the many diagenetic processes the Bluesky Formation underwent from the time of deposition. The thin sections are described based on the UWI (Unique Well Identification) number the thin sections were taken from. When looking at the photomicrographs, please refer to Table 6.0.

Minerals	Abbreviation
Chert	Crt
Glauconite	Glauc
Iron Calcite	Fe-Cal
Iron Dolomite	Fe-Dol
Kaolinite	Kaol
Micrite	Mic
Mudstone	Mds
Porosity	Por
Quartz	Qtz
Quartz Overgrowths	Qtz og
Sandstone	Sst
Siltstone	Slt

**Table 6.0.** Shows abbreviations used in thin section analysis and the minerals they correspond to.

### 06-25-061-18W5 Sample # SDWC 6 (Fig. 6.1)

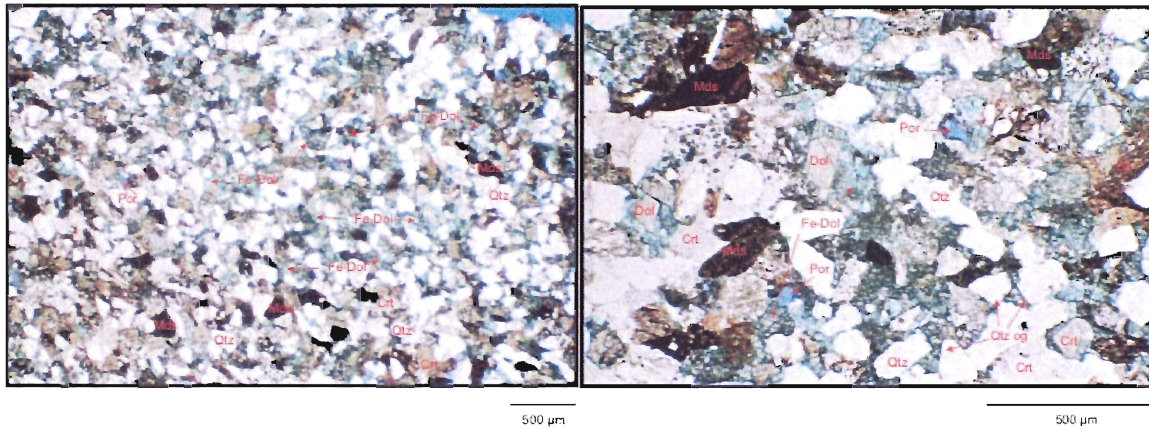
This section is composed mainly of lithic grains, quartz, and chert, with iron dolomite cement and kaolinite in pore spaces. Monocrystalline and polycrystalline quartz are present, as well as overgrowths of quartz, filling the open pore space. The 36X image shows a general overview of the rock while the 90X image shows a close up view. At the 90X magnification, it is apparent that iron dolomite has filled the open pore spaces, reducing porosity. The image also shows kaolinite and quartz overgrowths filling in the open pores. The edges of grain boundaries in this figure show the strain from compaction. Grain boundaries appear irregular and sutured, some grains have been partially or completely dissolved, creating secondary porosity. Some of the dark material lining open pore space in this section may be the remains of dissolved lithic grains or it may be small amounts of bitumen.



**Figure 6.1.** The above photos are of well 06-25-061-18W5, sample SDWC 6. The top photo was taken at 36X magnification and the bottom was taken at 90X magnification. The sample was taken at 2006.5 m depth. (Photo by Jason Lavigne, 2006).

**06-25-061-18W5 Sample # SDWC 7 (Fig. 6.2)**

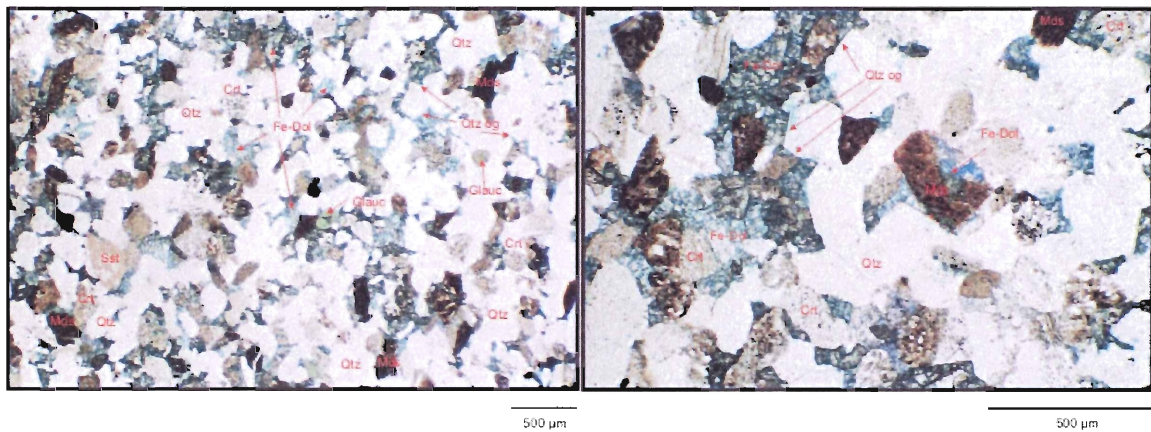
This section contains the same minerals listed in sample SDWC 6 but has a much higher percentage of iron dolomite cement and much lower porosity as a result. This section has a much smaller grain size than the sample SDWC 6 and there are more quartz overgrowths, reducing the porosity in the rock. The 90X image of sample SDWC 7 is approximately the same size as the 36X image of sample SDWC 6. Looking closely at the 36X image of sample SDWC 7, there appears to be some clustering of lithic material which may be in the early stages of stylolite formation.



**Figure 6.2.** The above photos are of well 06-25-061-18W5, sample SDWC 7. The top photo was taken at 36X magnification and the bottom was taken at 90X magnification. The sample was taken at 2007.45 m depth. (Photo by Jason Lavigne, 2006).

### 07-31-058-19W5 Sample # SDWC 8 (Fig. 6.3)

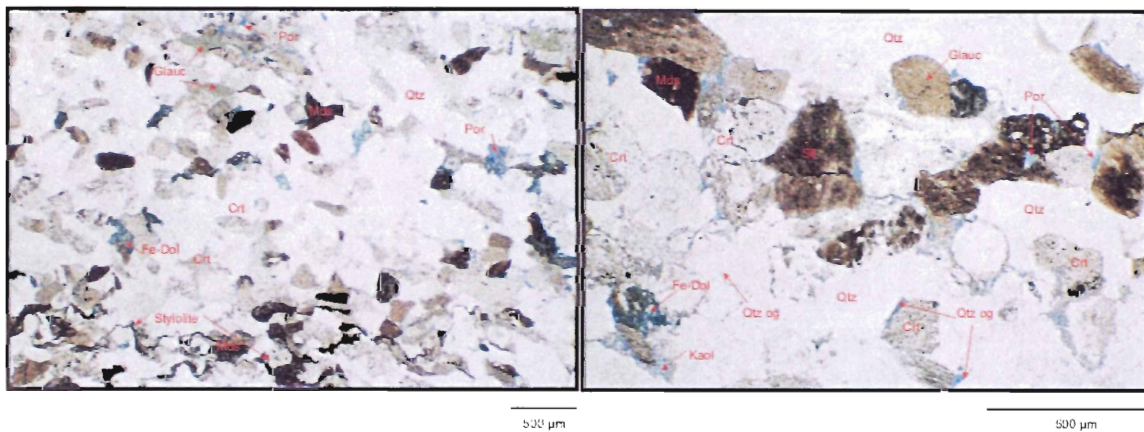
This section is composed mainly of lithic grains, quartz, and chert with iron dolomite cement. The iron dolomite cement has greatly reduced the porosity in this sample. Glauconite is present in trace amounts and appears as pellet grains, not as pore-filling cement. The section contains abundant quartz overgrowths which have also reduced the overall porosity of the rock. In the image taken at 90X magnification, a mudstone grain is being leached out and replaced with iron dolomite cement. This is an example of secondary porosity being created by the leaching of less resistant grains. However, the pore space has been partially filled with iron dolomite cement. The sutured and irregular grain boundaries show the degree of compaction in the formation.



**Figure 6.3.** The above photos are of well 07-31-058-19W5, sample SDWC 8. The top photo was taken at 36X magnification and the bottom was taken at 90X magnification. The sample was taken at 2223.4 m depth. (Photo by Jason Lavigne, 2006).

### 07-31-058-19W5 Sample # SDWC 9 (Fig. 6.4)

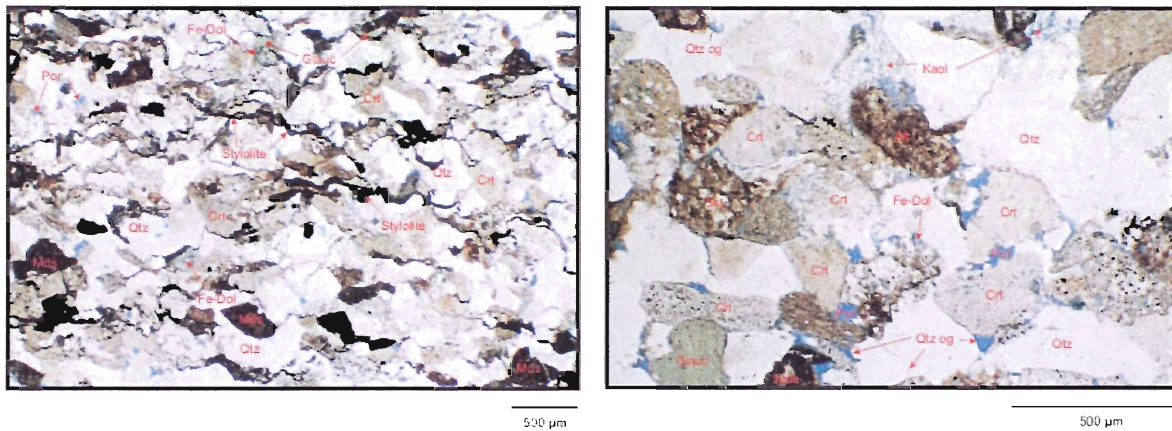
This section contains the same minerals listed in sample SDWC 8 but has a much lower percentage of iron dolomite cement and much lower porosity as a result of grain size, compaction, and formation of stylolites. This section has a slightly coarser grain size than SDWC 8 but with more quartz overgrowths, reducing the porosity. The abundance of quartz overgrowths as well as the presence of stylolites indicates the degree of compaction this rock has undergone. Comparing SDWC9 to SDWC 8, there is a change in the degree of compaction moving deeper down the core. The grain boundaries in the 90X magnification image of this section show more intense alteration (sutureing) than in SDWC 8, which suggest an increase in compaction despite only a few metres increase in depth.



**Figure 6.4.** The above photos are of well 07-31-058-19W5, sample SDWC 9. The top photo was taken at 36X magnification and the bottom was taken at 90X magnification. The sample was taken at 2227.85 m depth. (Photo by Jason Lavigne, 2006).

### 07-31-058-19W5 Sample # SDWC 10 (Fig. 6.5)

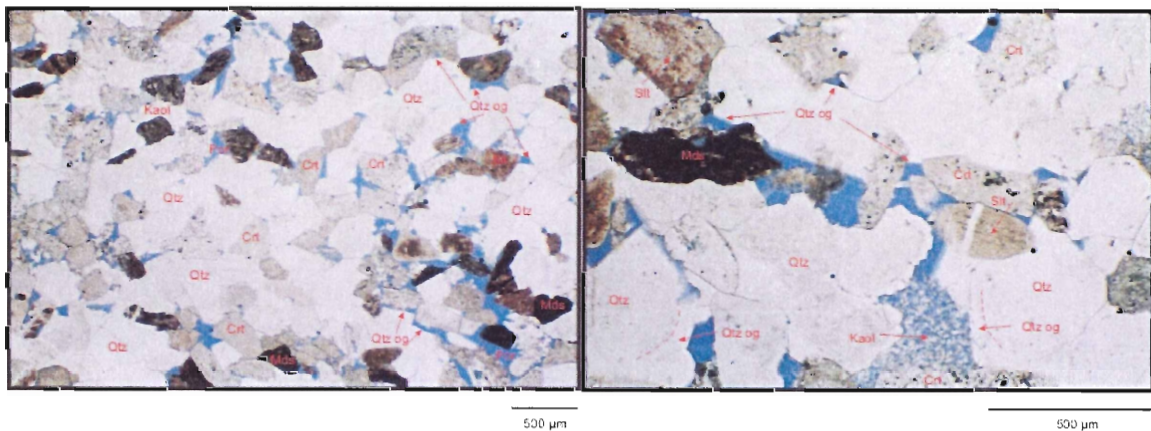
This thin section contains the same minerals listed in sample SDWC 9 but has a lower percentage of iron dolomite cement and much lower porosity, as a result of compaction, than either of the previous samples (SDWC 8 or SDWC 9). Dissolution of grains has created some secondary porosity. This section has a similar grain size as SDWC 8 and 9 but there are more quartz overgrowths reducing porosity. Looking at the upper portion of the slide in the 36X image of SDWC 10, there is clustering of stylolites and they appear to be connected. The abundance of quartz overgrowths as well as the presence of stylolites indicates the degree of compaction this rock has undergone. Comparing SDWC 8 and 9 to SDWC 10, there is an increase in the degree of compaction moving down the core.



**Figure 6.5.** The above photos are of well 07-31-058-19W5, sample SDWC 10. The top photo was taken at 36X magnification and the bottom was taken at 90X magnification. The sample was taken at 2231.4 m depth. (Photo by Jason Lavigne, 2006).

### 09-08-058-18W5 Sample # SDWC 5 (Fig. 6.6)

This section is composed mainly of lithic grains, quartz, chert, kaolinite cement, and quartz overgrowths. The long contacts along grain boundaries indicate the degree of strain put on the formation during compaction. This section contains both primary and secondary porosity. Grain boundaries appear irregular and slightly sutured. Some grains have partially or completely dissolved, creating the secondary porosity in this thin section. This sample shows 10 percent porosity which is moderate for the Bluesky Formation in the study area. It appears that this portion of the formation has not undergone as much compaction as other portions due to the lack of stylolites and the less altered grain boundaries. Some of the grain boundaries may appear less altered by the overgrowth of quartz covering the original boundary. This section contains dust rims where the overgrowth of quartz has covered the original quartz grain boundaries. These have been labeled with a red dotted line in the photos.

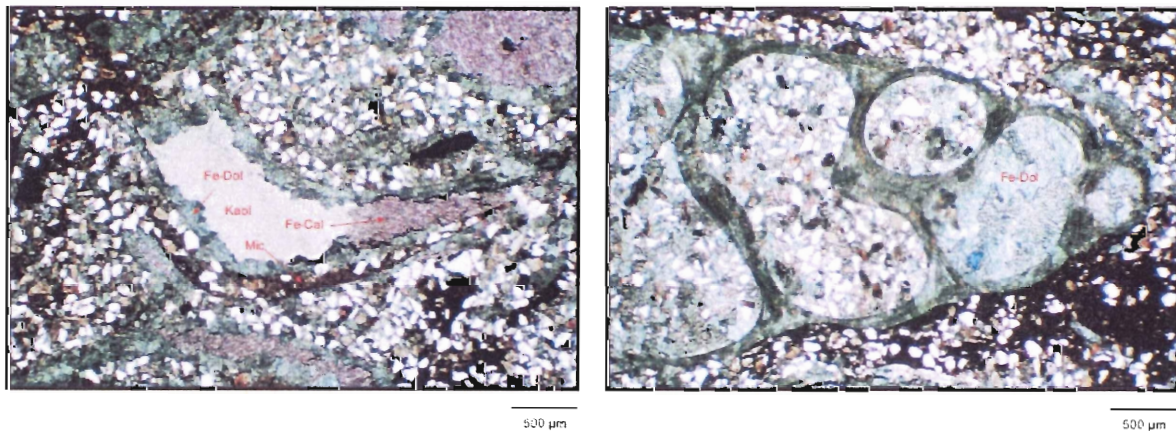


**Figure 6.6.** The above photos are of well 09-08-058-18W5, sample SDWC 5. The top photo was taken at 36X magnification and the bottom was taken at 90X magnification. The sample was taken at 2261.43 m depth. (Photo by Jason Lavigne, 2006).



### 03-31-060-18W5 Sample # SDWC 11 (Fig. 6.7)

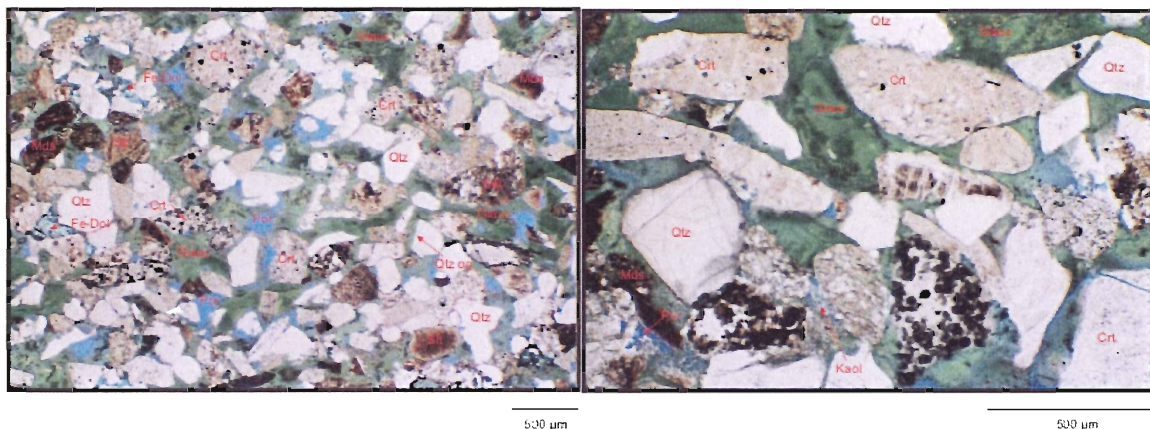
This sample was taken from a section of the core containing a shell bed. The photos show a bivalve shell and a gastropod shell, detrital grains, as well as the minerals that have filled the shell during the deposition and diagenetic process. This sample has not been included in the tables in Appendix A and no mineral percentages were taken because of the location of the sample within a shale section of the core. This section is important because it shows steps in the diagenetic process for this portion of formation and perhaps may be extrapolated to other cores in this study. The top photo shows a bivalve shell that has been outlined with micrite, then an inner lining of iron dolomite was emplaced, followed by the formation of a pyrite / bituminous lining (black lines around inner shell lining), followed by infilling of the shell with iron calcite, and finally the remaining space was filled with kaolinite. The gastropod shell shows only iron dolomite cement infilling. The remainder of the gastropod shell has been filled with clastic material.



**Figure 6.7.** The above photos are of well 03-31-060-18W5, sample SDWC 11. The photos were taken at 36X magnification. The sample was taken at 2053.7 m depth. (Photo by Jason Lavigne, 2006).

### 01-29-061-17W5 Sample # SDWC 3 (Fig. 6.8)

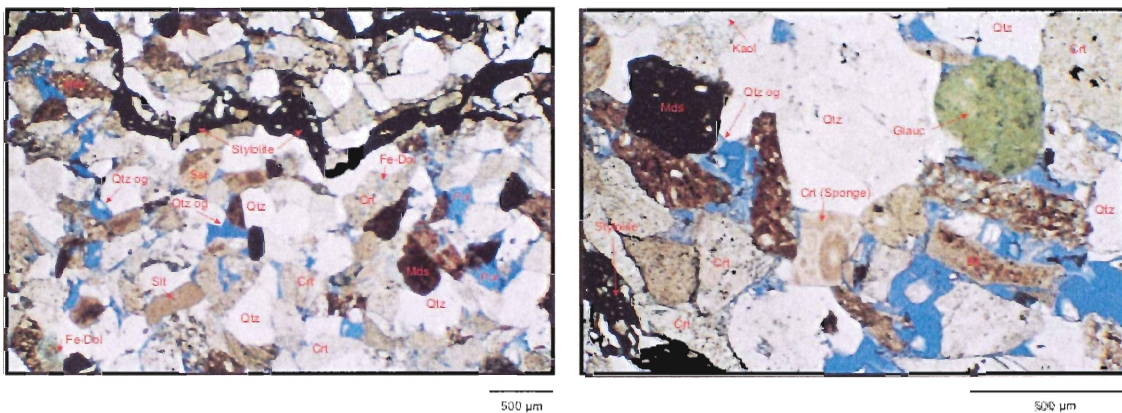
This section is composed mainly of lithic grains, quartz, chert, iron dolomite and glauconite cement, as well as quartz overgrowths. There is also a minor component of kaolinite filling pore space. The grain boundaries in this figure show some strain put on the formation from compaction. The long contacts along grain boundaries appear somewhat irregular and some grains have partially dissolved, creating minor secondary porosity. The sample shows approximately 15 percent porosity which is high for the Bluesky Formation in the study area. It appears that this portion of the formation has not undergone as much compaction as those in some of the other cores. Some of the grain boundaries may appear less irregular from the overgrowth of quartz covering the original boundary. The glauconite in this section has not filled in all the pore space as it has done in other samples and appears to have had little cementation. The 90X photo of the section shows a chert grain that contains crystals of iron calcite, visible as small dark coloured dots within the crystal.



**Figure 6.8.** The above photos are of well 01-29-061-17W5, sample SDWC 3. The top photo was taken at 36X magnification and the bottom was taken at 90X magnification. The sample was taken at 1905.43 m depth. (Photo by Jason Lavigne, 2006).

### 01-29-061-17W5 Sample # SDWC 4 (Fig. 6.9)

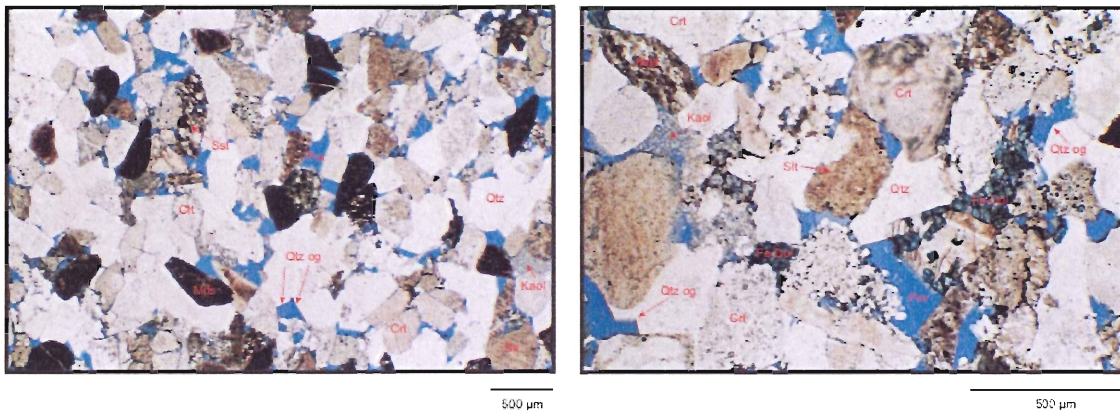
This section contains the same minerals present in sample SDWC 3 however the glauconite content is much lower. The glauconite is largely in the form of pellets and less wispy than the glauconite filling pore throats in sample SDWC 3. There is less cementation in this sample but the compaction is much greater than SDWC 3. Both photos show stylolites and sutured and irregular grain boundaries that are associated with leaching and dissolution during compaction. It appears that the lack of cement in this sample has been nearly offset by a higher degree of compaction, leaving similar porosity as that found in SDWC 3. The 90X image shows a large pore that was not destroyed during compaction but the pore has been partially reduced by quartz overgrowths. The image also shows the remnants of a microfossil, possibly a sponge spicule.



**Figure 6.9.** The above photos are of well 01-29-061-17W5, sample SDWC 4. The top photo was taken at 36X magnification and the bottom was taken at 90X magnification. The sample was taken at 1907.7 m depth. (Photo by Jason Lavigne, 2006).

### 12-24-058-18W5 Sample # SDWC 1 (Fig. 6.10)

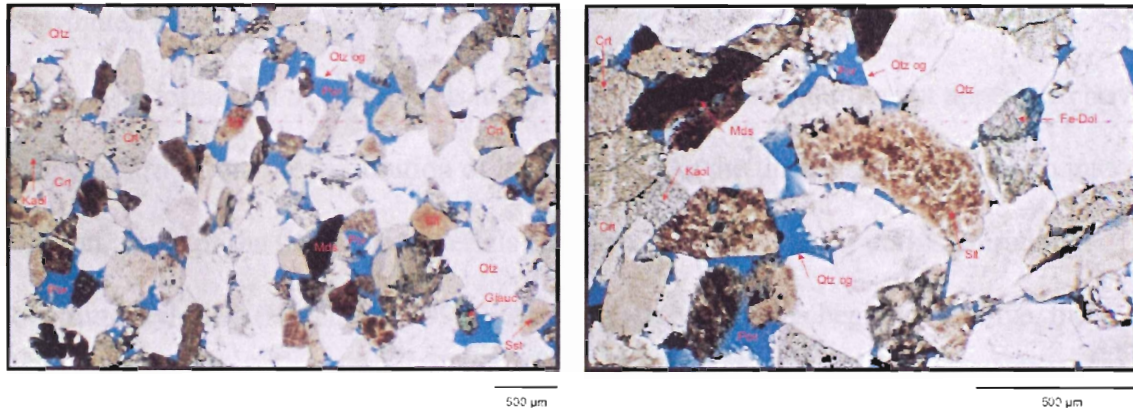
This section is composed mainly of lithic grains, quartz, chert, iron dolomite, kaolinite, and quartz overgrowths. This section has only trace amount of glauconite in the form of pellets. The section does not show the compaction features found in some other samples. Some of the chert grains appear to have been partially dissolved and replaced by what appears to be iron calcite. In the 90X image, several lithic clasts show partial dissolution and are replaced by iron dolomite. The pores in this sample are large but have some invasion from quartz overgrowths. Secondary porosity was created by the dissolution of lithic and chert clasts but a portion of that porosity was reduced by quartz overgrowths and iron dolomite cement. The chert grain the upper middle portion of the 90X image shows the same type of pattern as that in sample SDWC 4 and probably contains microfossils.



**Figure 6.10.** The above photos are of well 12-24-058-18W5, sample SDWC 1. The top photo was taken at 36X magnification and the bottom was taken at 90X magnification. The sample was taken at 2295.3 m depth. (Photo by Jason Lavigne, 2006).

### 12-24-058-18W5 Sample # SDWC 2 (Fig. 6.11)

This section contains the same minerals present in sample SDWC 1. There are more quartz overgrowths and greater compaction than seen in SDWC1, reducing the porosity. The iron dolomite cement and kaolinite are less abundant in this sample. The 90X image shows large pore spaces that have not been destroyed due to compaction but contain abundant quartz overgrowths. Some of the lithic grains are being dissolved and replaced by what appears to be iron dolomite. The removal of lithic grains has also created secondary porosity.



**Figure 6.11.** The above photos are of well 12-24-058-18W5, sample SDWC 2. The top photo was taken at 36X magnification and the bottom was taken at 90X magnification. The sample was taken at 2300.6 m depth. (Photo by Jason Lavigne, 2006).

### 6.3 Diagenesis of the Bluesky Formation

The thin sections show many diagenetic features that may be applied to the Bluesky Formation as a whole. The location of the wells used is spread over the study area and the different areas show slightly different aspects of diagenesis. The diagenetic process is complex and the exact order of the processes has not been established by this study. However, an attempt will be made to put the diagenetic processes in sequential order for all of the Bluesky Formation in the study area.

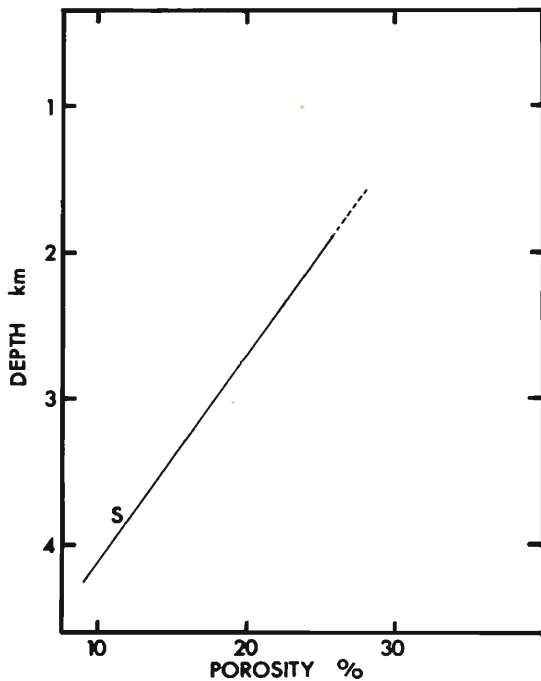
All the samples have some features in common. Quartz overgrowths are common to all samples and are a common feature of sandstones that have undergone strong compaction. As the quartz grains are pressured, silica begins to go into solution (pressure solution). The silica is then transported in the waters that percolate through the rock. Once the silica reaches an area of lower pressure, the silica precipitates out of the water and begins to grow new crystal faces onto existing quartz crystals. This most commonly occurs in the open pore space found in sandstone (Hutcheon, 1990). However, numerous other sources of silica (e.g., dissolution of siliceous fossils and chert) may have also contributed silica.

The formation of stylolites is also a result of pressure solution but appears to have been primarily from the dissolution of lithic clasts. As the lithic grains begin to go into solution, some of the insoluble materials combine, forming lines of dark material that constitute stylolites (Hutcheon, 1990). As the grain boundaries begin to dissolve, the rock compacts, squeezing off the open pore space and reducing the porosity of the rock.

Dissolution of less resistant lithic grains have in some cases created secondary porosity. Cementation and overgrowths seem in many cases to have offset any secondary porosity that may have been created from this process.

The early stages of grain dissolution and stylolite formation can be found in the samples. The suturing and dissolution of grain boundaries to create jagged, irregular edges are symptomatic of compaction in sandstone (Hutcheon, 1990). The driving force behind the formation of the diagenetic features presented thus far is compaction of the rock. This removes grains that contain soluble elements and concentrates the elements that are less soluble (stylolites). Figure 6.13 shows the effect burial depth and

compaction has on a sandstone reservoir. As burial depth increases, the porosity declines in a linear trend. As depth approaches 4 km, the reservoir may still have up to 10 % porosity remaining. This may indicate that something other than burial depth and compaction has the greatest control on reducing porosity.



**Figure 6.13.** A plot of change in porosity (%) with burial depth (km). (Modified from Schmidt and McDonald, 1979a).

The samples in this study have been subjected to burial depths of at least 1900 m and it can be assumed they have undergone diagenetic processes associated with at least that depth of burial and degree of pressure and associated compaction.

The authigenic clay in the Bluesky samples reduces the primary porosity that would have existed at the time of deposition of the sediment. The clays are transported to the pore space by waters rich in dissolved material. The water contains elements for the formation of the glauconite and kaolinite, the two main types of clay mineral seen in the thin section samples. The water and dissolved materials may come from a variety of sources such as connate saline water (seawater), percolating groundwater, or transfer of

pore waters from shale to sandstone (Hutcheon, 1990). The presence of glauconite in sample SDWC 3 is the controlling factor in the low porosity of the thin section. Glauconite seems to fill pore throats nearly completely, where present (Fig. 6.8). In this section, grains appear isolated, i.e., glauconite formed prior to much compaction or cementation of the rock. This may suggest that glauconite formed early, during deposition on the sea floor. Kaolinite is present in the majority of the samples but is rarely abundant and does not act as the primary pore reducing clay in the sample. Kaolinite fills pore throats that have quartz overgrowths projecting into them (Fig. 6.6). From this, it appears that the quartz overgrowths predate the kaolinite placement.

The cements commonly found in the samples are carbonate cements. Both iron dolomite and iron calcite are common in the samples but the iron calcite is usually found only in trace amounts whereas the iron dolomite forms the main cement in samples SDWC 7, SDWC 8. It is present in smaller amounts in nearly all of the other samples. Iron calcite and iron dolomite cement begin as waters rich in dissolved Fe, Mg, and Ca. As the water moves through the rock, carbonate cement containing iron is precipitated in open pore spaces. As the cement forms, it begins to close off the primary porosity (Prothero and Schwab, 1996). Figure 6.3 shows iron dolomite replacing a dissolved lithic grain. At least in this case, dolomite cement post-dated dissolution. This indicates that there may have been several stages of cementation.

The timing of formation of the cements may be summarized by the stages present in sample SDWC 11 (Fig. 6.7). The following are the proposed stages of cementation of the Bluesky Formation in the study area. The first stage was the development of iron dolomite which would have cemented the sands early in the diagenetic process, leaving



little room for any clay formation/migration. The second stage was the formation of small amounts of iron calcite cement and minor pyrite formation. The third stage was the formation of glauconite and kaolinite. During this process, some areas were either poor in carbonate cements from the beginning or the carbonates were dissolved leaving space for the clay minerals to replace the carbonate as the cement. While all of the precipitation and dissolution of cement was taking place, the formation was being buried to increasingly greater depths. The increase in compaction caused strain on grain boundaries and began to dissolve quartz and lithic grains. The dissolving materials were then in solution and proceeded to migrate through the formation until they precipitated in lower pressure areas, filling open pore space. The diagenetic process destroyed some primary porosity but created secondary porosity by dissolution of grains. Although stylolite formation liberated some material, whether that material acted as cement in pore space cannot be determined within the scope of this study. The dissolved materials may have come from many different sources at different times. The samples that have undergone strong compaction tend to have less carbonate cement, common quartz overgrowths, closer positioning of grains, smaller grain sizes, and stylolites. These all affect porosity and permeability and may indicate that the most important controls for reservoir quality are grain size and degree of compaction. It seems as though the intervals that were not cemented early may have undergone enhanced compaction.

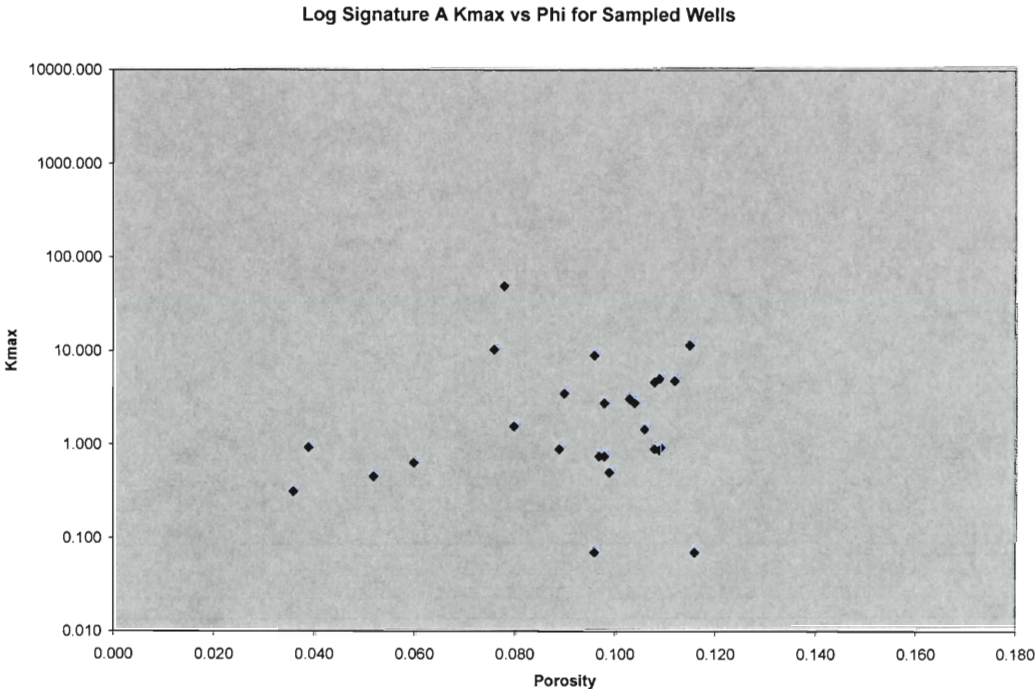
## **7.0 Discussion / Conclusions**

### *7.1 The Bluesky Formation in Whitecourt*

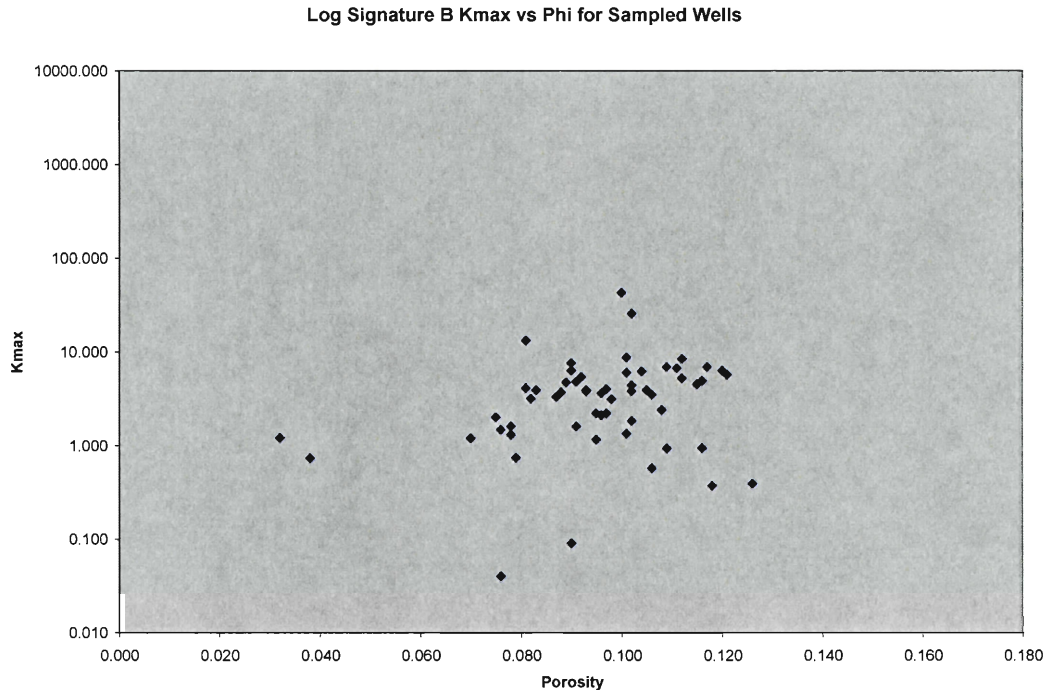
The Bluesky Formation in Whitecourt shows a wide range of permeability and porosity, not only from well to well, but also within the same sand body within a single well. This study has brought forth ideas with respect to what may cause the fluctuations in the porosity and permeability. The data seem to show fractures may be important in enhancing permeability but is localized. A well connected system of microfractures, not visible with the naked eye, could have the same effect as macro scale fracturing. Macrofracturing was not identified in the studied core nor was microfracturing found in the thin sections. They are believed to be present in some areas. The presence of prominent fractures, although possible, was not observed in any of the logged cores or reported in any of the data from the sampled wells (See Appendix A). Fracturing in the remaining wells used in the data set was noted by the technician running the porosity and permeability analyses on the core. The presence of fractures presents the question “are the fractures formed in response to the unloading of the core when it is brought to the surface or are they present and effective in the sub-surface as well?” Production from some wells in the study area show large volumes of gas from reservoirs that look poor on logs. Unfortunately these have not been cored. In these wells, has poor porosity been overcome by fracture enhanced permeability to create good reservoir? This cannot be resolved within the realm of this study but it is an important question left for future study.

Sedimentary features appear to have a minimal affect on permeability and porosity of the Bluesky Formation in Whitecourt. All of the wells used have been classified based on the log signature present in the well. The wells showing the Bluesky

“A” log signature tend to have a lower correlation coefficient than the Bluesky “B” log signature, however they both appear to be good reservoir regardless of the sedimentary features present. Comparison of the “A” (Fig. 7.1) and “B” (Fig. 7.2) cross plots show the relationship between porosity and permeability for signatures “A” and “B”.



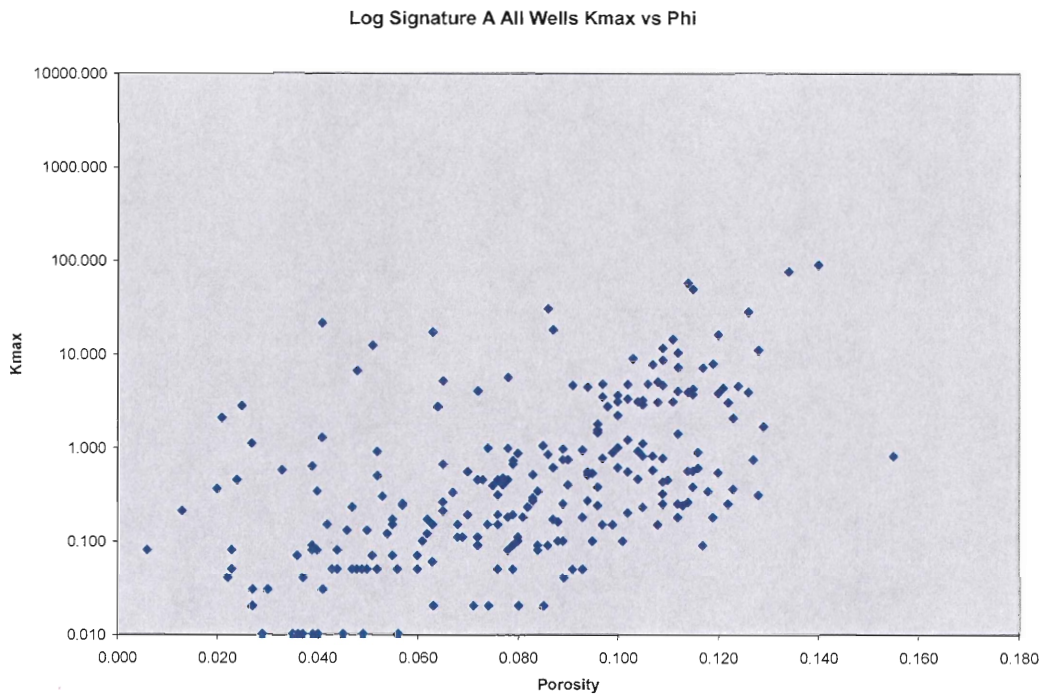
**Figure 7.1.** Cross plot of Kmax vs porosity for all of the sampled wells with the log signature “A” sand body.



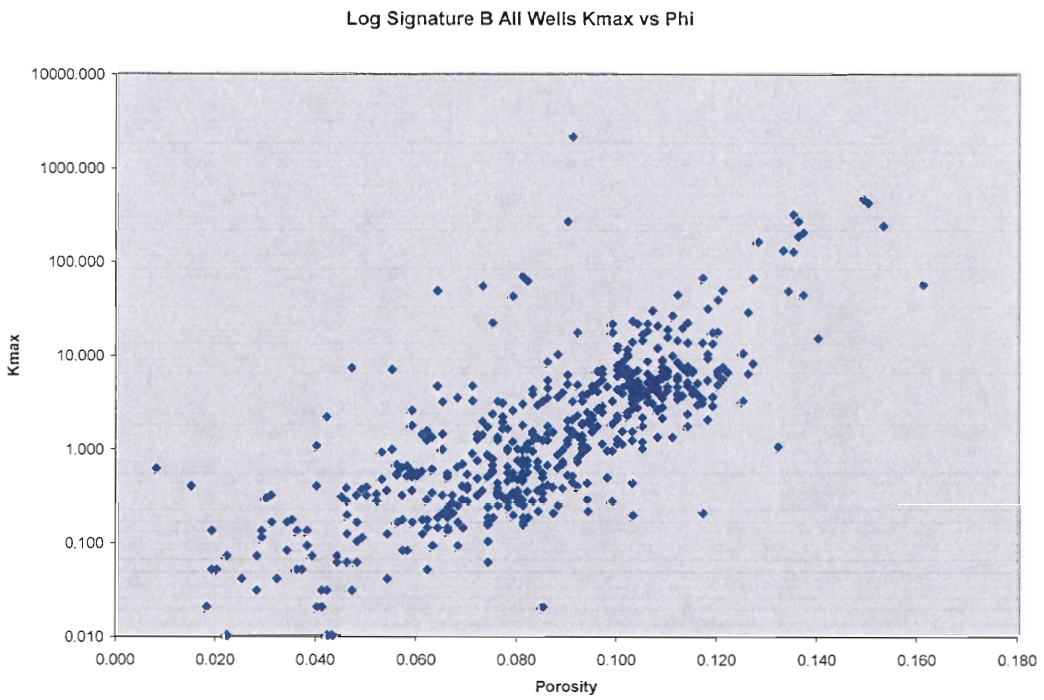
**Figure 7.2.** Cross plot of Kmax vs porosity for all of the sampled wells with the log signature “B” sand body.

The data for the sampled wells have also been cross plotted and show the same trend as the plots for the whole data set (Figs. 7.3, 7.4, 7.5). The sampled wells have data points that allow a comparison of permeability and porosity values from the EUB database with cores and thin sections.

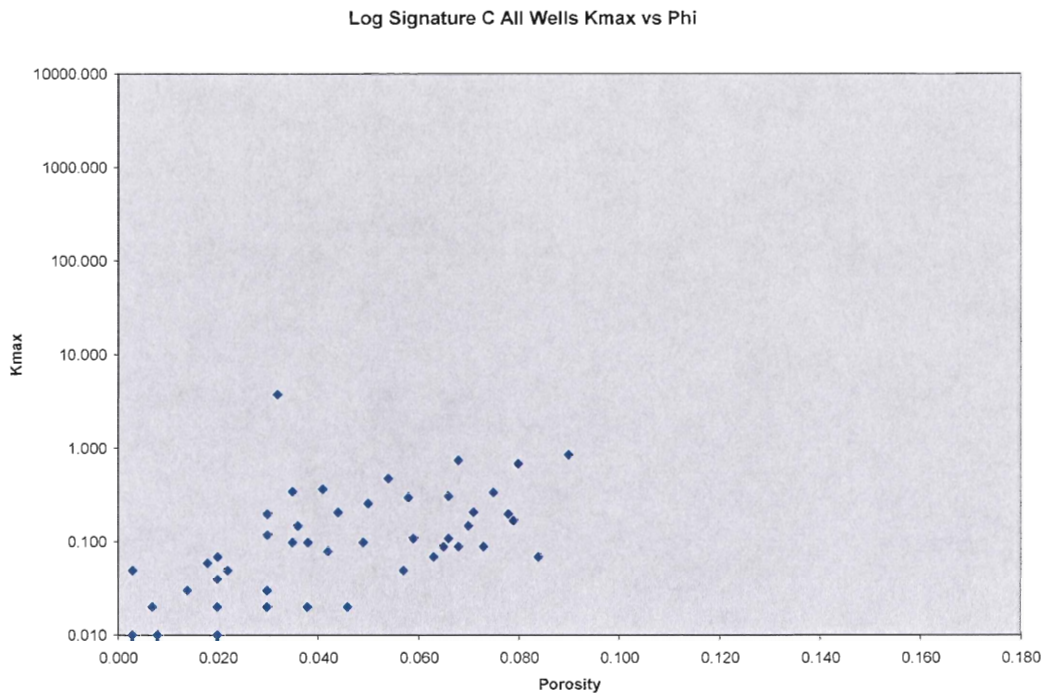
The “A” signature sands have high permeability and porosity and contain planar bedding, cross bedding, and may contain cryptic bioturbation. Mud and organic laminae have a dramatic effect on vertical permeability ( $K_{vert}$ ). In areas where there is moderate lamination, the vertical permeability is often less than 50% of the  $K_{max}$  and  $K_{90}$  values.



**Figure 7.3.** Cross plot of Kmax vs porosity for all of the wells in this study with the log signature “A” sand body.



**Figure 7.4.** Cross plot of Kmax vs porosity for all of the wells in this study with the log signature “B” sand body.



**Figure 7.5.** Cross plot of Kmax vs porosity for all of the wells in this study with the log signature “B” sand body.

The SDWC 6 and 7 thin sections show minor quartz overgrowths, minimal clay/mud content, and minor carbonate cement. In these samples, there is an obvious grain size difference. The coarser grained portion of the core has higher permeability and porosity values. The absence of stylolites in these samples may suggest that compaction in the area was less intense than in other portions of the formation, or perhaps compaction may have had less impact because of the coarser grain size and corresponding larger pore system.

The Bluesky “B” log signature sand body shows high permeability and porosity even though it appears to finer grained, have high clay/mud content, and the presence of quartz overgrowths. In areas where sand is finer grained, overgrowths are more abundant and seal off open pore spaces. Similar to the “A” signature sand, vertical permeability is greatly affected by mud and organic laminae. Glauconite does not appear to be abundant

in the sampled wells that have actual permeability and porosity data points. However, well 01-29-060-17W5 contains abundant glauconite and if the data were available it would show low porosity and permeability in the areas where the glauconite is prevalent.

The location of the Bluesky sand bodies within the proposed depositional environment appears to have at least a modest effect on the porosity and permeability of the Bluesky Formation in Whitecourt. The size of sand grains, abundance or lack of lamination, and degree of bioturbation, all affect reservoir quality. Sand found in the Bluesky “C” area of deposition would be undesirable for reservoir in an oil field but may produce economic volumes of gas. The sands are filled with baffles and barriers to flow but because gas can flow economically from lower permeabilities (Fig. 7.5) than oil, these targets may still be desirable, especially if found with either the “A” or “B” sands.

The thick sand found in the Bluesky “B” area of deposition seems an ideal target when looking only at the well log suite. However, these sand bodies may contain mud laminae that cannot be resolved on the logs and may also have abundant quartz overgrowths sealing off pores and reducing permeability through narrowing or elimination of pore throats. This exposes one limitation of porosity logs. They measure both effective and ineffective porosity. Porosity within a grain or in areas of narrow pore throats is not useful for trapping hydrocarbons and/or allowing fluid/gas to flow. The highest permeability and porosity areas in the Bluesky “B” sand have few overgrowths, low mud/clay content, and few laminations. The type of features present do not appear to be as important as the sand/mud content of the sediment and how it has been affected by diagenesis.

Well 07-31-58-19W5 is the deepest Bluesky well at a present depth of 2219.6 m, however, the current depth of burial does not necessarily imply original depth of burial. The rocks may have undergone stages of uplift and burial. It is apparent when looking at the thin sections that burial depth and compaction have had an effect on the porosity and permeability of the formation, as indicated by the fine grain size, dissolution, and migration of quartz and lithic grains, and suturing and elongation of grain boundaries. This Bluesky “B” sand body shows that reservoir quality is controlled equally by diagenesis and depositional setting. It is possible that effects of compaction may be reduced in wells with larger grain sizes because there is more surface area per grain to spread pressure over.

## 7.2 *Reservoir analysis*

The Bluesky Formation in Whitecourt produces a moderate amount of hydrocarbons but is a much more prolific producer in other areas of Alberta where the depositional setting is slightly different. The log signatures described in this study may serve as an initial guide to evaluating the Bluesky Formation in well logs. The log signatures are useful for eliminating sand bodies corresponding to the Bluesky “C” sand which is not likely to produce a worthwhile result if evaluated for liquid hydrocarbons due to the high clay content acting as a permeability barrier. The main sand bodies for exploration and development are signatures “A” and “B”. The “C” signature may also be present in the same well but is not the main target. Table 7.1 shows the hydrocarbons produced from these wells, the date the well was drilled, and the unique well identification number. All of these wells have been hydraulically fractured using sand as



the proppant. This is necessary for all Bluesky wells in the study area because of the low average permeability (Refer to Figs.5.1, 5.3, 5.4).

UWI	Rig Release Date	Cumulative Gas Production (mcf)	Daily Gas Production (mcf/d)	Cumulative Oil Production (bbl)	Daily Oil Production (bbl/d)	Log Signature
06-25-061-18W5/3	3/26/2000	315706	196	0	0	A & C
07-31-058-19W5/0	11/25/1994	0	0	0	0	B
09-08-058-18W5/0	10/19/1993	4997127	1109	0	0	B
03-31-060-18W5/2	12/9/1995	1151711	303	0	0	A & C
01-29-061-17W5/0	4/3/2001	1221073	627	0	0	B
12-24-058-18W5/0	1/4/1989	6616432	1181	4256	1	B

**Table 7.1.** Hydrocarbon production data for the wells sampled and used in this study.

The “A” log signature is a thin sand body but has proven to produce almost as well as the Bluesky “B” sand. This could be explained by the lateral extent of the “A” signature as shown in Figure 2.4a. If the area of a reservoir is large, there is a greater potential volume of recoverable hydrocarbons. However, the Bluesky Formation has low permeability (on average less than 0.1 millidarcies) so the drainage area is somewhat limited. Thin sand bodies are generally less favourable than thick sand bodies because thin sand spread laterally with low permeability will require more wells to get the same volume of hydrocarbons as a thick, localised sand body with the same permeability. Considering the above factors, drilling for thicker reservoirs is more economic. However, with fracture enhanced permeability and large area, thin reservoirs like the Bluesky “A” signature may still be attractive targets.

The Bluesky “B” log signature is a very thick sand body and could contain a large volume of hydrocarbons. These sand bodies are more limited in their distribution, as shown in Figure 2.4b. Their value as a reservoir is higher than “A” because their thickness means more area for hydrocarbons to accumulate and a larger area vertically to

draw from. Drilling one well in the thick sand may recover as much hydrocarbon as drilling several in a thin sand. Therefore detailed mapping of the “A” and “B” trend is important.

When drilling wells in the Bluesky formation in Whitecourt, Alberta, two main things should be considered; 1) Possible sedimentary and diagenetic factors that have altered the target sand body. It appears that the ranges of porosity and permeability may be explained by the following; very high porosity/permeability is due to fracturing, moderate to high porosity/permeability is due to remnant porosity, and secondary porosity, low to very low porosity/permeability is due to lack of early cementation, causing enhanced compaction and may or may not contain stylolites. 2) The type of log signature corresponding to the sand body being explored. Because coring wells is a very expensive process, most petroleum companies limit the number of cored wells, especially in developed fields. However, the only way to see the slight changes in depositional environment and diagenetic history that can cause decreases in productivity is to core every well and calibrate the core to the well logs. This is obviously not realistic; it is, however, realistic to combine all the available data for a large area and to map porosity and permeability changes. Doing this could possibly save money and allow companies to avoid drilling unproductive wells.

### *7.3 Future work*

Future work for the Bluesky Formation in Whitecourt should include more core analysis. Study of drill core provides a visual sense of the factors controlling reservoir quality. Sampling the cores and thin section analysis is also crucial to finding and developing a high quality reservoir. By taking additional cores in areas that have limited

core data it will increase understanding of the depositional setting. Point counting all of the thin sections would allow a much better analysis of the components making up the sand in the formation. Proportions were visually estimated in this study. Finally, mapping all data, whether it is permeability values or the presence of a specific log signature, will always bring a different perspective to the area being studied.

## 8.0 References:

- Agar, D. 2005. Personal Correspondence (e-mail). Porosity and Permeability techniques used by EUB Core Lab.
- Bhattacharya, J. P. and Walker, R. G. 1992. Deltas (Facies Models: response to sea level change). Edited by Walker, R. G. and James, N. P. Geological Association of Canada, St. John's, p. 157-179.
- Cant, D. J. 1989. Zuni Sequence: The Forland Basin Lower Zuni Sequence: Middle Jurassic to Middle Cretaceous (Western Canada Sedimentary Basin A Case History). Edited by Ricketts, B. D. Canadian Society of Petroleum Geologists, Calgary, p. 251-284
- Chafetz, H. S. and Reid, A. 2000. Syndepositional shallow-water precipitation of glauconitic minerals. *Sedimentary Geology*, 136, p. 29-42.
- Chiang, K. T. 1985. The Giant Hoadley gas field, South-Central Alberta (Elmworth Case Study Deep Basin Gas Field AAPG Memoir 38). Edited by Masters, J. A. American Association of Petroleum Geologists, p. 297-313.
- Cone, M. P. and Kersey, D. G. 1999. Porosity (Development Geology Reference Manual: AAPG Methods in Exploration Series, No. 10). Edited by Thompson, D. M., and Woods, A. M. American Association of Petroleum Geologists, p. 204-212.
- Dott Jr, R. H. 1964. Wacke, greywacke and matrix-what approach to immature sandstone classification? *Journal of Sedimentary Petrology*, vol. 34, no. 3, p. 625-633.
- Doyle, S. J. 2005. Bluesky A Gross Sand Isopach. Talisman Energy internal map. Scale 1:250000.
- Doyle, S. J. 2005. Bluesky B Gross Sand Isopach. Talisman Energy internal map. Scale 1:250000.
- Hutcheon, I. 1990. Aspects of the diagenesis of coarse-grained siliciclastic rocks(Diagenesis). Edited by McIlreath, I. A. and Morrow, D. W. The Runge Press Ltd, Ottawa, p. 165-177.
- Lavigne, J. 2006. Photo micrographs used in this study. Figures 6.1-6.11 inclusive.
- Legun, A. 1983. Stratigraphic and Depositional Relationships Between the Bluesky Marker Unit, Gething Marine Tongue, and Upper Coal Measures of the Gething

- Formation; in Geological Fieldwork. B.C. Ministry of Energy, Mines and Petroleum Resources, Paper 1984-1, p. 117-122.
- Lukie, T. 2004. Bluesky Formation in Edson: A Petrographic Study. Talisman Internal Report.
- Lukie, T. 2005. Core photographs used in this study. Figures 4.1.2-4.1.9, 4.2.2-4.2.7, 4.3.2-4.3.5, 4.4.2-4.4.6.
- Mossop, G. D., Shetson, I. 1994. Chapter 19. Cretaceous Mannville Group of the Western Canada Sedimentary Basin. In: Geological Atlas of the Western Canada Sedimentary Basin. Canadian Society of Petroleum Geologists and Alberta Research Council, p.
- Mussett, A. E., Khan, M. A. 2000. Looking into the Earth: An Introduction to Geological Geophysics. Cambridge University Press, p. 285-303.
- Ohen, H. A. and Kersey, D. G. 1999. Permeability (Development Geology Reference Manual: AAPG Methods in Exploration Series, No. 10). Edited by Thompson, D. M., and Woods, A. M. American Association of Petroleum Geologists, p. 210-213.
- Oppelt, H. P. 1985. Stratigraphy and character of the Bluesky Formation (94A, B, H, G;93I, O, P). British Columbia Ministry of Energy, Mines and Petroleum Resources, Geological Fieldwork, p.161-166.
- Pemberton, G. S. and MacEachern, J. A. 1995. The Sequence Stratigraphic Significance of Trace Fossils: Examples from the Cretaceous Foreland Basin of Alberta, Canada. *Memoirs- American Association of Petroleum Geologists*, Issue 64, p. 429-475.
- Pemberton, S. G. and MacEachern, J. A., Frey, R. W. 1992. Trace fossil facies models: environmental and allostratigraphic significance (Facies Models: response to sea level change). Edited by Walker, R. G. and James, N. P. Geological Association of Canada, St. John's, p. 47-73.
- Pemberton, S. G. and Van Wagoneer, J. C. 1992. Ichnofacies of a Wave-Dominated Shoreline (Applications of Ichnology to Petroleum Exploration). Society of Economic Paleontologists and Mineralogists, Core Workshop, 17, p. 339-382.
- Plint, A. G. 1988. Sharp-based shoreface sequences and "offshore bars" in the Cardium Formation of Alberta: their relationship to relative changes in sea level. *Sea-level Changes-An Integrated Approach*, SEPM Special Publication No. 42, p. 358-370.
- Prothero, D. R. and Schwab, F. 1996. Sedimentary Geology: an introduction to sedimentary rocks and stratigraphy. W. H. Freeman Company, New York, p. 69-101, 121-135, 170-227.

- Reinson, G. E. Transgressive barrier island and estuarine systems (Facies Models: response to sea level change). Edited by Walker, R. G. and James, N. P. Geological Association of Canada, St. John's, p. 179-195.
- Terzouli, A. and Walker, R. G. 1997. Estuarine valley fills in the Lower Cretaceous Bluesky Formation, Edson area, Alberta. Bulletin of Canadian Petroleum Geology, vol. 45, no. 2, p. 194-217.
- Trevena, A. S. and Clark, R. A. 1986. Diagenesis of Sandstone Reservoirs of Pattani Basin, Gulf of Thailand. American Association of Petroleum Geologists Bulletin, vol. 70, no. 3, p. 299-308.
- Walker, R. G. and Plint, A. G. 1992. Wave-and storm-dominated shallow marine systems (Facies Models: response to sea level change). Edited by Walker, R. G. and James, N. P. Geological Association of Canada, St. John's, p. 219-239.